Deriving Metallicities from Calcium Triplet Spectroscopy in combination with Near Infrared Photometry[⋆]

F. Mauro[1], C. Moni Bidin[1,2], D. Geisler[1], I. Saviane[3], G. S. Da Costa[4], A. C. Gormaz-Matamala[1], S. Vasquez[3,5], A.-N. Chené[1,6,7], R. Cohen[1], and B. Dias[3,8]

[1] Departamento de Astronomía, Universidad de Concepción, Casilla 160-C, Concepción, Chile
[2] Instituto de Astronomía, Universidad Católica del Norte, Av. Angamos 0610, Antofagasta, Chile
[3] European Southern Observatory, Ave. Alonso de Cordova 3107, Casilla 19, 19001 Santiago, Chile
[4] Research School of Astronomy & Astrophyiscs, Australian National University, Canberra ACT 0200 Australia.
[5] Instituto de Astrofísica, Facultad de Fisíca, Pontificia Universidad Católica de Chile, Av Vicuña MacKenna 4860, Santiago, Chile
[6] Gemini Observatory, Hawaii, USA
[7] Departamento de de Fisíca y Astronomía, Universidad de Valparaíso, Av. Gran Bretaña 1111, Playa Ancha, Casilla 5030, Chile
[8] Instituto de Astronomia, Geofísica e Ciências Atmosféricas, Universidade de São Paulo, Rua do Matão 1226, Cidade Universitária, São Paulo, 05508-900, SP, Brazil

Preprint online version: January 3, 2014

ABSTRACT

Context. When established with sufficient precision the ages, metallicities and kinematics of the Galactic globular clusters (GGCs) can shed much light on the dynamical and chemical evolution of the Galactic halo and bulge. While the most fundamental way to determine GC abundances is via high resolution spectroscopy, in practice this method is limited to only the brighter stars in the nearest and less reddened objects. This restriction has, over the years, led to the development of a large number of techniques that measure the overall abundance indirectly, from parameters that correlate with overall metallicity. One of the most efficient methods is the measurement of the equivalent width (EW) of the Calcium II Triplet (CaT) at $\lambda \approx 8500$Å in red giants, corrected for the luminosity and temperature effects via V magnitude differences from the horizontal branch (HB).
Aims. We establish a similar method in the NIR, combining the power of the differential magnitudes technique with the advantages of NIR photometry in minimizing differential reddening effects
Methods. We use the K_s magnitude difference between the star and the reddest part of the HB (RHB) or of the Red Clump (RC) to generate reduced equivalent widths (rEW) from the datasets presented in Saviane et al. (2012) and Rutledge et al. (1997) Subsequently we calibrated these rEW against three different metallicity scales: the one presented in Carretta et al. (2009), the metallicity values given in Harris (2010) and a version of the former corrected via high-resolution spectroscopic metallicities.
Results. We calculated the calibration relations for the two datasets and the three metallicity scales and found that they are approximately equivalent, with differences almost negligible. We compared our nIR calibrations with the corresponding optical ones, and found them to be equivalent, establishing that the luminosity-corrected rEW using the K_s magnitude is compatible with the one obtained from the V magnitude. We then used the metallicities obtained from the calibration to investigate the internal metallicity distributions of the GCs.
Conclusions. We have established that the ([Fe/H]:rEW) relation is independent from the magnitude used for the luminosity correction and find that the calibration relations only change slightly for different metallicity scales. The CaT technique using NIR photometry is thus a powerful tool to derive metallicities. In particular, it can be used to study the internal metallicity spread of a GC. We confirm the presence of at least two metallicity populations in NGC 6656 and find that several other GCs present peculiar metallicity distributions.

Key words. globular clusters: general

1. Introduction

Stellar population studies are one of our most powerful tools to study a wide variety of fundamental problems in stellar and galactic astrophysics. In particular, globular clusters (GCs) are perfect laboratories in this regard. GCs are testbeds for the understanding not only of stellar evolution and dynamics, but also of the formation of stellar exotica and the processes leading to disruption of massive stellar systems. GCs are cornerstones of the distance scale and serve as dynamical probes of a galaxy's complex kinematics and interaction history. They are unexcelled as tracers of the structure, formation and chemical evolution of a galaxy and its distinct components. Galactic GCs (GGCs) represent one of the fundamental systems that allow a reconstruction of the early evolution of the Milky Way: the knowledge of their ages, metallicities and kinematics has shed much light on the dynamical and chemical evolution of the Galactic halo and bulge (Zinn 1985; Minniti 1995; Ferraro et al. 2009).

While the most fundamental way to determine GC abundances is via high resolution (HR) spectroscopy, in practice this method is limited to only the brighter stars in the nearest GCs. This restriction has led over the years to the development of a large number of techniques aimed at indirectly measure the overall metal abundance, using parameters such as line strength, blanketing, or giant branch effective temperature, all of which correlate with overall metallicity. Even if these indices strictly

---

provide only criteria for ranking clusters by abundance, actual metallicities can be determined with appropriate calibration.

One of the most efficient methods is the measurement of the equivalent width (EW) of the Calcium II Triplet (CaT) at $\lambda \approx 8500$Å in red giants (Olszewski et al. 1991; Armandroff & Da Costa 1991). The CaT technique has many advantages. It is one of the most efficient ways to build up a large sample of accurate metallicity and velocity measurements even in distant GGCs. The brightest stars in the optical and IR in clusters older than ≈ 1Gyr are the red giants, and are thus the natural targets for precision measurements of cluster abundances and velocities. The CaT lines are extremely strong and near the peak flux of unreddened RGB stars, and the technique only requires moderate resolution ($R \sim 3000$). Because there are many giants in a typical GC, the derived mean abundance can be determined much more robustly than that based on only one or a few stars. A reasonable sample of stars must be observed in order to ensure cluster membership, especially in bulge GCs (BGC) where membership on the bright RGB may be as low as 20-50% due to strong field contamination (Saviane et al. 2012). Observing in the near Infrared (NIR) is also very advantageous for reddened BGCs, where optical indices can be strongly absorbed. Many authors have confirmed the accuracy and repeatability of CaT abundance measurements in combination with broad-band optical photometry and shown its very high sensitivity to metallicity and insensitivity to age (e.g., Cole et al. 2004). Additionally, as reported by Carrera et al. (2013), the strength of the CaT lines depends mainly on iron abundances, rather than on the Ca abundance, as has been pointed out also by several other investigations (e.g. Idiart et al. 1997; Battaglia et al. 2008).

In view of all of these advantages, many GGCs have had a sample of their RGB stars observed using CaT. A seminal paper in this regard is that of Rutledge et al. (1997, R97). They observed a total of 976 giants in 52 GGCs and showed that the CaT is both a very efficient and accurate technique for deriving GC velocities and metallicities. Recently, Saviane et al. (2012, S12) began an attempt to fill in CaT data for the large sample of GGCs remaining without such measurements. They obtained CaT abundances for 20 new GGCs. Still, this leaves more than one half of the GGCs without CaT data, including most bulge GCs (BGCs). The BGC system is one of the most important in our Galaxy and a thorough knowledge of metallicities and velocities can help to constrain bulge formation and evolution models. Nevertheless, substantial crowding or large and possibly variable reddening have combined to limit attempts to use even the CaT technique on many of these BGCs. One of the main reasons is because the traditional CaT technique, although it nominally involves only observations in the near IR, also requires optical photometry in order to calibrate the metallicity. It is well known that the CaT lines, in addition to being very metallicity sensitive, also depend on effective temperature and especially luminosity, and these effects must be removed in order to properly derive the metallicity. Traditionally, this is done by defining a reduced EW (rEW or W') for the sum of some combination of the 3 lines, which is then corrected for luminosity and temperature effects using the slope of the RGB, in particular the magnitude difference in V between the star and the horizontal branch (HB), $V_{HB} - V$. This differential method is very powerful as it also removes any dependence on distance or mean reddening. Unfortunately, it also requires good optical photometry, which is often problematic for BGCs. Indeed, for many BGCs V_{HB} is only very poorly known. Clearly, it would be very advantageous to develop a similar technique without these problems.

Here we establish a similar method in the IR, using as the fiducial magnitude the K_s magnitude of the reddest part of the HB (RHB) or of the Red Clump (RC). This combines the power of the differential technique with the advantages of IR observations in minimizing extinction and reddening effects.

A major advantage of this work is the possibility to exploit databases that are homogeneous both in terms of spectroscopy and photometry. Our photometric dataset consists of a catalog of GCs observed as part of the Vista Variables in the Via Lactea (VVV) Survey (Saito et al. 2012), calibrated on the system of the Two Micron All Sky Survey (2MASS, Skrutskie et al. 2006). This proves to be the ideal catalog for this purpose, since it is integrated with the 2MASS PSC. We used the spectroscopic dataset presented in S12, and also in R97, while we adopted as the metallicity reference the Carretta et al. (2009) scale, based on UVES and GIRAFFE HR spectra.

We note that an initial attempt at involving NIR photometry to calibrate CaT was made by Olszewski et al. (1991), where they used the absolute I magnitude of the red giant in order to correct for luminosity and temperature effects. Unfortunately, this requires an accurate distance, which is certainly problematic for BGCs. Another attempt of calibration of CaT in the nIR was made by Warren & Cole (2009) using spectra of 133 red giant stars from 10 Galactic open clusters and two Galactic globular clusters, and Zinn & West (1984) as metallicity scale. They found a linear correlation. However, the Zinn & West (1984) and Carretta et al. (2009) scales are not correlated properly by a simple linear relation, but by at least a quadratic expression. Previous works that used NIR photometry to correct CaT are Lane et al. (2010) and Warren & Cole (2009), but the former used as reference level the K_s magnitude of the Tip of the RGB, while the latter took the value of K_s at the RR Lyrae instability strip for the GCs.

The CaT method can also be applied to derive the metallicity for red giants in any stellar population for which V_{HB} is known, e.g. dwarf spheroidal galaxies, the Magellanic Clouds, extragalactic Globular Clusters or even M31 (Battaglia et al. 2011; Parisi et al. 2010; Foster et al. 2010; Jones et al. 1984; Cenarro et al. 2008). Adapting the technique to the IR allows us to apply it to any stellar population where reddening is problematic, opening up many additional targets for detailed study.

Here we first present our observations and reductions (Section 2). Next we present the metallicity calibration and discuss individual clusters (Section 3). Our conclusions are discussed in Section 4.

2. Observations and reductions

Our main target list consists of the GCs analyzed by S12. The nIR imaging collected in the context of the VVV Survey was used for all clusters included in the survey area. We also checked if any of the GCs in the dataset not observed by the VVV Survey had useful 2MASS photometry, permitting us to determine the RHB position. Including also these GCs allowed us to better constrain the calibration over a wider metallicity range with better sampling. We similarly selected GCs from the R97 catalog in order to determine a calibration for this dataset as well. All clusters analyzed in the current paper are listed in Tables 1. The complete data for all spectroscopic stars are presented in Table 8, and the metallicity values are listed in Tables 2-7, separated for spectroscopic dataset, only available in electronic form.

2.1. Spectroscopy

2.1.1. S12 data

The data were obtained in the z-band region of giant stars with FORS2 (Appenzeller et al. 1998), working at the Cassegrain focus of VLT/UT1-Antu. The approach used to assemble the list of clusters observed is discussed in S12. All spectra were extracted using the FORS2 pipeline version 1.2 (Izzo et al. 2010). The absorption lines of the CaT were used both to measure radial velocities and derive metallicities. Metal-rich clusters were measured with Gaussian plus Lorentzian function fits, while the equivalent widths for metal-poor clusters were computed with Gaussian fits only and transformed onto the scale established in Gullieuszik et al. (2009, G09). This decision is justified since we have verified that there is a one-to-one correspondence between widths measured with the two methods.

The final ΣW_{S12} for each star results from the sum of the EWs of the two strongest CaT lines (8542Å, 8662Å):

$$\Sigma W_{S12} = EW(8542Å) + EW(8662Å). \tag{1}$$

We refer to S12 for a more complete description of the observations, reduction procedure, and selection for cluster membership.

2.1.2. R97 data

We also retrieved the spectroscopic data from Rutledge et al. (1997, R97). Not all of the clusters in R97 were used because of the difficulty to identify the stars in the scanned finding charts. Anyway, we included all the more metal-poor and metal-rich GCs, the ones included in the VVV Survey, as well as others to cover properly the full metallicity range of GGCs.

In this case the final ΣW for each star is the weighted sum of the three CaT lines:

$$\Sigma W_{R97} = 0.5 \cdot EW(8498Å) + EW(8542Å) + 0.6 \cdot EW(8662Å). \tag{2}$$

We refer to R97 for a more complete description of the observations, reduction procedure, and selection for cluster membership.

2.2. Photometry

The VVV Survey (Minniti et al. 2010; Catelan et al. 2011) is one of six ESO Public Surveys carried out at the 4-meter Visible and Infrared Survey Telescope for Astronomy (VISTA), scanning the Galactic bulge ($-10 \leq l \leq +10$, $-10 \leq b \leq +5$) and the adjacent part of the southern disk ($-65 \leq l \leq -10$, $-2 \leq b \leq +2$). The survey collects data in five NIR bands ($ZYJHK_s$) with the VIRCAM camera (Emerson & Sutherland 2010), an array of sixteen 2048×2048 pixel detectors with a pixel scale of $0.''341/pix$. VVV images extend several magnitudes fainter than the 2MASS, and enjoy increased spatial resolution (Saito et al. 2010). Both of these factors are particularly important for mitigating contaminated photometry in crowded regions near the Galactic center and the cores of globular clusters. The VVV survey provides precise multi-epoch K_s-photometry for 39 Galactic globular clusters, that permits to obtain K_s magnitudes with good accuracy. For this reason, we preferred K_s magnitudes, instead of J or H ones, to correct the equivalent widths.

We retrieved from the Vista Science Archive website[1] the VVV images containing the GGCs targeted by S12 and R97, pre-reduced at the Cambridge Astronomical Survey Unit

---

[1] http://horus.roe.ac.uk/vsa/

(CASU)[2] with the VIRCAM pipeline (Irwin et al. 2004). We performed PSF-fitting photometry using the VVV-SkZ_pipeline code (Mauro et al. 2013), based on DAOPHOT suite (Stetson 1987, 1994), on the single 2048×2048 pixel chips extracted from the stacked VVV pawprints (Saito et al. 2012). The photometry was tied to the 2MASS system, as described in Moni Bidin et al. (2011) and Chené et al. (2012). The use of the 2MASS system as the standard photometric system permitted us to integrate our photometric database with the 2MASS PSC. The use of the VVV-SkZ_pipeline was fundamental for this work, since it is the only photometric procedure for VVV data that provides accurate photometry even for partially saturated stars, which are the bulk of the giants observed spectroscopically. As can be seen in Figures 1, almost 90% of the observed stars are brighter than the saturation limit for the VVV survey ($K_s = 12$), but our photometry is still reliable up to $K_s = 9 - 10$, as the comparison with 2MASS photometry demonstrates in Figure 2.

The stars with spectroscopic CaT measurements were identified in our VVV photometry. In some cases it was not possible to find a corresponding star in the VVV catalogs, i.e. very bright stars ($K_s < 9$) completely saturated on the VVV images. It this case, their photometric data were obtain from the 2MASS PSC catalog. The GC HP1 was excluded due to the difficulty in identifying the cluster RHB. The data for all spectroscopic stars are presented in Table 8, only available in electronic form.

2.2.1. Determination of the HB-level magnitude

The magnitude at the HB level was determined by the position of the peak in the luminosity distribution of the reddest part of the HB. The HB of some metal-poor GCs (like NGC 6121, NGC 6397 or NGC 6809) is well populated also at the red end, permitting an accurate determination of the RHB magnitude. For most of the metal-poor GCs, however, the red HB is not easily detectable in the color-magnitude diagram (CMD). We determined theoretically a "first-guess" position of the RHB in these cases, and compared it with the peaks in the luminosity distribution for the stars located along and next to the RGB, $2 - 3'$ from the cluster center. We used the metal-poor GCs with well-defined RHB to calibrate this procedure. The determination of the initial position was performed considering the results given by several procedures. We calculated a "theoretical" value based on Bressan et al. (2012) and Girardi & Salaris (2001), corrected for distance modulus and reddening of the GC. An empirical value was also calculated from the V_{HB} value listed in Harris (1996, 2010 edition, hereafter H10), corrected for distance modulus and reddening of the GC, for a mean ($V - K_s$) color taken from Bressan et al. (2012). The accuracy of these two methods depends strongly on the accuracy of the photometric parameters of the cluster. The CaT datasets include also the $\Delta V = V_{HB} - V$ for each star; we fitted the points in the ($\Delta V; K_s$) plane with a linear and quadratic[3] relations: the intercepts give an estimate of K_s magnitude of RGB stars that in the optical have the same luminosity of the RHB. We noted that this method can have an uncertainty as large as 0.5 mag, and depends strongly on the accuracy of V_{HB} and on the magnitude range covered by the data. We used these estimates, together with the values presented in Valenti et al. (2007, 2010), as an initial position to identify RHB among the peaks in the K_s luminosity distribution. Additionally, we used the empirical calibration for the

---

[2] http://casu.ast.cam.ac.uk/
[3] The locus of the points in the ($V_{HB} - V; K_s$) plane is not perfectly linear, but slightly convex.

RGB bump (Valenti et al. 2007) applied to the parameters listed in H10 to determine the position of the bump in the luminosity distribution, to avoid confusion between the peaks associated with the two different features. The results are presented in Table 1.

Table 1. List of RHB levels

ID	Photometric Source	$K_s(HB)$	σ
NGC6380	VVV	13.80	0.05
NGC6440	VVV	13.64	0.05
NGC6441	VVV	14.38	0.05
NGC6522	VVV	13.16	0.05
NGC6528	VVV	13.11	0.05
NGC6544	VVV	10.50	0.05
NGC6553	VVV	12.27	0.05
NGC6558	VVV	13.30	0.10
NGC6569	VVV	14.30	0.05
NGC6624	VVV	13.28	0.05
NGC6626	VVV	13.00	0.05
NGC6637	VVV	13.51	0.05
NGC6638	VVV	13.70	0.05
NGC6656	VVV	11.70	0.10
NGC2808	2MASS	14.02	0.05
NGC3201	2MASS	12.05	0.10
NGC4372	2MASS	12.05	0.20
NGC4590	2MASS	13.30	0.20
NGC6121	2MASS	9.97	0.05
NGC6139	2MASS	13.75	0.15
NGC6254	2MASS	11.87	0.05
NGC6325	2MASS	13.27	0.05
NGC6356	2MASS	14.60	0.05
NGC6397	2MASS	10.45	0.05
NGC6541	2MASS	13.00	0.20
NGC6809	2MASS	12.00	0.20
NGC6838	2MASS	11.78	0.05
NGC7078	2MASS	13.50	0.10
NGC7099	2MASS	13.40	0.15
Pal7	2MASS	12.55	0.05

The comparison between our $K_s(HB)$ values and the ones deduced from the $(V(HB) - V; K_s)$ fit suggests that the value of V_{HB} is not very accurate for most of the faintest GCs. In fact, 73% of GCs with $K_s(HB) < 13$ present an agreement between the two values within 0.2 mag, but this fraction reduces to 37% among fainter GCs.

2.3. Metallicities

The metallicities were taken from Carretta et al. (2009, hereafter C09), who measured [Fe/H] for 19 GCs from the analysis of spectra of about 2000 RGB stars using FLAMES@VLT (about 100 stars with GIRAFFE and about 10 with UVES, respectively, in each GC). With these data, they recalibrated their previous metallicity scale (e.g. Carretta & Gratton 1997, CG97) to the UVES scale, giving the calibration relations, and assembled a table of [Fe/H] values for 133 clusters present in the Harris (1996) catalog. The metallicities were computed based on the weighted average of indices published in four different studies, putting them on a single UVES scale. These values are reliable, but they were not obtained from spectroscopic analysis for all the clusters. Nevertheless, C09 has the advantage of being a homogeneous metallicity scale, and it is the main metallicity source for H10. We considered for the calibration only the values not derived from Harris (1996) (clus-

ters with a "1" in the Notes column of Appendix 1). The S12 dataset includes 8 of the GCs used in C09 as calibrators (NGC 2808, NGC 3201, NGC 6121, NGC 6254, NGC 6397, NGC 6441, NGC 6838, and NGC 7078), while 7 calibrators (NGC 2808, NGC 3201, NGC 4590, NGC 6121, NGC 6397, NGC 6809, and NGC 7099) are among the R97 sample used in this work.

We observed that, while the majority of GCs in the ([Fe/H]$_{C09}$; $\langle W' \rangle$) plane lie within $\sim 1\sigma$ to the fit, others (namely NGC 6528, NGC 6558 and NGC 6569) present larger differences. These clusters are not part of the 19 C09 calibrators, and their metallicities were derived through the weighted average of literature values. Checking the sources of the metallicities for these three objects, we found that NGC 6528 and NGC 6558 have recent HR spectroscopic metallicities in poor agreement with the C09 metallicity. H10 reports four sources of HR spectroscopic metallicity for NGC 6528. Carretta et al. (2001) based their estimate on observations carried out with the High Resolution Echelle Spectrometer (HIRES) at Keck I (final $R \approx 15,000$) of four HB stars. The Origlia et al. (2005) estimate is based on IR echelle spectra of four bright core giants, acquired with the IR spectrograph NIRSPEC ($R \sim 25,000$) mounted at the Keck II telescope. The other two are based on the same spectra acquired by Zoccali et al. (2004) with UVES ($R \sim 45,000 - 55,000$) of three stars (one HB star and two red giants). While the metallicity derived by Carretta et al. (2001) (and used in C09) is $+0.07 \pm 0.08$ dex, the Origlia et al. (2005) NIRSPEC metallicity is -0.17 ± 0.01 dex, and the UVES value is -0.1 ± 0.2 dex and -0.24 ± 0.19 dex, from Zoccali et al. (2004) and Sobeck et al. (2006) respectively. The photometric estimates obtained by Momany et al. (2003) are centered on the mean of field stars in Baade's Window, [Fe/H] = -0.25, as derived by McWilliam & Rich (1994). Anyway, we notice that the metallicity distributions of the stars in the S12 and R97 catalogs of this GC, according to our calibrations, are both almost flat, covering a metallicity range of ≈ 1 dex. For NGC 6558, Barbuy et al. (2007) estimate a metallicity of -0.97 ± 0.15 dex, based on the analysis of HR spectra of five giant stars (two are in common with our sample) acquired at the VLT with the multifiber spectrograph FLAMES in GIRAFFE mode ($R \sim 22,000$). C09 demonstrates that the metallicity scales obtained with UVES and GIRAFFE do not present systematic differences[4]. For NGC 6569, Valenti et al. (2011) find a metallicity of -0.79 ± 0.02 dex, based on six HR IR echelle spectra acquired with NIRSPEC ($R \sim 25,000$). The CG97 metallicity on the UVES/C09 scale is -0.90 dex, similar to the averaged photometric value of [Fe/H]$_= -0.88$ dex estimated in Valenti et al. (2005). For the R97 dataset, NGC 6624 presents recent HR spectroscopic metallicities in poor agreement with the C09 metallicity and a difference with our best fits of more than 2σ. NGC 6624 was analyzed with HR spectra in Valenti et al. (2011), where they found [Fe/H] = -0.69 dex. Our calibration yields values of metallicity on the C09 scale in better agreement with the metallicities estimated with HR spectroscopy than with C09 metallicities, suggesting that the C09 estimates for these GCs may have problems. Based on these considerations, we decided to construct a second metallicity scale called "corrected C09" (C09c) in order to check if these more recent values provide a better calibration relation. For NGC 6626, that was not used as a calibration cluster, we used for C09c the value [Fe/H] = -1.28 dex cal-

---

[4] mean difference "UVES minus GIRAFFE" of -0.015 ± 0.008 *dex* with a rms scatter of 0.037 dex from 19 of their GCs

culated by Da Costa & Armandroff (1995) through CaT method, as comparison.

We additionally calculated the calibration relations also for the metallicities given in H10, since it is a commonly-used source. All the metallicity values are listed in Tables 2-7.

2.4. Dependence of He abundance and contamination from AGB stars

S12 highlighted that the CaT method works on the assumption that V_{HB} depends almost exclusively on [Fe/H], the other stellar parameters playing only a secondary role. While this is true for the age of old stellar systems like GGCs (Salaris & Girardi 2002; Ferraro et al. 2006), cluster-to-cluster differences in helium abundance can instead be significant, and might cause higher residuals in the calibration, supposing these differences are not correlated with metallicity. In general, halo GGCs share a common He abundance (Buzzoni et al. 1983; Zoccali et al. 2000; Cassisi et al. 2003), but things might be different for BGCs. Nataf et al. (2013) recently postulated that bulge stars have a He enhancement $\Delta Y = 0.06$ with respect to halo GCs (see also Renzini 1994) to explain the difference between the luminosity of the RGB bump of the Galactic bulge and that predicted by the luminosity-metallicity relation of GGCs. S12 conclude that the cluster-to-cluster scatter in He content should not affect the results of the CaT method, and we refer the reader to their analysis for more details. We expect similar behavior for $K_s(HB)$, and the small scatter that the C09 calibrator GCs have around the fitting curves confirms this expectation.

Another potential concern is that, particularly in the differentially reddened clusters, the possibility that AGB stars are included in the selected "RGB" samples may lead to additional scatter in the $(\Sigma W, K_s - K_s(HB))$ plane, and thus to increased uncertainty in the derived abundances. On the other hand this effect is expected to be quite small ($\Delta W = 0.04$Å), as shown by Cole et al. (2000).

3. Results

Assuming the relation

$$\Sigma W = a[K_s(HB) - K_s] + W' , \qquad (3)$$

the slope a is calculated through a least-square fit[5], with the constraint that it must be the same for all the clusters. To a good approximation, the slope is independent of metallicity within the range spanned by our GCs.

Subsequently, we calculated W' for all stars in each cluster, empirically removing the EW dependence on the star's gravity and temperature. We calculated $\langle W' \rangle$ for each GC, through a weighted average of W' of all stars. We preferred this approach instead of the intercept value provided by the least-square fit method because, while the two estimates negligibly differ, the uncertainties associated with the fit heavily depend on the number of data, and are thus overestimated. Finally the [Fe/H] vs. $\langle W' \rangle$ relation was calculated for each metallicity scale with a polynomial fit to define the best calibration relation. The unbiased residual mean square (hereafter urms or σ) was assumed as the uncertainty of our fit. It consists in the square root of the sum of the square of the residuals, divided by the number of degrees

of freedom for error[6], instead of the number of data points, in order to remove the bias on the estimate of the variance of the unobserved errors.

3.1. Calibration of reduced equivalent widths from S12

The ΣW_{S12} values are plotted vs. $K_s(RHB) - K_s$ in Figure 3. For the slope we obtain $a = -0.385$ Å/mag with a urms of 0.013 Å/mag. The $\langle W' \rangle$ cover a range of 2-5.8 Å.

The calibration relations for [Fe/H] on the C09 scale and the nIR $\langle W' \rangle$ on the G09 scale are shown in Figure 4, defined in a [Fe/H] range from -2.33 dex to $+0.07$ dex. As can be seen in the Figure, both the cubic and the quadratic relations well reproduce the observed trend, while the linear one does not fit properly the more metal-rich GCs. The fourth- and fifth-order polynomials do not differ noticeably from the third-order one. The cubic calibration relation is

$$[Fe/H]_{C09} = -4.61 + 1.842\langle W' \rangle - 0.4428\langle W' \rangle^2 + 0.04517\langle W' \rangle^3, \qquad (4)$$

with a urms of 0.214 dex (0.113 dex considering only the 8 GCs used as calibrators in C09). The quadratic calibration relation

$$[Fe/H]_{C09} = -2.63 + 0.040\langle W' \rangle + 0.0653\langle W' \rangle^2, \qquad (5)$$

with a urms of 0.237 dex (0.110 dex considering only the 8 calibrators). The differences in metallicity between the cubic and the quadratic fit are less than 0.1 dex in absolute value in the range of definition ($2 < \langle W' \rangle < 5.5$, $-2.3 < [Fe/H] < -0.3$), increasing up to 0.35 for $\langle W' \rangle = 6$ ([Fe/H] ~ 0.1).

The calibration relations for [Fe/H] on the C09c scale and the nIR $\langle W' \rangle$ on the G09 scale are shown in Figure 5. They are defined over an [Fe/H] range from -2.33 dex to -0.17 dex. The differences between the cubic and quadratic calibration relations are slightly smaller than for C09 scale. The cubic calibration relation in this revised system is

$$[Fe/H]_{C09c} = -4.09 + 1.341\langle W' \rangle - 0.2919\langle W' \rangle^2 + 0.03098\langle W' \rangle^3, \qquad (6)$$

with a urms of 0.173 dex (0.114 dex considering only the 8 calibrators). The quadratic calibration relation

$$[Fe/H]_{C09c} = -2.73 + 0.103\langle W' \rangle + 0.0568\langle W' \rangle^2, \qquad (7)$$

with a urms of 0.180 dex (0.110 dex considering only the 8 calibrators).

The calibration relations for [Fe/H] on the H10 scale and the nIR $\langle W' \rangle$ on the G09 scale are shown in Figure 6. They are defined over an [Fe/H] range from -2.37 dex to -0.11 dex. The differences between the cubic and quadratic calibration relations are slightly smaller than for C09 scales. The cubic calibration relation is

$$[Fe/H]_{H10} = -4.14 + 1.371\langle W' \rangle - 0.3032\langle W' \rangle^2 + 0.03263\langle W' \rangle^3, \qquad (8)$$

with a urms of 0.165 dex. The quadratic calibration relation is

$$[Fe/H]_{H10} = -2.45 - 0.080\langle W' \rangle + 0.0839\langle W' \rangle^2, \qquad (9)$$

with a urms of 0.165 dex.

---

[5] the algorithm is based on a series of five lectures presented at "V Escola Avancada de Astrofisica" by Peter B. Stetson http://ned.ipac.caltech.edu/level5/Stetson/Stetson_contents.html

[6] The number of data points less the number of the coefficients of the curve used to fit them.

3.1.1. Comparison between reference scales

We compared the three calibration relations for the S12 dataset obtained in this study with the one calculated at optical wavelengths in S12. The cubic and the quadratic fits do not differ noticeably, and S12 presented a cubic relation, hence the 3rd-order solution was adopted in the comparison. As can be seen in Figure 7, the four relations are approximately the same, with differences less than 0.1 dex over the whole metallicity range. The three relations from this work differ among each other generally less than $0.02 - 0.04$ dex, with a maximum value of 0.08 dex between the solutions C09 and C09c at the metal-rich end. This demonstrates that the three scales are approximately the same, and the smallest values of urms could indicate a more precise calibration. This overall comparison demonstrates that the photometric correction to the CaT equivalent widths is independent of the passband used, since the same calibration relation can be adopted when using both optical and NIR magnitudes. Additionally, the good agreement over the whole metallicity range demonstrates that the HB level was determined with sufficient accuracy in our work.

Comparing the C09 metallicities with those obtained from our equation (see Table 2), 6 of the 19 GCs present a difference greater than 1σ. However, the metallicity of three of these is controversial, and is poorly known for the other two. Only NGC 6569 among these GCs presents a difference greater than 2σ. We derived a metallicity of -1.20 dex for it, similar to those of NGC 2808 and NGC 6121, versus the C09 value of -0.72 dex. We get [Fe/H] $= -0.58$ dex (instead of -0.35 dex) for NGC 6356, -0.19 dex (instead of $+0.07$ dex) for NGC 6528, and -1.09 dex (instead of -1.37 dex) for NGC 6558. For the two GCs with poorly known metallicity, the equation gives -1.47 dex for NGC 6139 (C09 suggests -1.71 dex), and -0.73 dex for NGC 6380 (-0.40 dex). The statistic is similar in the comparison with the C09c scale (see Table 3): 6 GCs with $|\Delta[\text{Fe/H}]| > 1\sigma$, with NGC 6569 still the only one with $|\Delta[\text{Fe/H}]| > 2\sigma$. We obtain now a difference smaller than 1σ for NGC 6528 and NGC 6558, while the discrepancy for NGC 6440 and NGC 6441 is now greater than before: the equation gives -0.41 dex (against the C09 value of -0.20 dex), and -0.65 dex (-0.44 dex), respectively. We note that, in these two C09-based scales, NGC 6441 is the only one of the 8 C09 calibrators that presents a $\Delta[\text{Fe/H}] > 0.3\sigma$. For the H10 scale (see Table 4), only four of the 19 GCs present $|\Delta[\text{Fe/H}]| > 1\sigma$, namely NGC 6139, NGC 6558, NGC 6569, and NGC 6656 (-1.90 dex instead of -1.70 dex).

3.2. Calibration of reduced equivalent widths from R97

The ΣW_{R97} values are plotted vs. $K_s - K_{sRHB}$ in Figure 8. For the R97 dataset we obtain $a = -0.380$ Å/mag with a urms of 0.014 Å/mag. This value differs from the one for S12 by only 0.005 Å/mag ($\approx 0.4\sigma$), consequently the slope is independent of the way the equivalent width is calculated. Such variation would cause a change in the mean rEW less than 0.02 Å in our case, which is completely negligible. The $\langle W' \rangle$ cover a range of 1.6-5.1 Å.

The calibration relations for [Fe/H] on the C09 scale and the nIR $\langle W' \rangle$ are shown in Figure 9, defined over an [Fe/H] range from -2.33 dex to $+0.07$ dex. The calibrations based on a fourth- and fifth-order polynomial are not suitable, and were consequently rejected. The best fits are obtained with the cubic and quadratic relations, while the linear one does not fit properly

the more metal-rich GCs, as observed also for the S12 dataset, or the more metal-poor GCs. The quadratic calibration relation is

$$[\text{Fe/H}]_{\text{C09}} = -2.24 - 0.254\langle W' \rangle + 0.13094\langle W' \rangle^2, \qquad (10)$$

with a urms of 0.102 dex (0.114 dex considering only the 7 GCs used as calibrators in C09), while the cubic calibration relation is

$$[\text{Fe/H}]_{\text{C09}} = -2.90 + 0.393\langle W' \rangle - 0.0684\langle W' \rangle^2 + 0.01939\langle W' \rangle^3, \qquad (11)$$

with a urms of 0.113 dex (0.130 dex considering only the 7 calibrators). The differences in metallicity between the cubic and the quadratic fits are less than 0.06 dex in absolute values in almost all the range of definition ($1.7 < \langle W' \rangle < 5.0$, $-2.2 < [\text{Fe/H}] < -0.3$), increasing up to 0.2 for $\langle W' \rangle = 5.3$ ($[\text{Fe/H}] \sim 0.0$).

The calibration relations for [Fe/H] on the C09c scale and the nIR $\langle W' \rangle$ are shown in Figure 10. They are defined over an [Fe/H] range from -2.33 dex to -0.16 dex. The differences between the cubic and quadratic calibration relations are slightly smaller than for the C09 scale. The quadratic calibration relation is

$$[\text{Fe/H}]_{\text{C09c}} = -2.39 - 0.143\langle W' \rangle + 0.1116\langle W' \rangle^2, \qquad (12)$$

with a urms of 0.096 dex (0.115 dex considering only the 7 calibrators). The cubic calibration relation is

$$[\text{Fe/H}]_{\text{C09c}} = -2.66 + 0.125\langle W' \rangle + 0.0285\langle W' \rangle + 0.00809\langle W' \rangle^3, \qquad (13)$$

with a urms of 0.104 dex (0.133 dex considering only the 7 calibrators).

The calibration relations for [Fe/H] on the H10 scale and the nIR $\langle W' \rangle$ are shown in Figure 11. They are defined over an [Fe/H] range from -2.27 dex to -0.11 dex. The differences between the cubic and quadratic calibration relations are less than 0.06 dex in the whole range. The quadratic calibration relation is

$$[\text{Fe/H}]_{\text{H10}} = -2.53 - 0.037\langle W' \rangle + 0.09658\langle W' \rangle^2 \qquad (14)$$

has a urms dispersion around the fit of 0.110 dex. The cubic calibration relation is

$$[\text{Fe/H}]_{\text{H10}} = -0.66 - 1.821\langle W' \rangle + 0.6211\langle W' \rangle^2 - 0.04848\langle W' \rangle^3 \qquad (15)$$

has a urms dispersion around the fit of 0.103 dex.

3.2.1. Comparison between the reference scales

For the comparison between the three metallicity scales, we chose to use the quadratic relations, since they are the ones with the lower urms values. Our three relations are approximately the same, even for this dataset, as can be seen in Figure 12. The differences are negligible, being less than ~ 0.03 dex over most of the metallicity range, with a maximum value of 0.08 dex at the more metal-rich GCs. The H10 relation presents a systematic over-estimate of ~ 0.04 dex compared to the other two.

The linear relation between the V-band rEW and [Fe/H] presented by C09 was defined in the ranges $1.5 < \langle W' \rangle < 4.7$ and $-2.33 < [\text{Fe/H}] < -0.7$, thus excluding the most metal-rich GCs. Anyway, as can be noted in Figures 9-11, in this metallicity range the difference among the cubic and quadratic fits and the linear one is $\lesssim 1\sigma$. As a matter of fact, if we recalculate the urms for our linear fits in the same metallicity range, we obtain results more similar to the urms of the quadratic equation

(0.116, 0.099, and 0.149 dex, respectively for the three scales), showing that a non-linear fit is needed including also the metal-rich end. We compared both the quadratic and the linear calibration relations for the nIR rEW with the one from C09. While the quadratic relations present an obvious difference with the optical one, the comparison among the four linear relations (see lower plot in Fig. 12) confirms that the ([Fe/H] vs rEW) relation can be considered almost independent of the passband used for the photometry.

Comparing the C09 metallicities with the ones obtained from our equations (see Table 5), the quadratic equation yields a metallicity different by more than 1σ for four GCs, namely NGC 2808, NGC 6397, NGC 6624, NGC 6626. The problems related to the controversial metallicity of the last two GCs were already discussed in Section 2.3. The cubic solution gives a difference Δ[Fe/H] $> 1\sigma$ even for NGC 6528. NGC 6624 is only cluster with Δ[Fe/H] $> 2\sigma$, with an estimated metallicity of -0.67 dex, against the C09 value of -0.42 dex. We obtain [Fe/H] $= -1.31$ dex for NGC 2808, while C09 gives -1.18 dex and S12 equation ~ -1.14 dex, -2.14 dex for NGC 6397, versus -1.99 dex, for both C09 and S12 equation, and -1.31 dex for NGC 6626, instead of -1.46 dex. Considering the six GCs in common with S12 dataset, the metallicity obtained for NGC 3201 and NGC 6121 are in perfect agreement, while NGC 6553 presents a difference Δ[Fe/H] $\approx 1\sigma$. NGC 6528 shows an even larger discrepancy, but its metallicity is controversial and, along with NGC 6553, it is sensitive to the fit uncertainties at high metallicities. Considering the C09c scale (see Table 6), we have only three GCs with $|\Delta$[Fe/H]$| > 1\sigma$, namely NGC 2808, NGC 6397 and NGC 6528. This last is the only one with $|\Delta$[Fe/H]$| > 2\sigma$, with a resulting [Fe/H] $= +0.04$ dex, against the adopted value of -0.17 dex. The equation for the H10 scale (see Table 7) presents more discrepancies, since five clusters show $|\Delta$[Fe/H]$| > 1\sigma$, namely NGC 2808, NGC 3201 (-1.42 dex instead of -1.59 dex), NGC 6528 ($+0.04$ dex instead of -0.11 dex), NGC 6624 (again with Δ[Fe/H] $> 2\sigma$), and NGC 6809 (-1.81 dex instead of -1.94 dex). The equations from the R97 dataset presented more discrepancies in the derived metallicities for the C09 calibrators with respect to the S12 data, maybe due to the method used to determine the EWs, or to larger uncertainties in the measured EWs.

3.3. Metallicity Distributions

We used the cubic calibration relations for the S12 dataset and the quadratic ones for the R97 dataset to calculate the metallicity for each star and obtain the metallicity distribution in each GC. The results for the clusters discussed in this Section are shown in Figures 15-29, while similar histograms for all the clusters in our sample are shown in Figures 30-42, only available in electronic form. The convolved frequency is drawn with a solid line, while the classical frequency is plotted with a dotted histogram. We chose a bin width of 0.08 dex. The convolved frequency was obtained shifting the position of the bin by a step of 0.02 dex, a quarter of the bin width, instead of using bins placed side by side. The analysis of the convolved frequency permits to remove the bias introduced by the choice of the minimum value. We show the C09 distribution for the GCs included in both spectroscopic datasets, and both the C09 and H10 distributions for the GCs with only one spectroscopic dataset.

NGC 6656 (M 22) presents a clear multimodal distribution (see Figure 13), similar to the one shown in Da Costa et al. (2009), based on the same spectroscopic data. In Figure 14 we show the distributions of the metallicities obtained from the op-

tical rEW, and sampled in the same way as our distributions, for both the values calculated in Da Costa et al. (2009, upper plot) and S12 (lower plot). Both studies analyzed 51 stars, but their data reduction differed. The metallicity bimodality stands out more clearly with our rEW than it did with the optical data from Da Costa et al. (2009) and S12. The metallicity distributions based on optical magnitudes have a FWHM of ≈ 0.4 dex, while it reduces to 0.3 dex when based on nIR photometry. In the latter case, the peaks are also 30-50% higher. This result can be explained by the smaller effect of differential reddening using the K_s data. The calibration is not a source of these differences, because the ([Fe/H];$\langle W' \rangle$) relation for optical and nIR data are very similar and approximately linear in the metallicity range under study. The main peak (located at [Fe/H] $\simeq -1.90$ dex in all the distributions) and the overall distribution is quite similar in both plots based on optical photometry, although the secondary peak is more evident in the Da Costa data (with a mean [Fe/H] value of ~ -1.60) with respect to the S12 data, where is also located at ~ -1.70 dex. Hence, the differences in data reduction have not influenced the results noticeably. In our distribution, the two peaks are located at -1.77 and -1.90 dex, presenting a systematic shift of ≈ 0.08 dex with respect to the results found by Marino et al. (2009), that determined a mean [Fe/H] values of -1.68 and -1.82 dex for stars rich and poor in s-process element, respectively.

NGC 6656 is not the only GC in our sample that shows a structured metallicity distribution suggesting a complex mix of stellar populations with different metallicity. The most peculiar distributions are those of NGC 6528 and NGC 6553, which are nearly flat and cover a ~ 1 dex range in metallicity. Membership cannot be considered certain, since it is based only on position and radial velocity. They are also the two most metal-rich clusters, and the literature presents controversial values for their metallicity.

4. Discussion and Conclusions

We determined $K_s(HB)$ values for 30 Galactic Globular clusters (GCs). We then calculated the calibration equations between the metallicity and the reduced equivalent widths (rEW) of the Calcium Triplet (CaT) using nIR photometry. We considered the GCs in the catalogs of equivalent widths presented in S12 and R97. We presented the calibration equations on three metallicity scales: the one presented in C09, the C09 with recent high-resolution spectroscopic metallicities (C09c, see Section 2.3), and the values listed in H10. For the S12 dataset, the cubic relations (Eq. 4, 6 and 8) have the smallest urms, while for the R97 dataset the quadratic relations (Eq. 10, 12 and 14) yield the best fits. The analysis of these solutions and of the metallicities obtained through them provide the following important points:

– The comparison between the calibration equations on the three metallicity scales demonstrates that, within ~ 0.05 dex, the three scales are equivalent. This similarity is not surprising since the other two scales are based on C09, even if they differ in individual values and in the determination. This result assures the overall validity of the obtained equations, because the differences in the metallicities of some GCs slightly affect the fit. The validity of the solutions for the S12 dataset is assured by the small scatter shown by the C09 calibrator GCs, that can be assumed to have a well-determined metallicity (7 out 8 of the calibrators included in the S12 dataset present $|\Delta$[Fe/H]$| \leq 0.05$ dex).

– The calibration is independent of the passband used to calculate the rEW, as demonstrated by the comparison between the calibrations obtained from visible ($\sim 0.5~\mu m$) and nIR ($\sim 2~\mu m$) photometry. This result permits one to apply our relations even to $\langle W' \rangle$ calculated with magnitudes from other passbands.

– The comparison between the metallicity distributions for NGC 6656 (M 22) presented in Da Costa et al. (2009) and the one obtained from our calibrations (see Figures 13 and 14) demonstrates that nIR CaT rEW are less affected by internal scatter (most likely produced by differential reddening in this cluster). The separation between the two main peaks in our distribution is in agreement with the metallicity difference between stars rich and poor in s-process element found by Marino et al. (2009), while the absolute positions are shift of ~ 0.08 dex. The well-defined peaks demonstrates that the nIR CaT rEW is very promising as a powerful tool to study metallicity distributions of GCs, especially clusters belonging to the Galactic bulge, where differential reddening is much stronger.

– The analysis of the metallicity distribution of the our sample (Figures 15-29) suggests peculiarities in some of the GCs. NGC 6528 and NGC 6553 (the two most metal-rich ones) show a almost flat distribution that cover approximately 0.5-1 dex. For NGC 6553, a similar spread of 0.5 dex was already pointed out by Alves-Brito et al. (2006) for HR spectroscopic values present in the literature.

– NGC 3201 presents a spread in the metallicity distribution that suggests the presence of a complex metallicity population, as already proposed by Simmerer et al. (2013), where the metallicity of 24 RGB stars were analyzed. This was also supported by Muñoz et al. (2013). Our distributions present a similar spread in [Fe/H] of 0.3 dex, but also a hint of a double peak. 7 of the 24 stars are in common with the 17 selected from R97 catalog, while only one is present in the S12 sample. The stars in common with R97 present a metallicity difference less than ~ 0.1 dex with a mean value of +0.04 dex, and the same value for the difference with the C09 metallicity; 5 stars present an absolute metallicity difference less than 0.05 dex with a mean difference of +0.02 dex, where Simmerer et al. (2013) declared a total uncertainty in [Fe/H] less than 0.15 dex. This result confirms the accuracy of the [Fe/H] values obtained through the CaT method with respect to those obtained with HR spectroscopy.

– We detected the presence of possible complex distributions also for other GCs, namely NGC 2808, NGC 6121 (M 4), NGC 6356, NGC 6440, NGC 6522, NGC 6541, NGC 6569, NGC 6624, NGC 6626 (M 28), NGC 6637 (M 69), NGC 6638, and Pal 7 (IC 1276). NGC 6440 and NGC 6569 are also suggested to have a double horizontal branch in Mauro et al. (2012), while NGC 6626 is a metal-poor cluster that presents parameters very similar to NGC 6656, such as metallicity, absolute magnitude and CMD shape. For these three GCs, HR spectra were obtained and are under study.

A comparison with previous results of metallicities obtained from CaT method with NIR photometry did not lead to relevant conclusions. Both Warren & Cole (2009) and Lane et al. (2010) calibrated on different scales (CG97 and Harris 1996, respectively) and, except for NGC 6656, all the other GCs in common are also calibrators of C09, whose metallicities are in good agreement with our results.

References

Alves-Brito, A., Barbuy, B., Zoccali, M., et al. 2006, A&A, 460, 269
Appenzeller, I., Fricke, K., Fürtig, W., et al. 1998, The Messenger, 94, 1
Armandroff, T. E. & Da Costa, G. S. 1991, AJ, 101, 1329
Barbuy, B., Zoccali, M., Ortolani, S., et al. 2007, AJ, 134, 1613
Battaglia, G., Irwin, M., Tolstoy, E., et al. 2008, MNRAS, 383, 183
Battaglia, G., Tolstoy, E., Helmi, A., et al. 2011, MNRAS, 411, 1013
Bressan, A., Marigo, P., Girardi, L., et al. 2012, MNRAS, 427, 127
Buzzoni, A., Pecci, F. F., Buonanno, R., & Corsi, C. E. 1983, A&A, 128, 94
Carrera, R., Pancino, E., Gallart, C., & del Pino, A. 2013, MNRAS
Carretta, E., Bragaglia, A., Gratton, R. G., et al. 2009, A&A, 505, 117
Carretta, E., Cohen, J. G., Gratton, R. G., & Behr, B. B. 2001, AJ, 122, 1469
Carretta, E. & Gratton, R. G. 1997, A&AS, 121, 95
Cassisi, S., Salaris, M., & Irwin, A. W. 2003, ApJ, 588, 862
Catelan, M., Minniti, D., Lucas, P. W., et al. 2011, in RR Lyrae Stars, Metal-Poor Stars, and the Galaxy, ed. A. McWilliam, Vol. 5, 145
Cenarro, A. J., Cardiel, N., & Gorgas, J. 2008, in Astronomical Society of the Pacific Conference Series, Vol. 390, Pathways Through an Eclectic Universe, ed. J. H. Knapen, T. J. Mahoney, & A. Vazdekis, 292
Chené, A.-N., Borissova, J., Clarke, J. R. A., et al. 2012, A&A, 545, A54
Cole, A. A., Smecker-Hane, T. A., & Gallagher, III, J. S. 2000, AJ, 120, 1808
Cole, A. A., Smecker-Hane, T. A., Tolstoy, E., Bosler, T. L., & Gallagher, J. S. 2004, MNRAS, 347, 367
Da Costa, G. S. & Armandroff, T. E. 1995, AJ, 109, 2533
Da Costa, G. S., Held, E. V., Saviane, I., & Gullieuszik, M. 2009, ApJ, 705, 1481
Emerson, J. & Sutherland, W. 2010, The Messenger, 139, 2
Ferraro, F. R., Dalessandro, E., Mucciarelli, A., et al. 2009, Nature, 462, 483
Ferraro, F. R., Valenti, E., & Origlia, L. 2006, ApJ, 649, 243
Foster, C., Forbes, D. A., Proctor, R. N., et al. 2010, AJ, 139, 1566
Girardi, L. & Salaris, M. 2001, MNRAS, 323, 109
Gullieuszik, M., Held, E. V., Saviane, I., & Rizzi, L. 2009, A&A, 500, 735
Harris, W. E. 1996, AJ, 112, 1487
Harris, W. E. 2010, ArXiv e-prints: 1012.3224
Idiart, T. P., Thevenin, F., & de Freitas Pacheco, J. A. 1997, AJ, 113, 1066
Irwin, M. J., Lewis, J., Hodgkin, S., et al. 2004, in Society of Photo-Optical Instrumentation Engineers (SPIE) Conference Series, Vol. 5493, Society of Photo-Optical Instrumentation Engineers (SPIE) Conference Series, ed. P. J. Quinn & A. Bridger, 411–422
Izzo, C., de Bilbao, L., Larsen, J., et al. 2010, in Society of Photo-Optical Instrumentation Engineers (SPIE) Conference Series, Vol. 7737, Society of Photo-Optical Instrumentation Engineers (SPIE) Conference Series
Jones, J. E., Alloin, D. M., & Jones, B. J. T. 1984, ApJ, 283, 457
Lane, R. R., Kiss, L. L., Lewis, G. F., et al. 2010, MNRAS, 401, 2521
Marino, A. F., Milone, A. P., Piotto, G., et al. 2009, A&A, 505, 1099
Mauro, F., Moni Bidin, C., Chené, A.-N., et al. 2013, Rev. Mexicana Astron. Astrofis., 49, 189
Mauro, F., Moni Bidin, C., Cohen, R., et al. 2012, ApJ, 761, L29
McWilliam, A. & Rich, R. M. 1994, ApJS, 91, 749
Minniti, D. 1995, A&AS, 113, 299
Minniti, D., Lucas, P. W., Emerson, J. P., et al. 2010, New A, 15, 433
Momany, Y., Ortolani, S., Held, E. V., et al. 2003, A&A, 402, 607
Moni Bidin, C., Mauro, F., Geisler, D., et al. 2011, A&A, 535, A33
Muñoz, C., Geisler, D., & Villanova, S. 2013, MNRAS, 433, 2006
Nataf, D. M., Gould, A. P., Pinsonneault, M. H., & Udalski, A. 2013, ApJ, 766, 77
Olszewski, E. W., Schommer, R. A., Suntzeff, N. B., & Harris, H. C. 1991, AJ, 101, 515
Origlia, L., Valenti, E., & Rich, R. M. 2005, MNRAS, 356, 1276
Parisi, M. C., Geisler, D., Grocholski, A. J., Clariá, J. J., & Sarajedini, A. 2010, AJ, 139, 1168
Renzini, A. 1994, A&A, 285, L5
Rutledge, G. A., Hesser, J. E., & Stetson, P. B. 1997, PASP, 109, 907
Saito, R., Hempel, M., Alonso-García, J., et al. 2010, The Messenger, 141, 24
Saito, R. K., Hempel, M., Minniti, D., et al. 2012, A&A, 537, A107

Salaris, M. & Girardi, L. 2002, MNRAS, 337, 332
Saviane, I., da Costa, G. S., Held, E. V., et al. 2012, A&A, 540, A27
Simmerer, J., Ivans, I. I., Filler, D., et al. 2013, ApJ, 764, L7
Skrutskie, M. F., Cutri, R. M., Stiening, R., et al. 2006, AJ, 131, 1163
Sobeck, J. S., Ivans, I. I., Simmerer, J. A., et al. 2006, AJ, 131, 2949
Stetson, P. B. 1987, PASP, 99, 191
Stetson, P. B. 1994, PASP, 106, 250
Valenti, E., Ferraro, F. R., & Origlia, L. 2007, AJ, 133, 1287
Valenti, E., Ferraro, F. R., & Origlia, L. 2010, MNRAS, 402, 1729
Valenti, E., Origlia, L., & Ferraro, F. R. 2005, MNRAS, 361, 272
Valenti, E., Origlia, L., & Rich, R. M. 2011, MNRAS, 414, 2690
Warren, S. R. & Cole, A. A. 2009, MNRAS, 393, 272
Zinn, R. 1985, ApJ, 293, 424
Zinn, R. & West, M. J. 1984, ApJS, 55, 45
Zoccali, M., Barbuy, B., Hill, V., et al. 2004, A&A, 423, 507
Zoccali, M., Cassisi, S., Bono, G., et al. 2000, ApJ, 538, 289
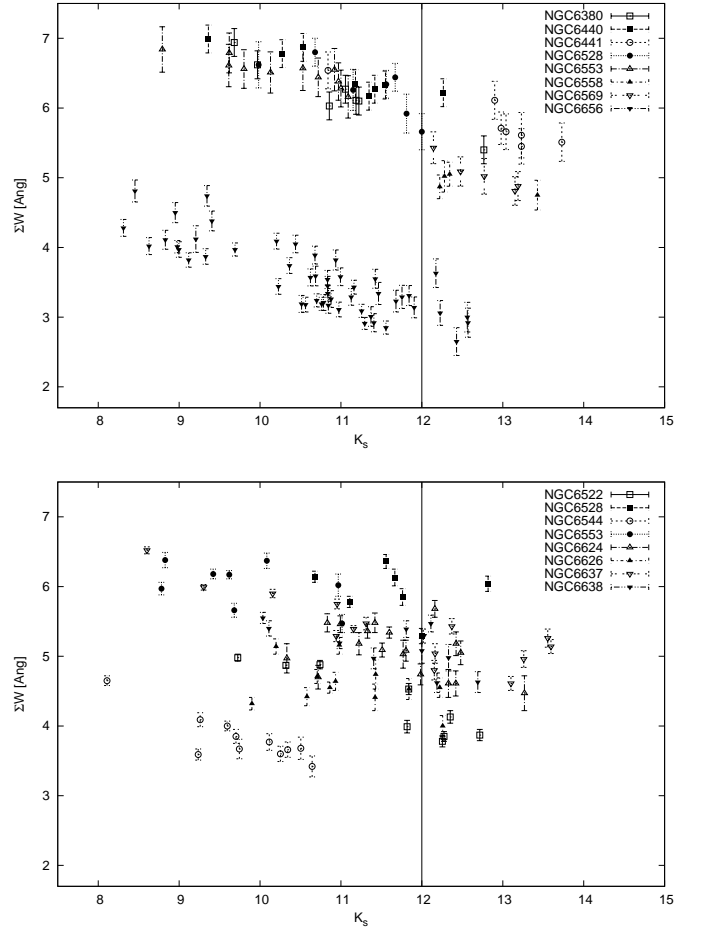
Fig. 1. Plot of Ca II line strength against K_s magnitude for VVV clusters in S12 and R97 catalogs. The vertical bold line at $K_s = 12$ is the saturation limit for the VVV survey. Vertical bars on each point show the measurement uncertainty in the line strengths. The measurement uncertainty in magnitude are too small to be noticed.
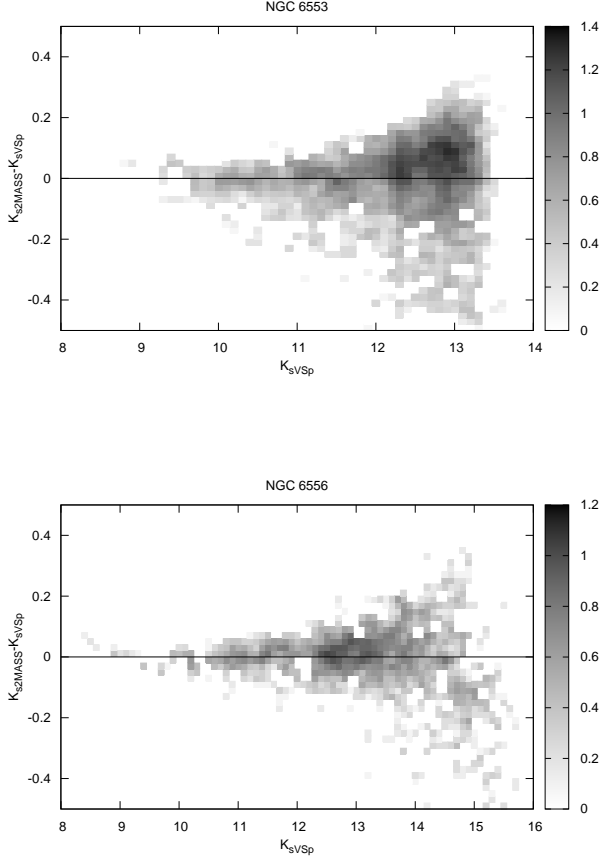
Fig. 2. Density map in logarithmic scale of the photometric differences in K_s between 2MASS and VSp catalogs, as a function of K_s magnitude obtained with VVV-SkZ_pipeline (VSp, upper figure for NGC 6553, lower figure for NGC 6656). No systematic offset exists, especially for the brighter ($K_s < 12$) stars, which are saturated in the VVV data.
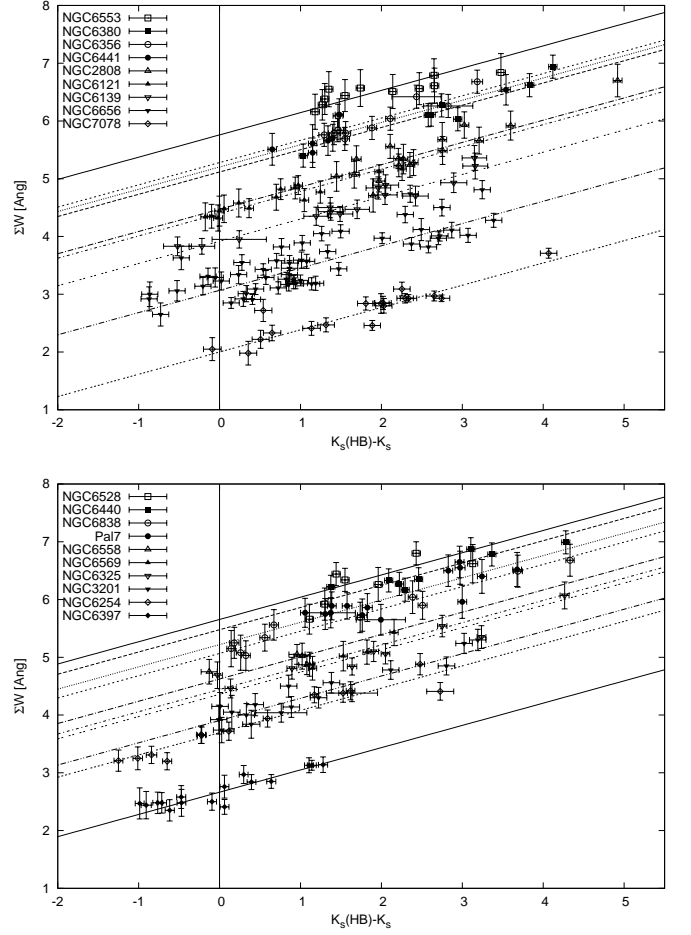
Fig. 3. Plot of summed Ca II line strength $\sum W_{S12}$ against magnitude difference from the red clump $K_s(HB) - K_s$ for the selected clusters. The data for each cluster has been fit with a line of slope -0.385 Å/mag with a urms of 0.013 Å/mag. The data are split to avoid too much overlap.
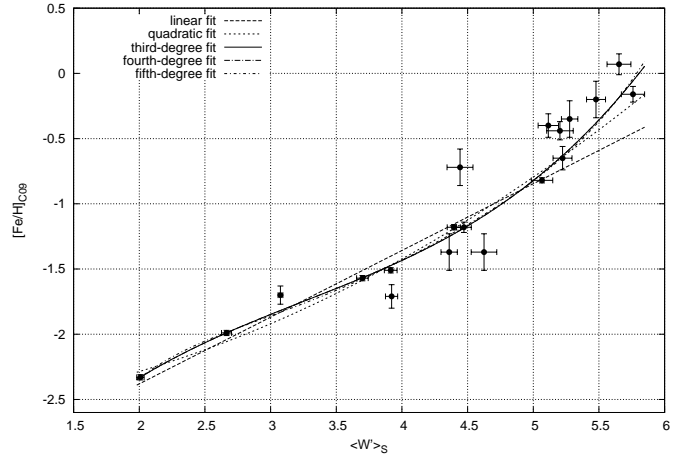
Fig. 4. The calibration relations among [Fe/H] on the C09 scale and the nIR $\langle W' \rangle$ on the G09 scale.
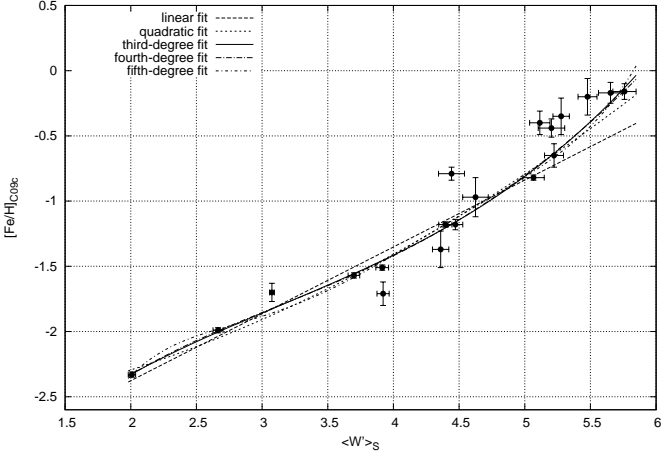
Fig. 5. The calibration relations among [Fe/H] on the "corrected C09" scale and the nIR $\langle W' \rangle$ on the G09 scale.
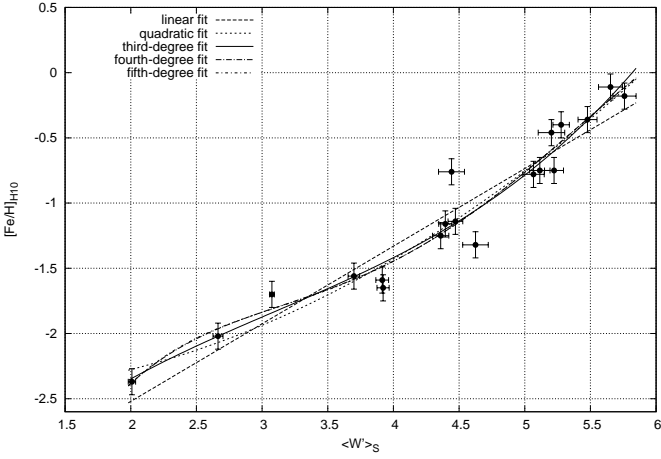
Fig. 6. The calibration relations among [Fe/H] on the H10 scale and the nIR $\langle W' \rangle$ on the G09 scale.
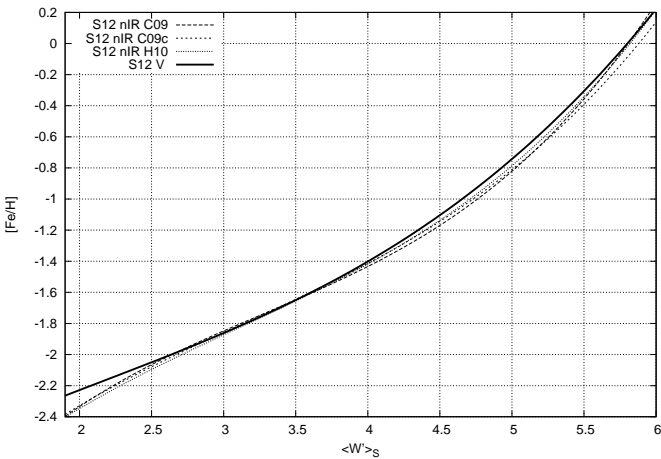
Fig. 7. Comparison among the cubic calibration relations [Fe/H] vs nIR $\langle W' \rangle$ on the G09 scale in the three metallicity scale and the one obtained in S12 for the visible.
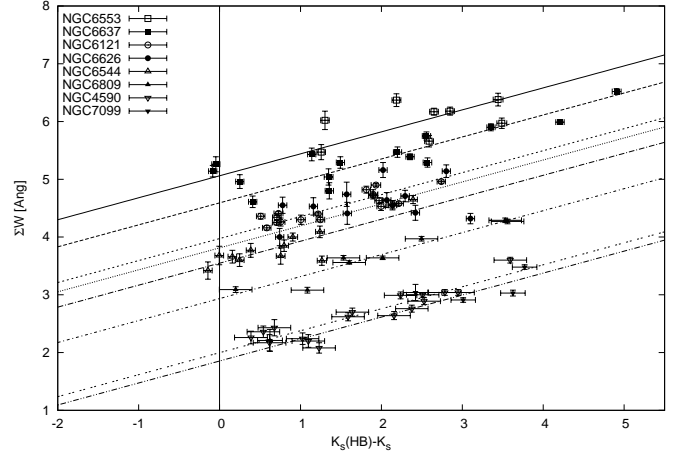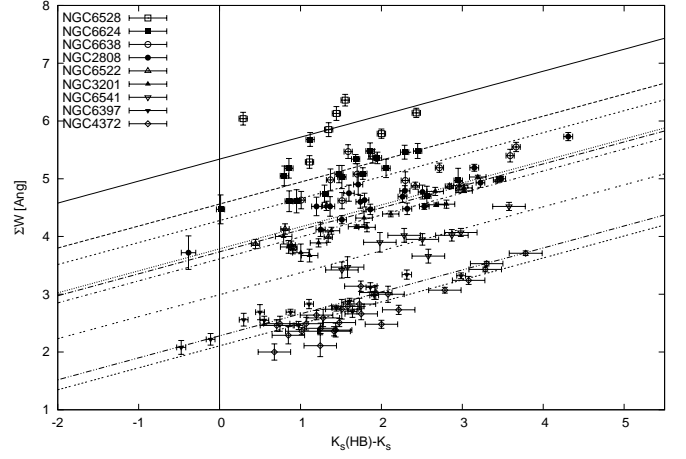
Fig. 8. Plot of summed Ca II line strength ($\sum W_{R97}$) against magnitude difference from the red clump $K_s(RHB) - K_s$ for the selected clusters. The data for each cluster has been fit with a line of slope -0.348 Å/mag. The data are split to avoid too much overlap.
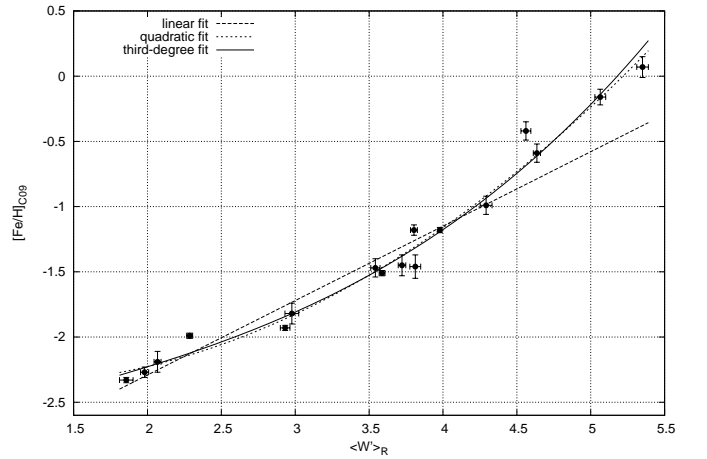
Fig. 9. The calibration relations among [Fe/H] on the C09 scale and the nIR $\langle W' \rangle$ on the R97 scale.

11
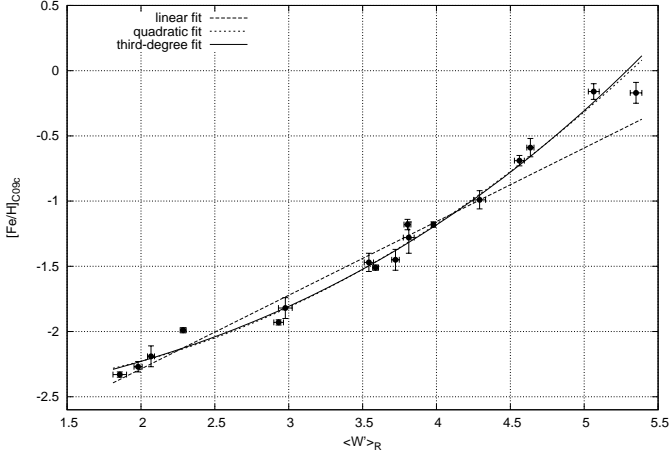
Fig. 10. The calibration relations among [Fe/H] on the "corrected C09" scale and the nIR $\langle W' \rangle$ on the R97 scale.
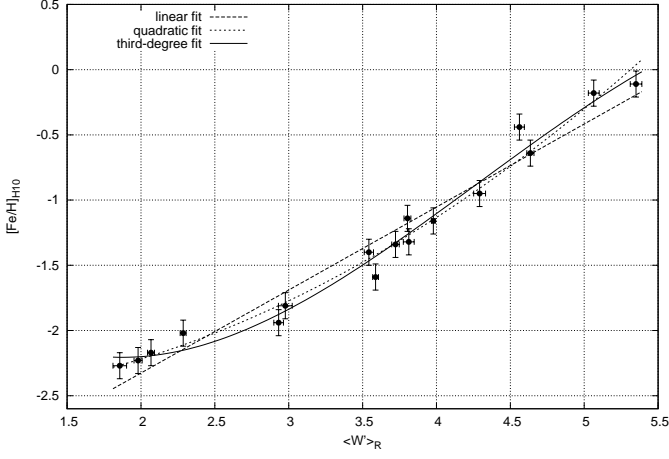
Fig. 11. The calibration relations among [Fe/H] on the H10 scale and the nIR $\langle W' \rangle$ on the R97 scale.
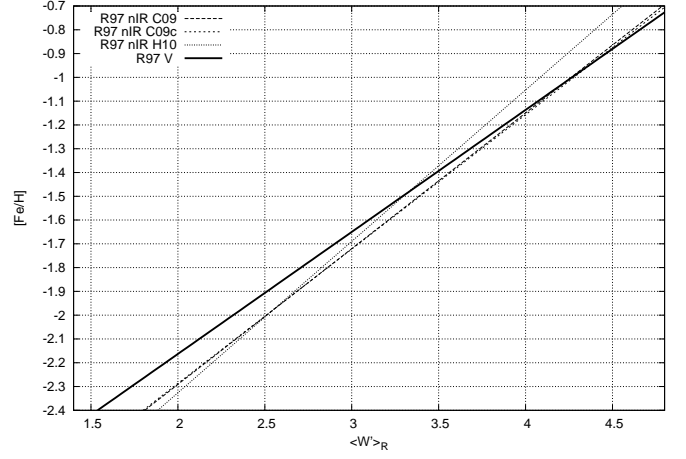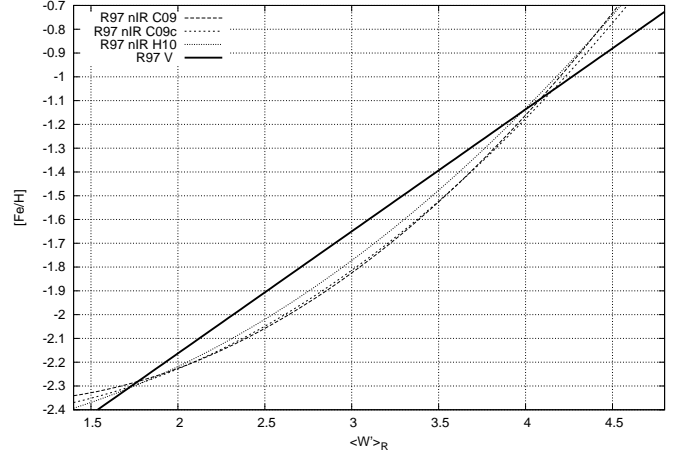
Fig. 12. Comparison among the quadratic (upper figure) and linear (lower figure) calibration relations [Fe/H] vs nIR $\langle W' \rangle$ on the three metallicity scales and the one obtained by C09 for R97 for the visible.
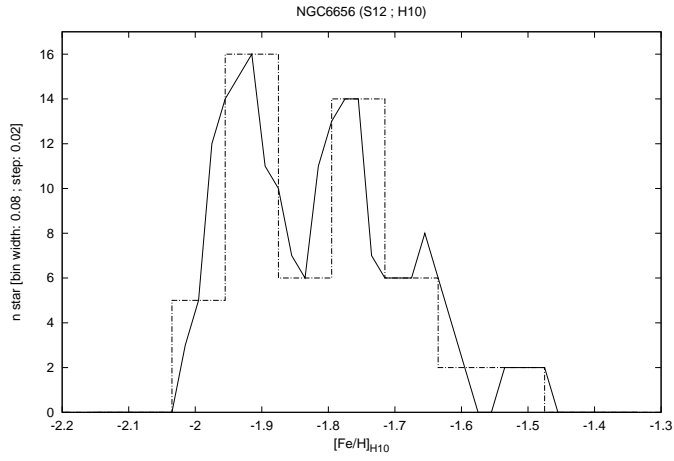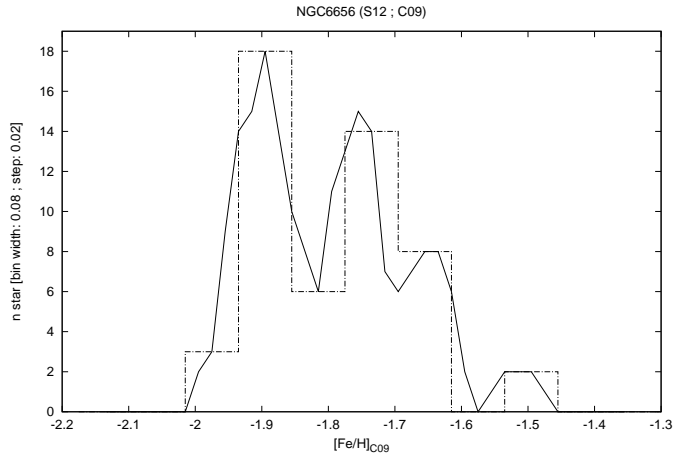
Fig. 13. Distribution in metallicity on the C09 (upper plot) and H10 (lower plot) scales for NGC 6656 stars in the S12 sample.
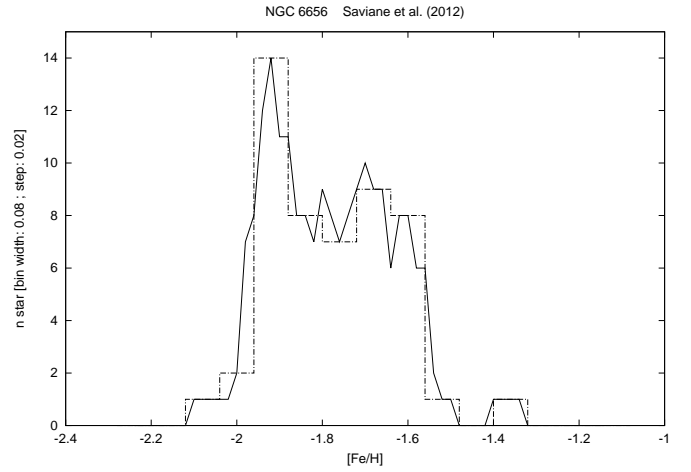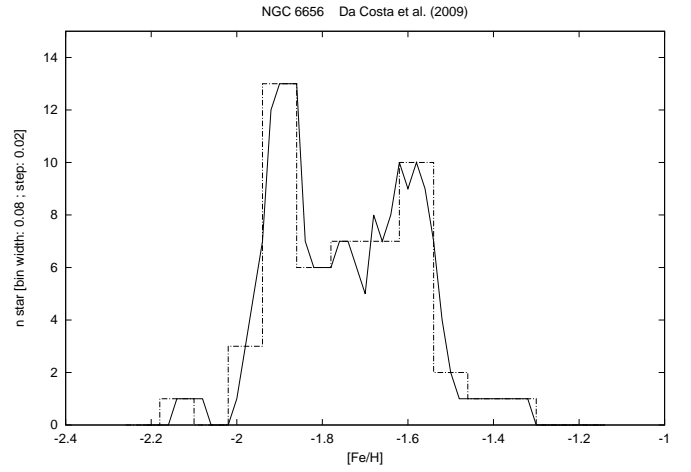
Fig. 14. Distribution in metallicity for NGC 6656 stars from optical rEW.
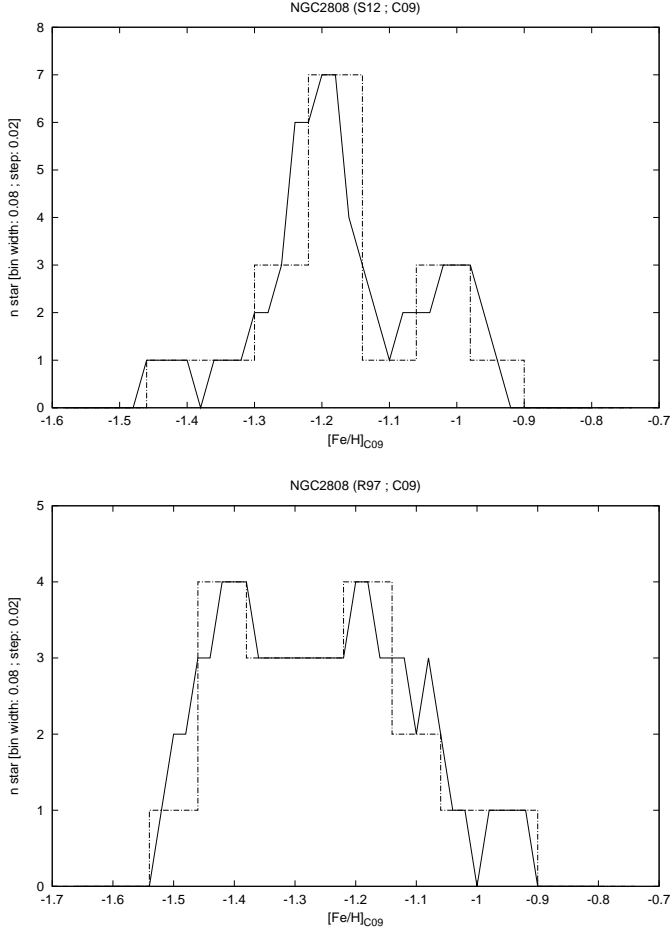
Fig. 15. Distribution in metallicity on the C09 scale for NGC 2808 stars in the S12 (upper plot) and R97 (lower plot) samples.
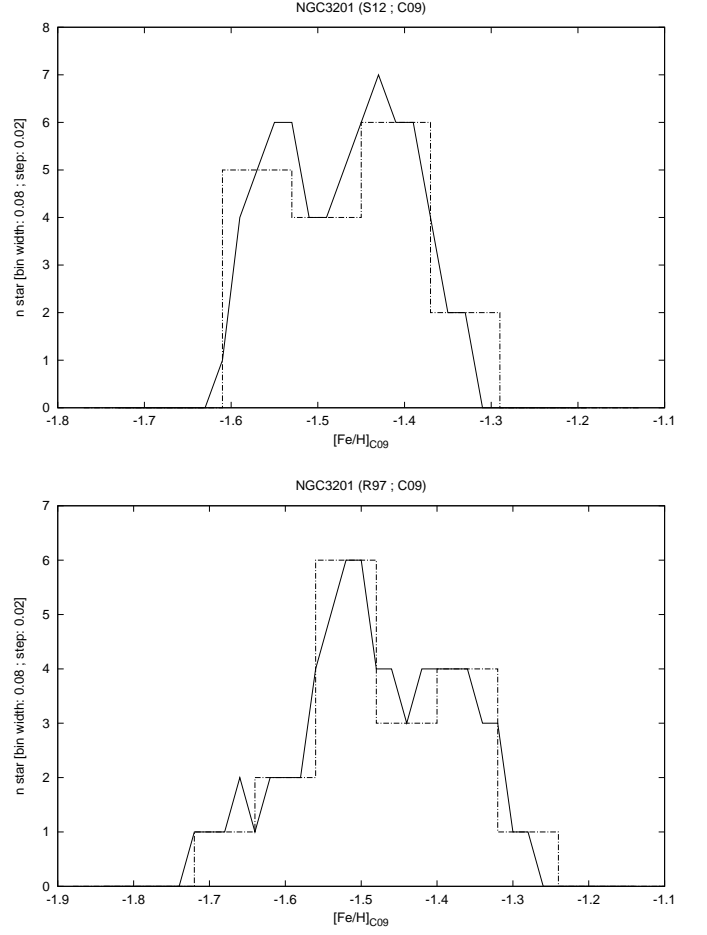
Fig. 16. Distribution in metallicity on the C09 scale for NGC 3201 stars in the S12 (upper plot) and R97 (lower plot) samples.
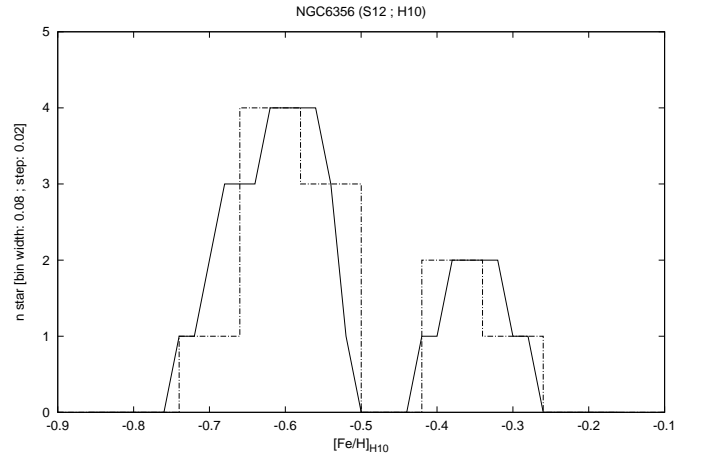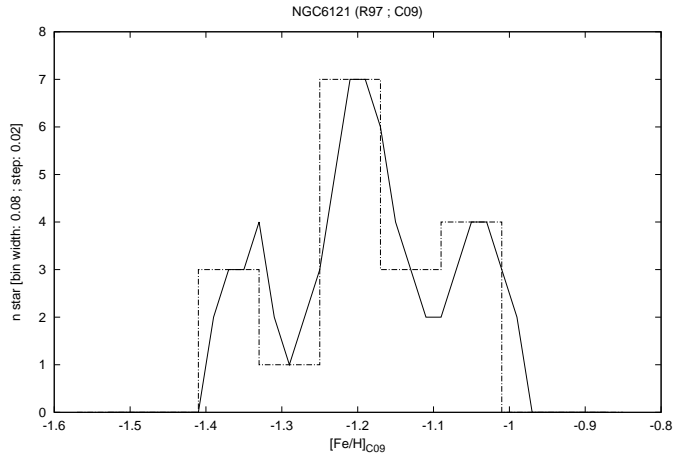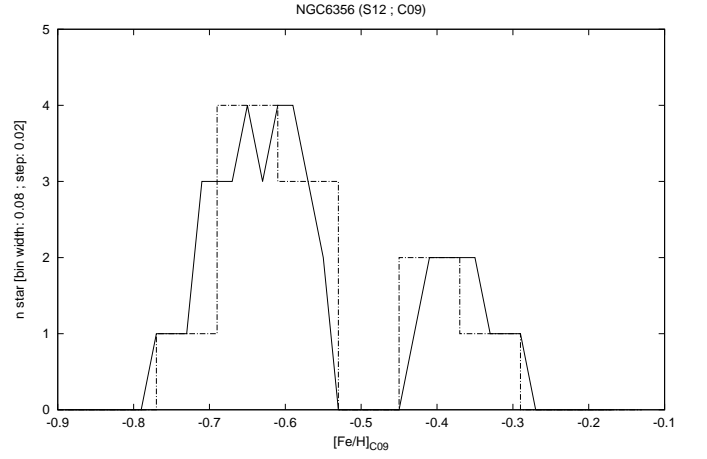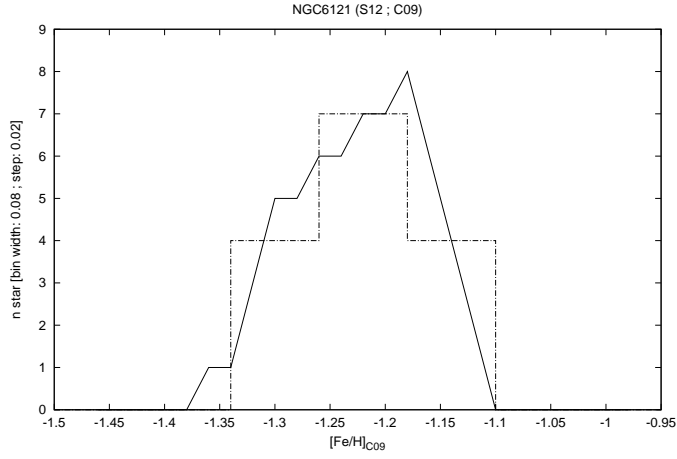
Fig. 17. Distribution in metallicity on the C09 scale for NGC 6121 stars in the S12 (upper plot) and R97 (lower plot) samples.

Fig. 18. Distribution in metallicity on the C09 (upper plot) and H10 (lower plot) scales for NGC 6356 stars in the S12 sample.
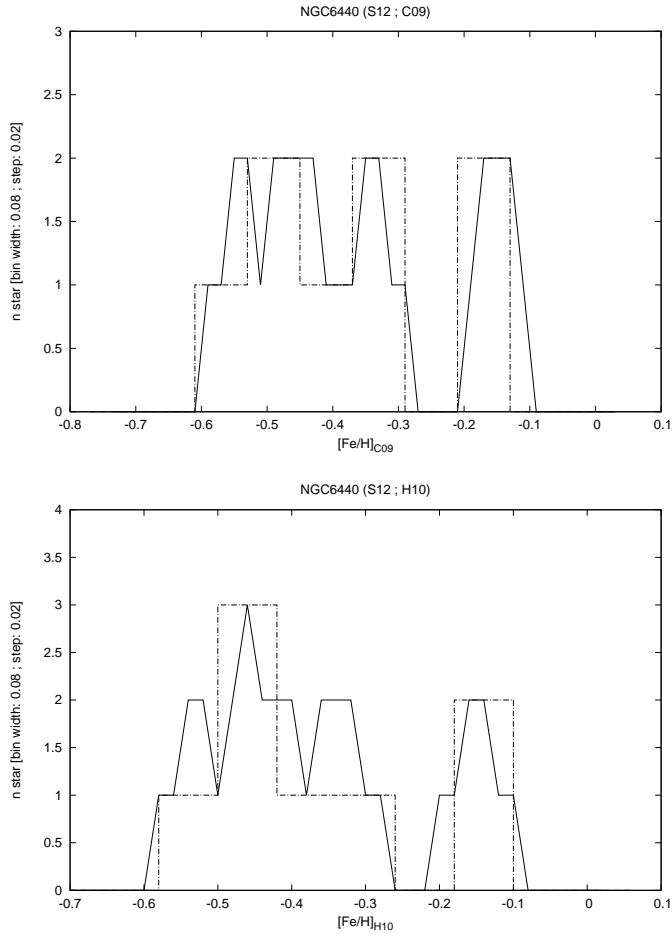
Fig. 19. Distribution in metallicity on the C09 (upper plot) and H10 (lower plot) scales for NGC 6440 stars in the S12 sample.
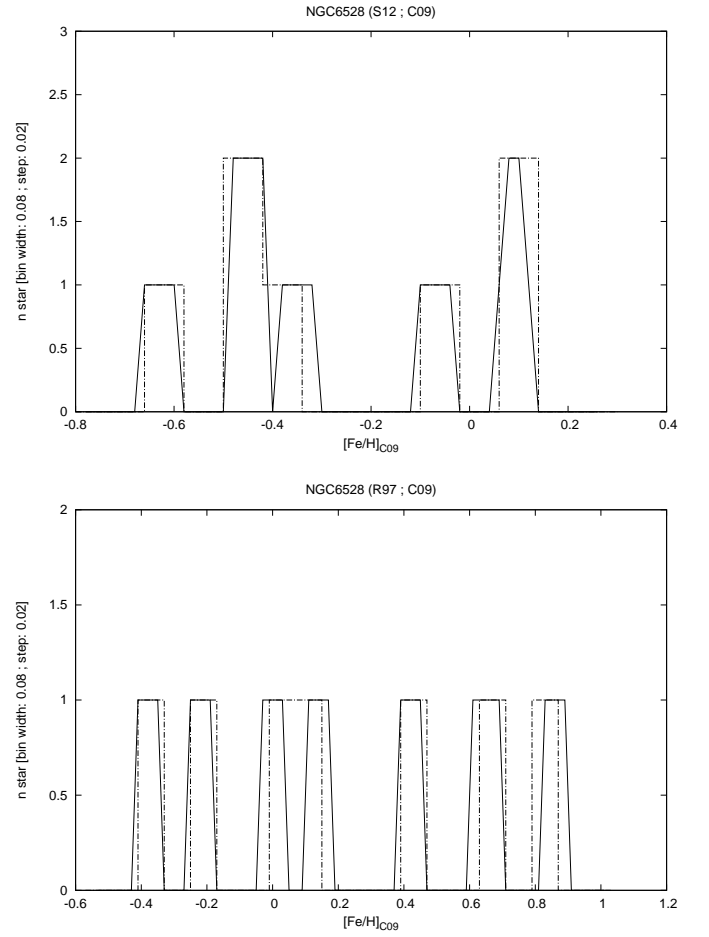
Fig. 20. Distribution in metallicity on the C09 scale for NGC 6528 stars in the S12 (upper plot) and R97 (lower plot) samples.
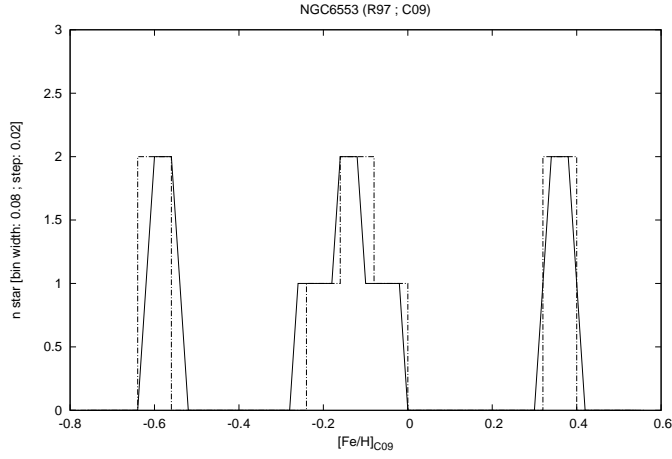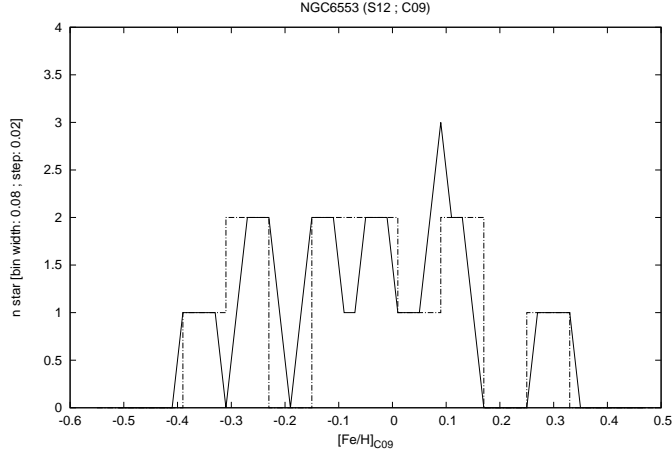
Fig. 21. Distribution in metallicity on the C09 scale for NGC 6553 stars in the S12 (upper plot) and R97 (lower plot) samples.
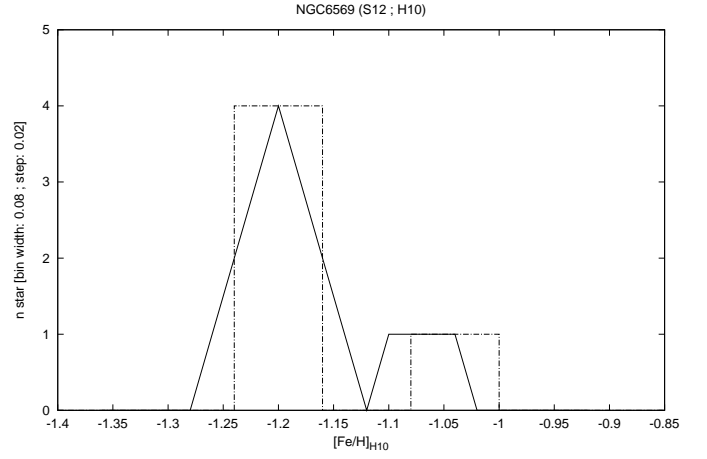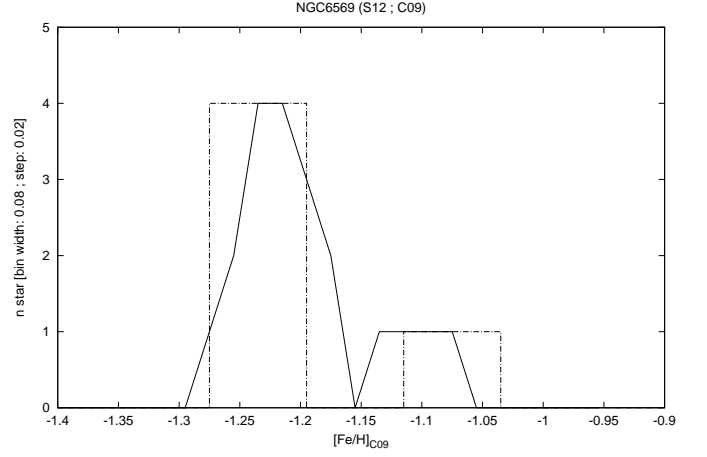
Fig. 22. Distribution in metallicity on the C09 (upper plot) and H10 (lower plot) scales for NGC 6569 stars in the S12 sample.
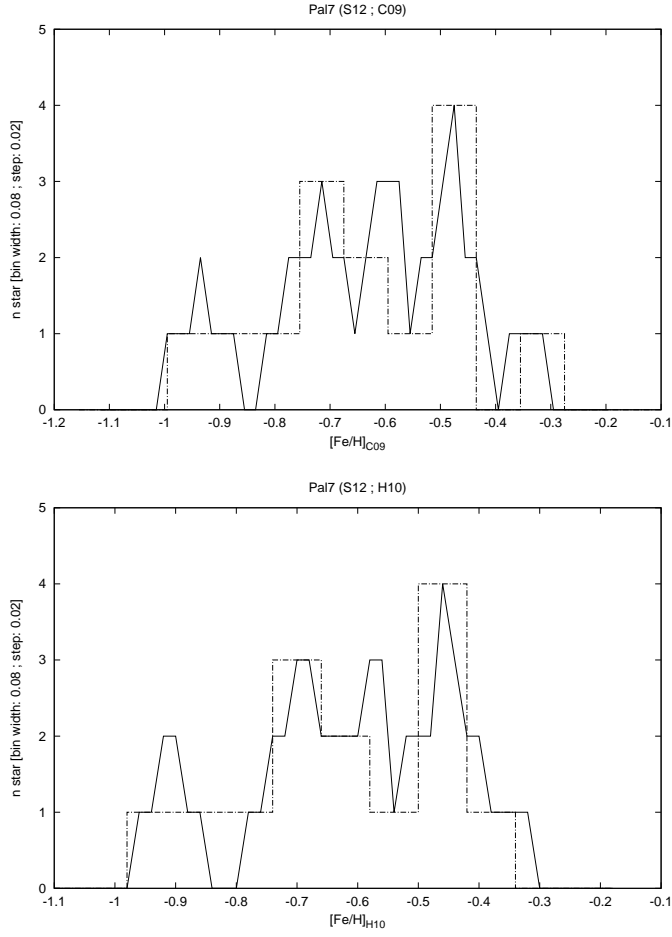
Fig. 23. Distribution in metallicity on the C09 (upper plot) and H10 (lower plot) scales for Pal 7 stars in the S12 sample.
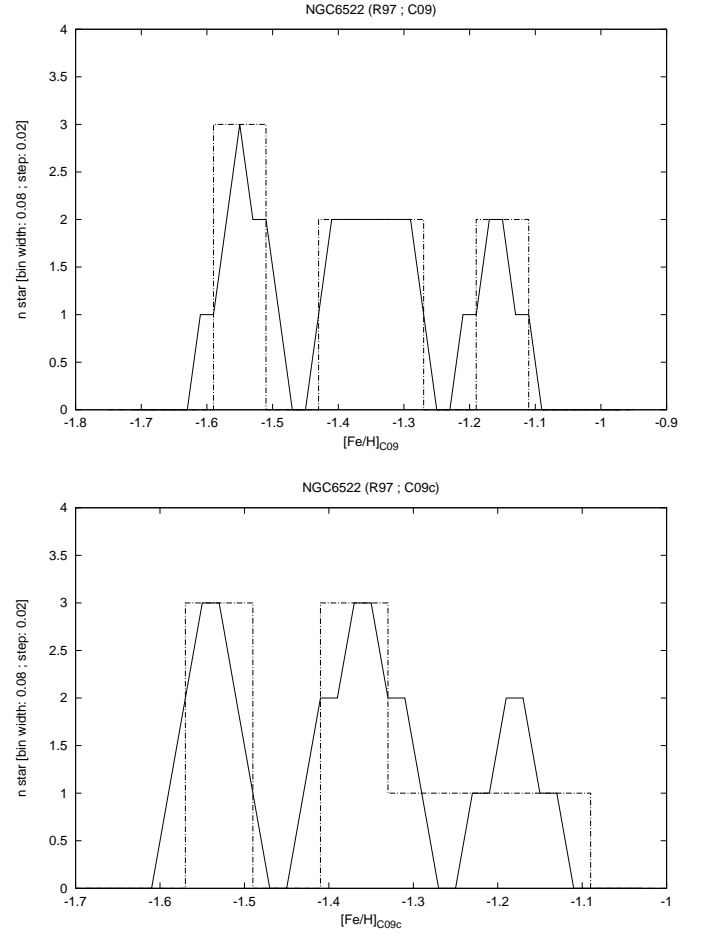
Fig. 24. Distribution in metallicity on the C09 (upper plot) and C09c (lower plot) scales for NGC 6522 stars in the R97 sample.
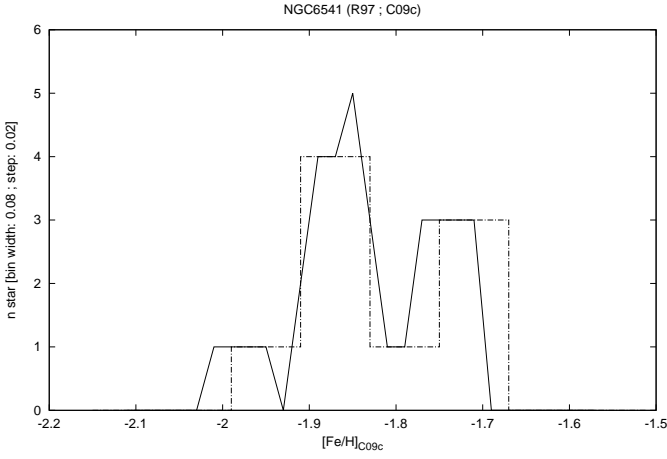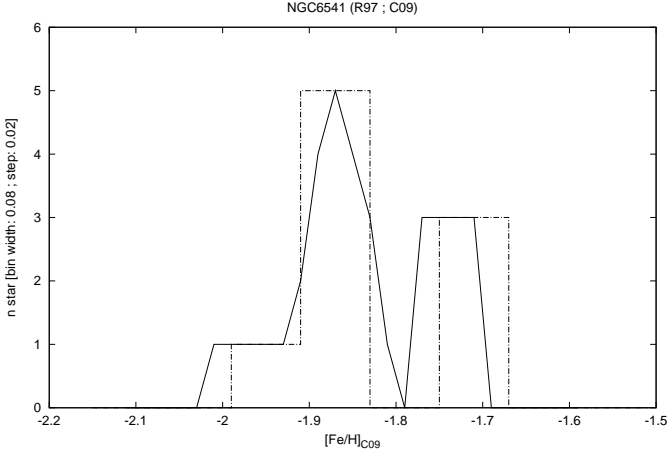
Fig. 25. Distribution in metallicity on the C09 (upper plot) and C09c (lower plot) scales for NGC 6541 stars in the R97 sample.
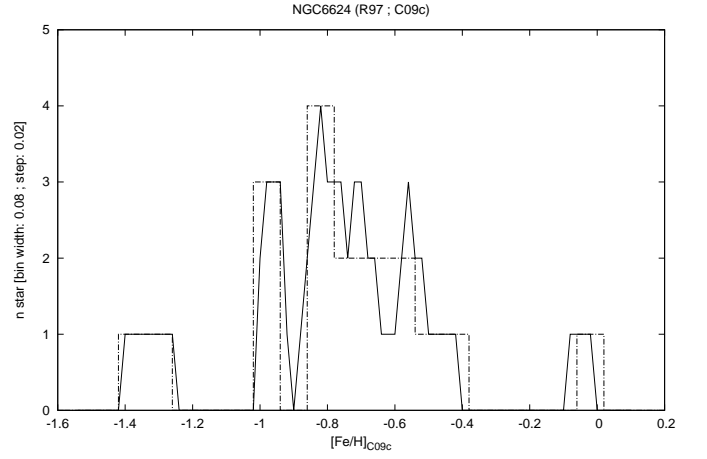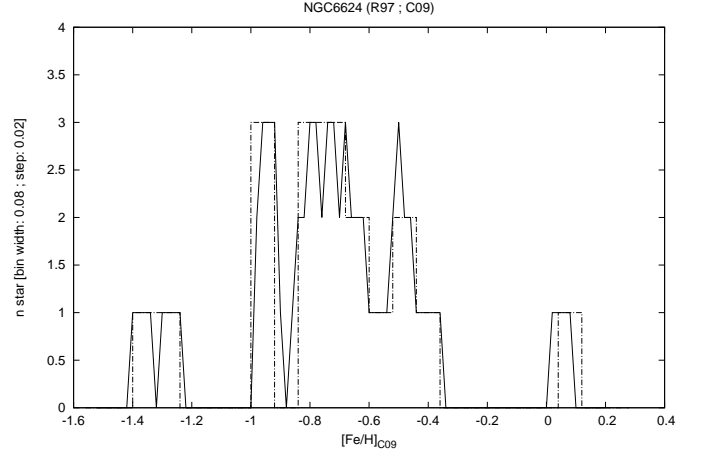
Fig. 26. Distribution in metallicity on the C09 (upper plot) and C09c (lower plot) scales for NGC 6624 stars in the R97 sample.
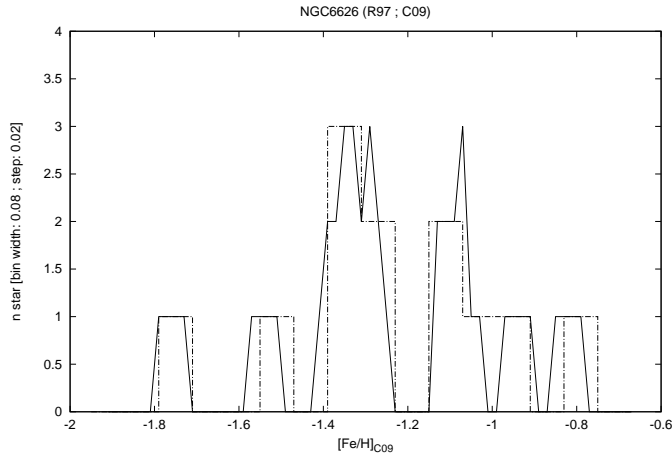
Fig. 27. Distribution in metallicity on the C09 (upper plot) and C09c (lower plot) scales for NGC 6626 stars in the R97 sample.
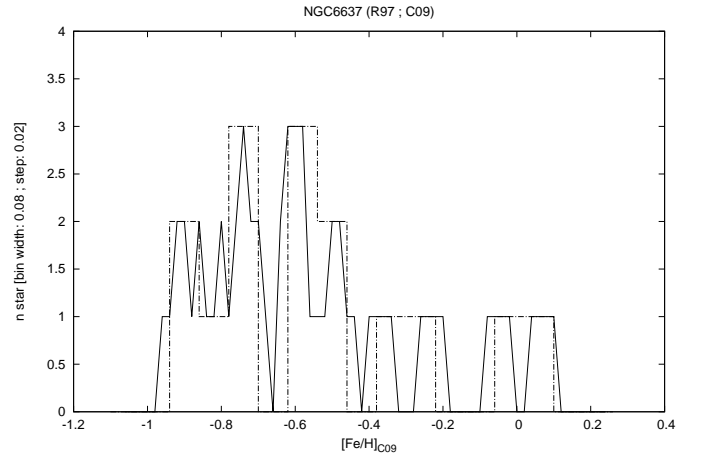
Fig. 28. Distribution in metallicity on the C09 (upper plot) and C09c (lower plot) scales for NGC 6637 stars in the R97 sample.
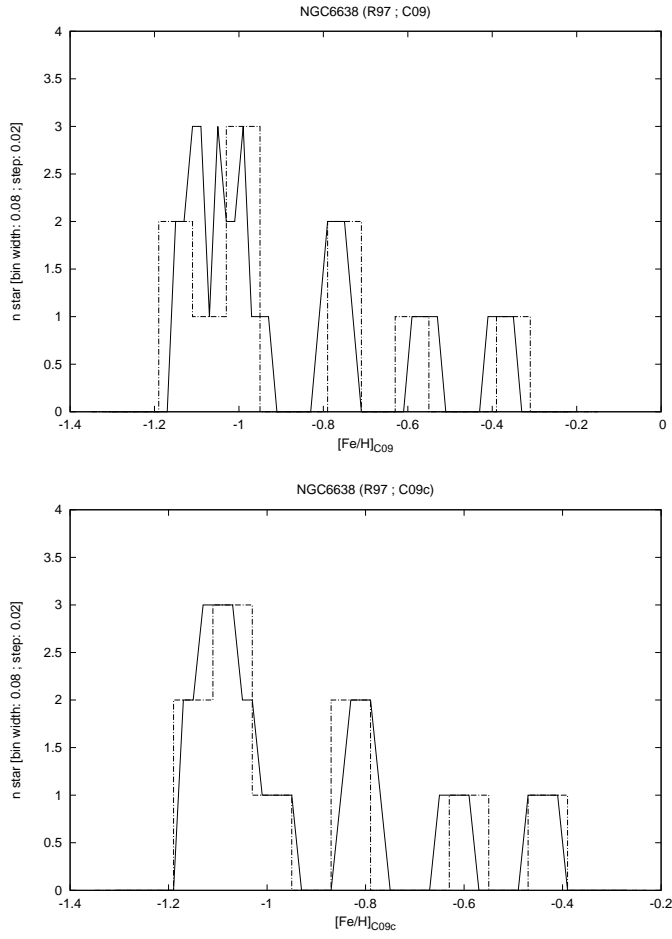
Fig. 29. Distribution in metallicity on the C09 (upper plot) and C09c (lower plot) scales for NGC 6638 stars in the R97 sample.

Table 2. Metallicities for the S12 GCs in C09 scale. Column (1) lists the cluster ID (the GCs marked with * were not used to calculate the calibration). Column (2) is the metallicity according the scale. Column (3) is the calculated rEW. Column (Xa) is the metallicity based on the calibration using a polynomial of degree X. Column (Xb) is the difference between the calculated and the scale metallicity. Column (Xc) is the former difference in r.m.s.

GC (1)	[Fe/H] (2)	$\langle W' \rangle$ (3)	[Fe/H]$_1$ (Ia)	Δ (Ib)	Δ/σ (Ic)	[Fe/H]$_2$ (IIa)	Δ (IIb)	Δ/σ (IIc)	[Fe/H]$_3$ (IIIa)	Δ (IIIb)	Δ/σ (IIIc)	[Fe/H]$_4$ (IVa)	Δ (IVb)	Δ/σ (IVc)	[Fe/H]$_5$ (Va)	Δ (Vb)	Δ/σ (Vc)
NGC2808	-1.18	4.47	-1.12	-0.06	-0.2	-1.14	-0.04	-0.2	-1.19	+0.01	+0.0	-1.19	+0.01	+0.0	-1.18	-0.00	-0.0
NGC3201	-1.51	3.91	-1.40	-0.11	-0.4	-1.47	-0.04	-0.2	-1.47	-0.04	-0.2	-1.47	-0.04	-0.2	-1.47	-0.04	-0.1
NGC6121	-1.18	4.40	-1.16	-0.02	-0.1	-1.19	+0.01	+0.0	-1.23	+0.05	+0.2	-1.23	+0.05	+0.2	-1.22	+0.04	+0.2
NGC6139*	-1.71	3.92	-1.40	-0.31	-1.1	-1.47	-0.24	-1.1	-1.47	-0.24	-1.1	-1.47	-0.24	-1.1	-1.47	-0.24	-1.0
NGC6254	-1.57	3.70	-1.51	-0.06	-0.2	-1.59	+0.02	+0.1	-1.57	-0.00	-0.0	-1.57	-0.00	-0.0	-1.58	+0.01	+0.0
NGC6325	-1.37	4.36	-1.17	-0.20	-0.7	-1.21	-0.16	-0.7	-1.25	-0.12	-0.6	-1.25	-0.12	-0.5	-1.24	-0.13	-0.5
NGC6356	-0.35	5.28	-0.70	+0.35	+1.2	-0.60	+0.25	+1.1	-0.58	+0.23	+1.1	-0.58	+0.23	+1.0	-0.59	+0.24	+1.0
NGC6380*	-0.40	5.11	-0.79	+0.39	+1.3	-0.72	+0.32	+1.4	-0.73	+0.33	+1.5	-0.73	+0.33	+1.5	-0.74	+0.34	+1.4
NGC6397	-1.99	2.66	-2.04	+0.05	+0.2	-2.06	+0.07	+0.3	-1.99	-0.00	-0.0	-1.99	-0.00	-0.0	-1.98	-0.01	-0.0
NGC6440	-0.20	5.48	-0.60	+0.40	+1.4	-0.45	+0.25	+1.1	-0.38	+0.18	+0.8	-0.38	+0.18	+0.8	-0.39	+0.19	+0.8
NGC6441	-0.44	5.20	-0.74	+0.30	+1.0	-0.65	+0.21	+0.9	-0.65	+0.21	+1.0	-0.65	+0.21	+0.9	-0.66	+0.22	+0.9
NGC6528	+0.07	5.65	-0.51	+0.58	+2.0	-0.32	+0.39	+1.7	-0.19	+0.26	+1.2	-0.19	+0.26	+1.1	-0.19	+0.26	+1.1
NGC6553	-0.16	5.76	-0.46	+0.30	+1.0	-0.23	+0.07	+0.3	-0.06	-0.10	-0.5	-0.06	-0.10	-0.5	-0.04	-0.12	-0.5
NGC6558	-1.37	4.62	-1.04	-0.33	-1.1	-1.05	-0.32	-1.4	-1.09	-0.28	-1.3	-1.09	-0.28	-1.2	-1.08	-0.29	-1.2
NGC6569	-0.72	4.44	-1.13	+0.41	+1.4	-1.16	+0.44	+1.9	-1.20	+0.48	+2.3	-1.20	+0.48	+2.2	-1.19	+0.47	+2.0
NGC6656	-1.70	3.07	-1.83	+0.13	+0.5	-1.89	+0.19	+0.8	-1.82	+0.12	+0.6	-1.82	+0.12	+0.5	-1.83	+0.13	+0.5
NGC6838	-0.82	5.07	-0.81	-0.01	-0.0	-0.75	-0.07	-0.3	-0.77	-0.05	-0.2	-0.77	-0.05	-0.2	-0.77	-0.05	-0.2
NGC7078	-2.33	2.01	-2.38	+0.05	+0.2	-2.28	-0.05	-0.2	-2.33	-0.00	-0.0	-2.33	-0.00	-0.0	-2.33	+0.00	+0.0
Pal7 *	-0.65	5.22	-0.73	+0.08	+0.3	-0.64	-0.01	-0.1	-0.63	-0.02	-0.1	-0.63	-0.02	-0.1	-0.64	-0.01	-0.0

Table 3. Metallicities for the S12 GCs in C09c scale. Column (1) lists the cluster ID (the GCs marked with * were not used to calculate the calibration). Column (2) is the metallicity according the scale. Column (3) is the calculated rEW. Column (Xa) is the metallicity based on the calibration using a polynomial of degree X. Column (Xb) is the difference between the calculated and the scale metallicity. Column (Xc) is the former difference in r.m.s.

GC (1)	[Fe/H] (2)	$\langle W' \rangle$ (3)	[Fe/H]$_1$ (Ia)	Δ (Ib)	Δ/σ (Ic)	[Fe/H]$_2$ (IIa)	Δ (IIb)	Δ/σ (IIc)	[Fe/H]$_3$ (IIIa)	Δ (IIIb)	Δ/σ (IIIc)	[Fe/H]$_4$ (IVa)	Δ (IVb)	Δ/σ (IVc)	[Fe/H]$_5$ (Va)	Δ (Vb)	Δ/σ (Vc)
NGC2808	-1.18	4.47	-1.11	-0.07	-0.3	-1.13	-0.05	-0.3	-1.16	-0.02	-0.1	-1.16	-0.02	-0.1	-1.13	-0.05	-0.2
NGC3201	-1.51	3.91	-1.40	-0.11	-0.5	-1.45	-0.06	-0.3	-1.46	-0.05	-0.3	-1.46	-0.05	-0.3	-1.46	-0.05	-0.2
NGC6121	-1.18	4.40	-1.15	-0.03	-0.1	-1.18	-0.00	-0.0	-1.21	+0.03	+0.1	-1.21	+0.03	+0.1	-1.18	-0.00	-0.0
NGC6139*	-1.71	3.92	-1.39	-0.32	-1.4	-1.45	-0.26	-1.4	-1.45	-0.26	-1.5	-1.46	-0.25	-1.4	-1.46	-0.25	-1.2
NGC6254	-1.57	3.70	-1.51	-0.06	-0.3	-1.57	+0.00	+0.0	-1.56	-0.01	-0.1	-1.56	-0.01	-0.0	-1.59	+0.02	+0.1
NGC6325	-1.37	4.36	-1.17	-0.20	-0.9	-1.20	-0.17	-0.9	-1.23	-0.14	-0.8	-1.23	-0.14	-0.8	-1.20	-0.17	-0.9
NGC6356	-0.35	5.28	-0.70	+0.35	+1.5	-0.60	+0.25	+1.4	-0.59	+0.24	+1.4	-0.59	+0.24	+1.3	-0.62	+0.27	+1.4
NGC6380*	-0.40	5.11	-0.78	+0.38	+1.6	-0.72	+0.32	+1.8	-0.72	+0.32	+1.9	-0.72	+0.32	+1.8	-0.74	+0.34	+1.7
NGC6397	-1.99	2.66	-2.04	+0.05	+0.2	-2.05	+0.06	+0.3	-2.00	+0.01	+0.1	-2.00	+0.01	+0.0	-1.98	-0.01	-0.0
NGC6440	-0.20	5.48	-0.59	+0.39	+1.7	-0.46	+0.26	+1.4	-0.41	+0.21	+1.2	-0.41	+0.21	+1.2	-0.45	+0.25	+1.2
NGC6441	-0.44	5.20	-0.73	+0.29	+1.3	-0.65	+0.21	+1.2	-0.65	+0.21	+1.2	-0.65	+0.21	+1.1	-0.68	+0.24	+1.2
NGC6528	-0.17	5.65	-0.50	+0.33	+1.4	-0.33	+0.16	+0.9	-0.24	+0.07	+0.4	-0.25	+0.08	+0.5	-0.25	+0.08	+0.4
NGC6553	-0.16	5.76	-0.45	+0.29	+1.2	-0.25	+0.09	+0.5	-0.13	-0.03	-0.2	-0.15	-0.01	-0.0	-0.11	-0.05	-0.3
NGC6558	-0.97	4.62	-1.03	+0.06	+0.3	-1.04	+0.07	+0.4	-1.07	+0.10	+0.6	-1.06	+0.09	+0.5	-1.04	+0.07	+0.4
NGC6569	-0.79	4.44	-1.12	+0.33	+1.4	-1.15	+0.36	+2.0	-1.18	+0.39	+2.2	-1.18	+0.39	+2.2	-1.15	+0.36	+1.8
NGC6656	-1.70	3.07	-1.83	+0.13	+0.5	-1.87	+0.17	+1.0	-1.83	+0.13	+0.7	-1.82	+0.12	+0.7	-1.86	+0.16	+0.8
NGC6838	-0.82	5.07	-0.80	-0.02	-0.1	-0.75	-0.07	-0.4	-0.76	-0.06	-0.3	-0.75	-0.07	-0.4	-0.77	-0.05	-0.2
NGC7078	-2.33	2.01	-2.37	+0.04	+0.2	-2.29	-0.04	-0.2	-2.32	-0.01	-0.0	-2.33	-0.00	-0.0	-2.33	+0.00	+0.0
Pal7 *	-0.65	5.22	-0.72	+0.07	+0.3	-0.64	-0.01	-0.0	-0.64	-0.01	-0.1	-0.63	-0.02	-0.1	-0.66	+0.01	+0.1

Table 4. Metallicities for the S12 GCs in H10 scale. Column (1) lists the cluster ID (the GCs marked with * were not used to calculate the calibration). Column (2) is the metallicity according the scale. Column (3) is the calculated rEW. Column (Xa) is the metallicity based on the calibration using a polynomial of degree X. Column (Xb) is the difference between the calculated and the scale metallicity. Column (Xc) is the former difference in r.m.s.

GC (1)	[Fe/H] (2)	$\langle W' \rangle$ (3)	[Fe/H]$_1$ (Ia)	Δ (Ib)	Δ/σ (Ic)	[Fe/H]$_2$ (IIa)	Δ (IIb)	Δ/σ (IIc)	[Fe/H]$_3$ (IIIa)	Δ (IIIb)	Δ/σ (IIIc)	[Fe/H]$_4$ (IVa)	Δ (IVb)	Δ/σ (IVc)	[Fe/H]$_5$ (Va)	Δ (Vb)	Δ/σ (Vc)
NGC2808	-1.14	4.47	-1.05	-0.09	-0.5	-1.13	-0.01	-0.1	-1.15	+0.01	+0.1	-1.17	+0.03	+0.1	-1.16	+0.02	+0.1
NGC3201	-1.59	3.91	-1.38	-0.21	-1.1	-1.48	-0.11	-0.7	-1.46	-0.13	-0.8	-1.49	-0.10	-0.6	-1.49	-0.10	-0.6
NGC6121	-1.16	4.40	-1.10	-0.06	-0.3	-1.18	+0.02	+0.1	-1.20	+0.04	+0.2	-1.22	+0.06	+0.3	-1.21	+0.05	+0.3
NGC6139	-1.65	3.92	-1.38	-0.27	-1.4	-1.48	-0.17	-1.1	-1.46	-0.19	-1.2	-1.48	-0.17	-1.0	-1.49	-0.16	-0.9
NGC6254	-1.56	3.70	-1.51	-0.05	-0.3	-1.60	+0.04	+0.2	-1.56	+0.00	+0.0	-1.58	+0.02	+0.1	-1.59	+0.03	+0.2
NGC6325	-1.25	4.36	-1.12	-0.13	-0.7	-1.21	-0.04	-0.3	-1.22	-0.03	-0.2	-1.24	-0.01	-0.1	-1.24	-0.01	-0.1
NGC6356	-0.40	5.28	-0.57	+0.17	+0.9	-0.54	+0.14	+0.8	-0.55	+0.15	+0.9	-0.53	+0.13	+0.8	-0.53	+0.13	+0.7
NGC6380	-0.75	5.11	-0.67	-0.08	-0.4	-0.67	-0.08	-0.5	-0.69	-0.06	-0.3	-0.67	-0.08	-0.5	-0.67	-0.08	-0.5
NGC6397	-2.02	2.66	-2.13	+0.11	+0.6	-2.07	+0.05	+0.3	-2.02	+0.00	+0.0	-1.96	-0.06	-0.3	-1.96	-0.06	-0.3
NGC6440	-0.36	5.48	-0.45	+0.09	+0.5	-0.37	+0.01	+0.1	-0.36	+0.00	+0.0	-0.35	-0.01	-0.0	-0.36	-0.00	-0.0
NGC6441	-0.46	5.20	-0.61	+0.15	+0.8	-0.60	+0.14	+0.8	-0.62	+0.16	+1.0	-0.59	+0.13	+0.8	-0.59	+0.13	+0.8
NGC6528	-0.11	5.65	-0.35	+0.24	+1.3	-0.22	+0.11	+0.7	-0.18	+0.07	+0.5	-0.20	+0.09	+0.6	-0.20	+0.09	+0.5
NGC6553	-0.18	5.76	-0.28	+0.10	+0.5	-0.13	-0.05	-0.3	-0.07	-0.11	-0.7	-0.11	-0.07	-0.4	-0.11	-0.07	-0.4
NGC6558	-1.32	4.62	-0.96	-0.36	-1.9	-1.03	-0.29	-1.8	-1.06	-0.26	-1.6	-1.06	-0.26	-1.6	-1.06	-0.26	-1.5
NGC6569	-0.76	4.44	-1.07	+0.31	+1.6	-1.15	+0.39	+2.4	-1.17	+0.41	+2.5	-1.18	+0.42	+2.5	-1.18	+0.42	+2.4
NGC6656	-1.70	3.07	-1.88	+0.18	+1.0	-1.90	+0.20	+1.2	-1.84	+0.14	+0.9	-1.81	+0.11	+0.7	-1.81	+0.11	+0.6
NGC6838	-0.78	5.07	-0.70	-0.08	-0.4	-0.70	-0.08	-0.5	-0.73	-0.05	-0.3	-0.71	-0.07	-0.4	-0.71	-0.07	-0.4
NGC7078	-2.37	2.01	-2.52	+0.15	+0.8	-2.27	-0.10	-0.6	-2.34	-0.03	-0.2	-2.38	+0.01	+0.0	-2.38	+0.01	+0.0
Pal7	-0.75	5.22	-0.60	-0.15	-0.8	-0.58	-0.17	-1.0	-0.60	-0.15	-0.9	-0.58	-0.17	-1.0	-0.58	-0.17	-1.0

Table 5. Metallicities for the R97 GCs in C09 scale. Column (1) lists the cluster ID (the GCs marked with * were not used to calculate the calibration). Column (2) is the metallicity according the scale. Column (3) is the calculated rEW. Column (Xa) is the metallicity based on the calibration using a polynomial of degree X. Column (Xb) is the difference between the calculated and the scale metallicity. Column (Xc) is the former difference in r.m.s.

GC (1)	[Fe/H] (2)	$\langle W' \rangle$ (3)	$[Fe/H]_1$ (Ia)	Δ (Ib)	Δ/σ (Ic)	$[Fe/H]_2$ (IIa)	Δ (IIb)	Δ/σ (IIc)	$[Fe/H]_3$ (IIIa)	Δ (IIIb)	Δ/σ (IIIc)
NGC2808	-1.18	3.80	-1.26	+0.08	+0.4	-1.31	+0.13	+1.3	-1.32	+0.14	+1.3
NGC3201	-1.51	3.59	-1.39	-0.12	-0.6	-1.47	-0.04	-0.4	-1.47	-0.04	-0.3
NGC4372	-2.19	2.07	-2.25	+0.06	+0.3	-2.21	+0.02	+0.2	-2.20	+0.01	+0.1
NGC4590	-2.27	1.98	-2.30	+0.03	+0.1	-2.23	-0.04	-0.4	-2.23	-0.04	-0.3
NGC6121	-1.18	3.98	-1.16	-0.02	-0.1	-1.18	-0.00	-0.0	-1.19	+0.01	+0.1
NGC6397	-1.99	2.29	-2.13	+0.14	+0.6	-2.14	+0.15	+1.4	-2.12	+0.13	+1.2
NGC6522	-1.45	3.72	-1.31	-0.14	-0.7	-1.37	-0.08	-0.8	-1.38	-0.07	-0.6
NGC6528	+0.07	5.35	-0.38	+0.45	+2.1	+0.15	-0.08	-0.8	+0.22	-0.15	-1.3
NGC6541	-1.82	2.98	-1.73	-0.09	-0.4	-1.84	+0.02	+0.2	-1.82	+0.00	+0.0
NGC6544	-1.47	3.54	-1.41	-0.06	-0.3	-1.50	+0.03	+0.3	-1.50	+0.03	+0.3
NGC6553	-0.16	5.06	-0.54	+0.38	+1.8	-0.17	+0.01	+0.1	-0.14	-0.02	-0.2
NGC6624	-0.42	4.56	-0.83	+0.41	+1.9	-0.67	+0.25	+2.5	-0.69	+0.27	+2.3
NGC6626*	-1.46	3.81	-1.26	-0.20	-0.9	-1.31	-0.15	-1.5	-1.32	-0.14	-1.3
NGC6637	-0.59	4.64	-0.79	+0.20	+0.9	-0.60	+0.01	+0.1	-0.61	+0.02	+0.2
NGC6638	-0.99	4.29	-0.98	-0.01	-0.0	-0.92	-0.07	-0.7	-0.94	-0.05	-0.5
NGC6809	-1.93	2.93	-1.76	-0.17	-0.8	-1.86	-0.07	-0.7	-1.84	-0.09	-0.8
NGC7099	-2.33	1.86	-2.37	+0.04	+0.2	-2.26	-0.07	-0.7	-2.28	-0.05	-0.5

Table 6. Metallicities for the R97 GCs in C09c scale. Column (1) lists the cluster ID (the GCs marked with * were not used to calculate the calibration). Column (2) is the metallicity according the scale. Column (3) is the calculated rEW. Column (Xa) is the metallicity based on the calibration using a polynomial of degree X. Column (Xb) is the difference between the calculated and the scale metallicity. Column (Xc) is the former difference in r.m.s.

GC	[Fe/H]	$\langle W' \rangle$	$[Fe/H]_1$	Δ	Δ/σ	$[Fe/H]_2$	Δ	Δ/σ	$[Fe/H]_3$	Δ	Δ/σ
(1)	(2)	(3)	(Ia)	(Ib)	(Ic)	(IIa)	(IIb)	(IIc)	(IIIa)	(IIIb)	(IIIc)
NGC2808	-1.18	3.80	-1.27	+0.09	+0.5	-1.32	+0.14	+1.5	-1.32	+0.14	+1.4
NGC3201	-1.51	3.59	-1.39	-0.12	-0.7	-1.47	-0.04	-0.5	-1.47	-0.04	-0.4
NGC4372	-2.19	2.07	-2.25	+0.06	+0.4	-2.21	+0.02	+0.2	-2.21	+0.02	+0.2
NGC4590	-2.27	1.98	-2.30	+0.03	+0.2	-2.23	-0.04	-0.4	-2.24	-0.03	-0.3
NGC6121	-1.18	3.98	-1.17	-0.01	-0.1	-1.19	+0.01	+0.1	-1.20	+0.02	+0.2
NGC6397	-1.99	2.29	-2.13	+0.14	+0.8	-2.13	+0.14	+1.5	-2.13	+0.14	+1.3
NGC6522	-1.45	3.72	-1.31	-0.14	-0.8	-1.38	-0.07	-0.8	-1.38	-0.07	-0.7
NGC6528	-0.17	5.35	-0.39	+0.22	+1.4	+0.04	-0.21	-2.2	+0.07	-0.24	-2.3
NGC6541	-1.82	2.98	-1.73	-0.09	-0.5	-1.83	+0.01	+0.1	-1.82	-0.00	-0.0
NGC6544	-1.47	3.54	-1.42	-0.05	-0.3	-1.50	+0.03	+0.3	-1.50	+0.03	+0.3
NGC6553	-0.16	5.06	-0.56	+0.40	+2.4	-0.25	+0.09	+1.0	-0.24	+0.08	+0.8
NGC6624	-0.69	4.56	-0.84	+0.15	+0.9	-0.72	+0.03	+0.3	-0.72	+0.03	+0.3
NGC6626*	-1.28	3.81	-1.26	-0.02	-0.1	-1.31	+0.03	+0.3	-1.32	+0.04	+0.4
NGC6637	-0.59	4.64	-0.80	+0.21	+1.3	-0.66	+0.07	+0.7	-0.66	+0.07	+0.6
NGC6638	-0.99	4.29	-0.99	+0.00	+0.0	-0.95	-0.04	-0.4	-0.95	-0.04	-0.3
NGC6809	-1.93	2.93	-1.76	-0.17	-1.0	-1.85	-0.08	-0.8	-1.84	-0.09	-0.8
NGC7099	-2.33	1.86	-2.37	+0.04	+0.2	-2.27	-0.06	-0.6	-2.28	-0.05	-0.5

Table 7. Metallicities for the R97 GCs in H10 scale. Column (1) lists the cluster ID (the GCs marked with * were not used to calculate the calibration). Column (2) is the metallicity according the scale. Column (3) is the calculated rEW. Column (Xa) is the metallicity based on the calibration using a polynomial of degree X. Column (Xb) is the difference between the calculated and the scale metallicity. Column (Xc) is the former difference in r.m.s.

GC (1)	[Fe/H] (2)	$\langle W' \rangle$ (3)	[Fe/H]$_1$ (Ia)	Δ (Ib)	Δ/σ (Ic)	[Fe/H]$_2$ (IIa)	Δ (IIb)	Δ/σ (IIc)	[Fe/H]$_3$ (IIIa)	Δ (IIIb)	Δ/σ (IIIc)
NGC2808	-1.14	3.80	-1.18	+0.04	+0.2	-1.27	+0.13	+1.2	-1.26	+0.12	+1.2
NGC3201	-1.59	3.59	-1.32	-0.27	-1.8	-1.42	-0.17	-1.5	-1.43	-0.16	-1.5
NGC4372	-2.17	2.07	-2.28	+0.11	+0.7	-2.19	+0.02	+0.2	-2.19	+0.02	+0.2
NGC4590	-2.23	1.98	-2.34	+0.11	+0.7	-2.23	-0.00	-0.0	-2.20	-0.03	-0.3
NGC6121	-1.16	3.98	-1.07	-0.09	-0.6	-1.15	-0.01	-0.1	-1.12	-0.04	-0.4
NGC6397	-2.02	2.29	-2.14	+0.12	+0.8	-2.11	+0.09	+0.8	-2.15	+0.13	+1.3
NGC6522	-1.34	3.72	-1.23	-0.11	-0.7	-1.33	-0.01	-0.1	-1.33	-0.01	-0.1
NGC6528	-0.11	5.35	-0.19	+0.08	+0.5	+0.04	-0.15	-1.3	-0.04	-0.07	-0.7
NGC6541	-1.81	2.98	-1.70	-0.11	-0.7	-1.78	-0.03	-0.2	-1.85	+0.04	+0.4
NGC6544	-1.40	3.54	-1.34	-0.06	-0.4	-1.45	+0.05	+0.5	-1.47	+0.07	+0.6
NGC6553	-0.18	5.06	-0.38	+0.20	+1.3	-0.24	+0.06	+0.6	-0.24	+0.06	+0.6
NGC6624	-0.44	4.56	-0.70	+0.26	+1.7	-0.69	+0.25	+2.3	-0.64	+0.20	+1.9
NGC6626	-1.32	3.81	-1.17	-0.15	-1.0	-1.27	-0.05	-0.5	-1.26	-0.06	-0.6
NGC6637	-0.64	4.64	-0.65	+0.01	+0.1	-0.63	-0.01	-0.1	-0.58	-0.06	-0.6
NGC6638	-0.95	4.29	-0.87	-0.08	-0.5	-0.91	-0.04	-0.4	-0.86	-0.09	-0.9
NGC6809	-1.94	2.93	-1.73	-0.21	-1.3	-1.81	-0.13	-1.2	-1.88	-0.06	-0.6
NGC7099	-2.27	1.86	-2.42	+0.15	+1.0	-2.27	-0.00	-0.0	-2.21	-0.06	-0.6
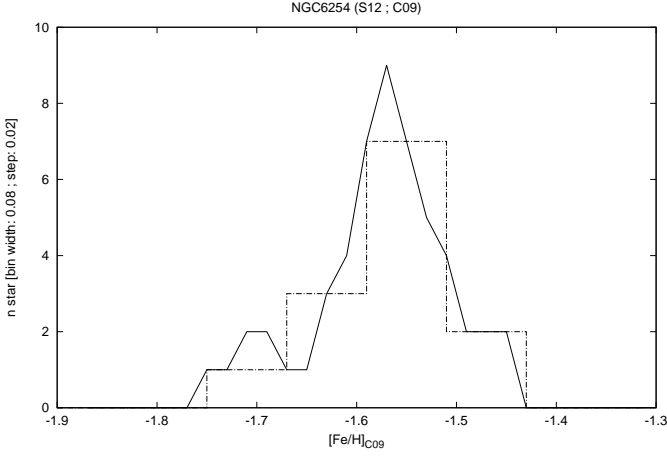
Fig. 30. Distribution in metallicity on the C09 scale for NGC 6254 stars in the S12 sample.
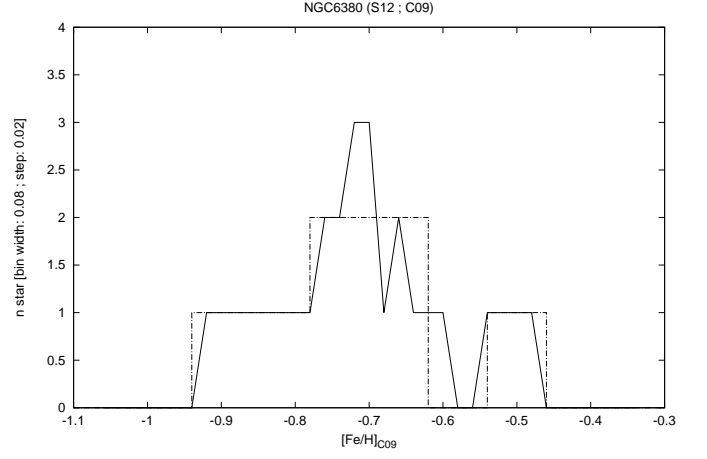
Fig. 32. Distribution in metallicity on the C09 scale for NGC 6380 stars in the S12 sample.
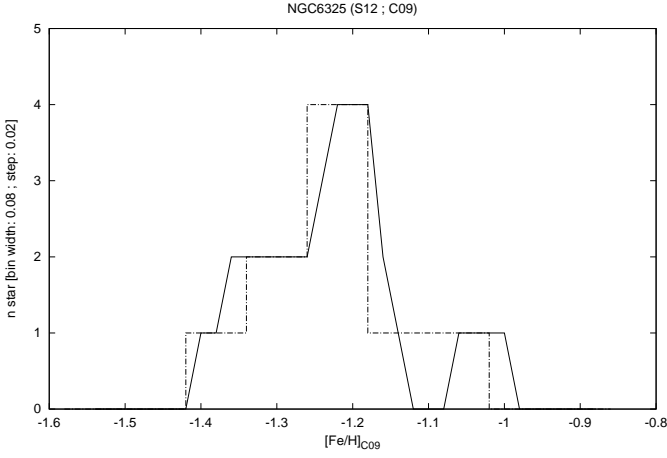
Fig. 31. Distribution in metallicity on the C09 scale for NGC 6325 stars in the S12 sample.
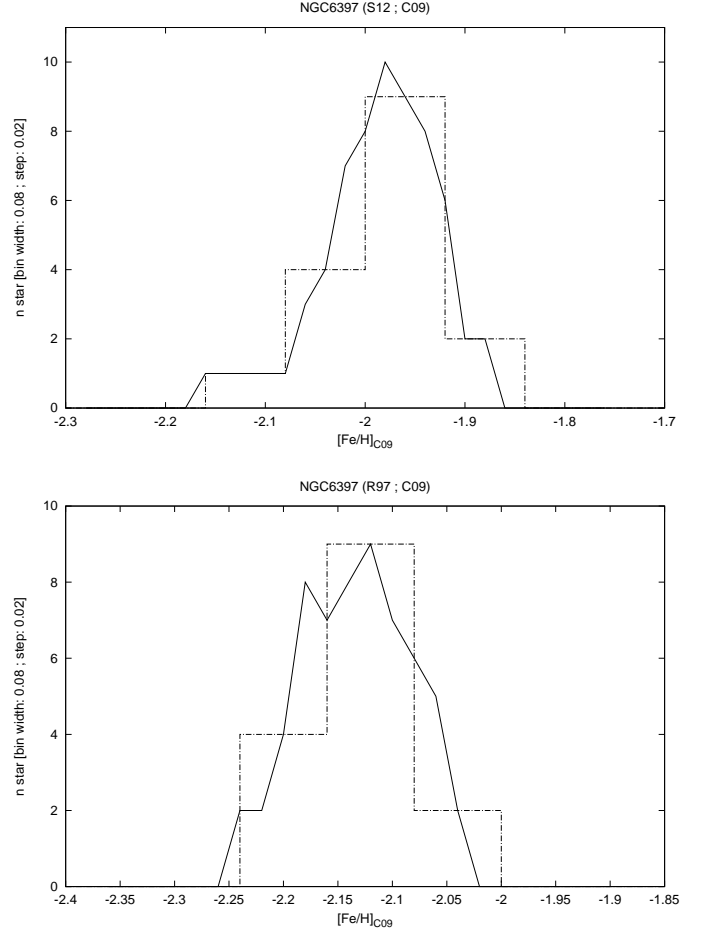
Fig. 33. Distribution in metallicity on the C09 scale for NGC 6397 stars in the S12 (upper plot) and R97 (lower plot) samples.
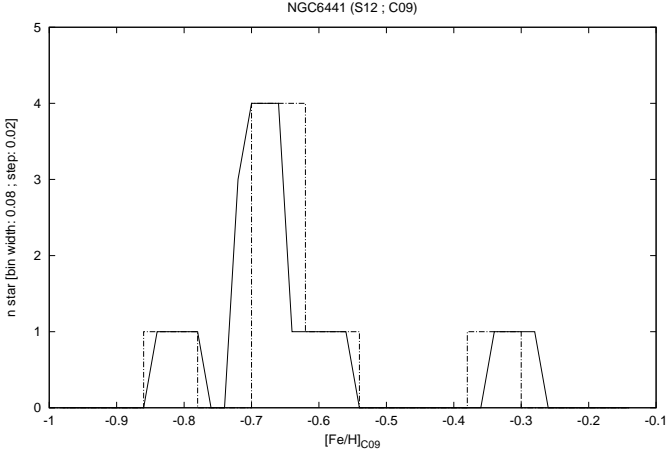
Fig. 34. Distribution in metallicity on the C09 scale for NGC 6441 stars in the S12 sample.
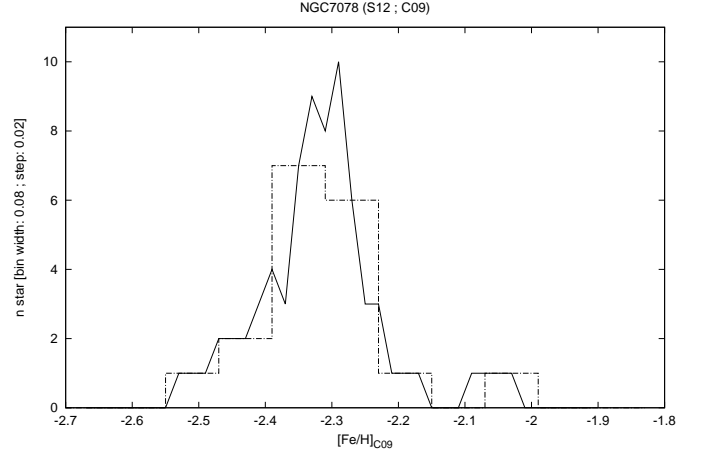
Fig. 37. Distribution in metallicity on the C09 scale for NGC 7078 stars in the S12 sample.
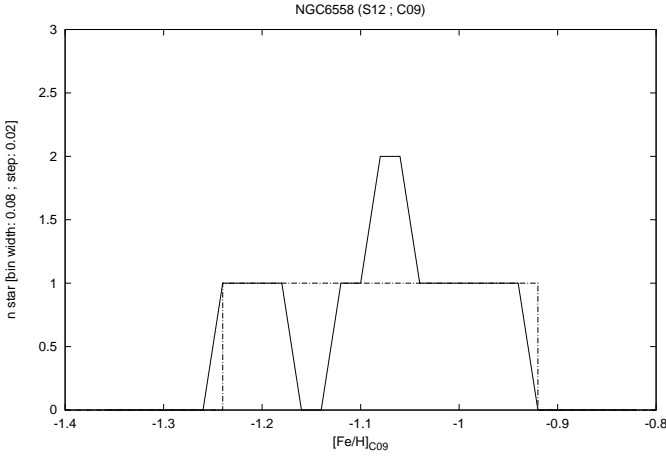
Fig. 35. Distribution in metallicity on the C09 scale for NGC 6558 stars in the S12 sample.
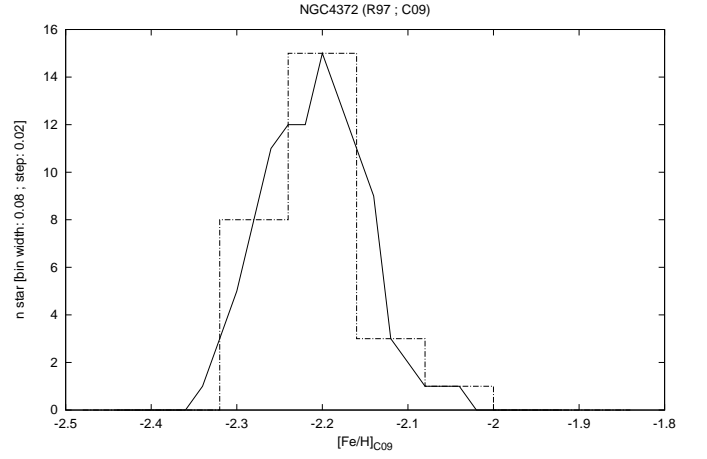
Fig. 38. Distribution in metallicity on the C09 scale for NGC 4372 stars in the R97 sample.
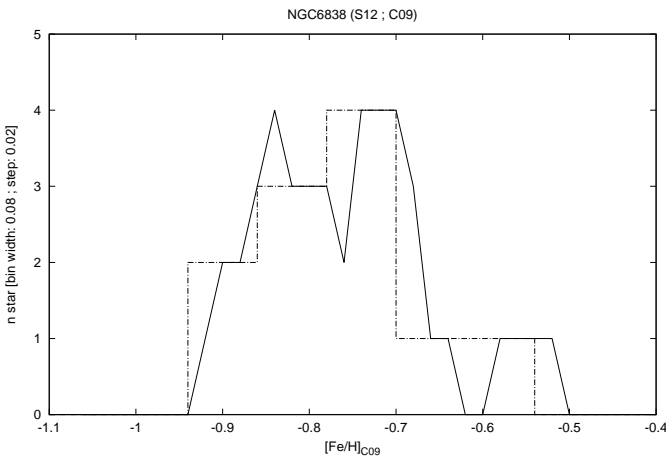
Fig. 36. Distribution in metallicity on the C09 scale for NGC 6838 stars in the S12 sample.
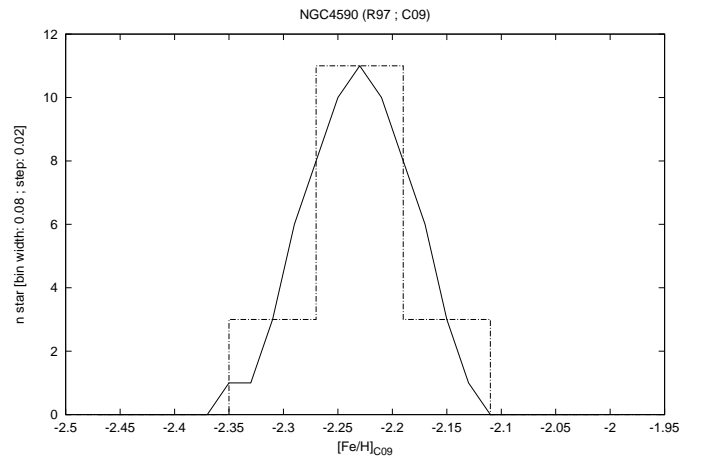
Fig. 39. Distribution in metallicity on the C09 scale for NGC 4590 stars in the R97 sample.
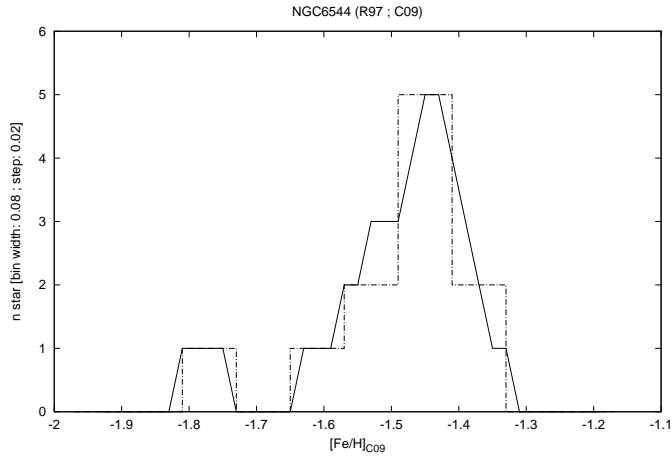
Fig. 40. Distribution in metallicity on the C09 scale for NGC 6544 stars in the R97 sample.
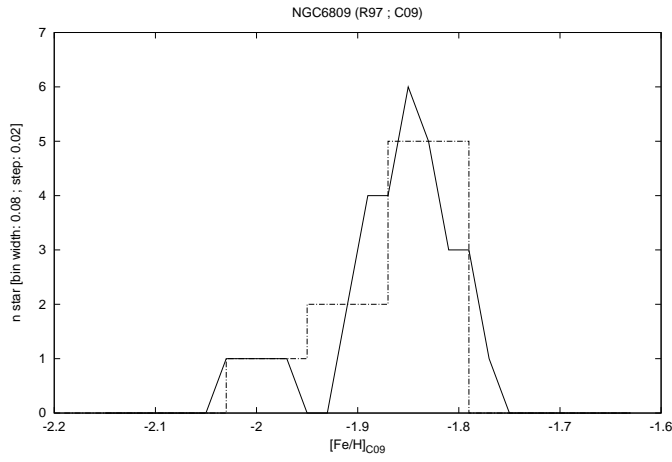
Fig. 41. Distribution in metallicity on the C09 scale for NGC 6809 stars in the R97 sample.
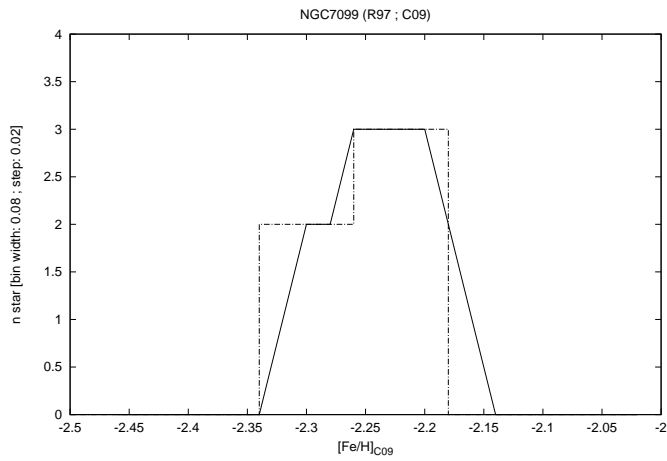
Fig. 42. Distribution in metallicity on the C09 scale for NGC 7099 stars in the R97 sample.

Table 8. Data

Cluster	ra(J2000)	dec(J2000)	J	σ_J	H	σ_H	K_s	σ_{Ks}	EW	σ_{EW}	source
NGC2808	137.944550	-64.870630	11.6660	0.0260	10.9670	0.0300	10.8120	0.0210	5.660	0.233	S12
NGC2808	138.069940	-64.867500	10.2290	0.0280	9.3530	0.0240	9.1010	0.0230	6.700	0.282	S12
NGC2808	137.940140	-64.858480	12.8840	0.0320	12.3110	0.0410	12.1220	0.0270	4.710	0.288	S12
NGC2808	138.076100	-64.852680	11.9450	0.0330	11.1770	0.0320	10.9950	0.0240	5.930	0.228	S12
NGC2808	138.070550	-64.847130	12.8550	0.0620	12.2170	0.0630	12.0500	0.0540	4.960	0.189	S12
NGC2808	138.090370	-64.842770	13.1930	0.0440	12.5020	0.0390	12.3290	0.0300	5.340	0.230	S12
NGC2808	138.008410	-64.834180	13.2110	0.0250	12.5690	0.0220	12.3560	0.0360	5.070	0.233	S12
NGC2808	138.031650	-64.826760	12.4970	0.0370	11.7930	0.0350	11.6670	0.0320	5.240	0.214	S12
NGC2808	137.989130	-64.820710	12.4720	0.0260	11.7770	0.0260	11.6230	0.0240	5.280	0.225	S12
NGC2808	138.041730	-64.809250	12.7460	0.0280	12.0570	0.0290	11.9110	0.0230	5.560	0.208	S12
NGC2808	137.999900	-64.920920	13.3910	0.0430	12.8020	0.0440	12.5740	0.0460	5.040	0.256	S12
NGC2808	138.025400	-64.911880	12.1420	0.0320	11.4400	0.0300	11.2640	0.0260	5.490	0.242	S12
NGC2808	137.979440	-64.903970	11.3580	0.0250	10.5680	0.0210	10.4230	0.0240	5.920	0.251	S12
NGC2808	138.027750	-64.896890	12.5400	0.0430	11.9540	0.0420	11.8050	0.0330	5.230	0.197	S12
NGC2808	138.008810	-64.890870	12.6080	0.0230	11.9360	0.0260	11.8110	0.0240	5.350	0.175	S12
NGC2808	138.074800	-64.884940	12.6050	0.0290	11.9240	0.0270	11.7480	0.0210	5.340	0.256	S12
NGC2808	137.941540	-64.878910	12.1440	0.0260	11.4530	0.0330	11.2680	0.0210	5.680	0.294	S12
NGC3201	154.454720	-46.416050	11.4380	0.0210	10.8110	0.0240	10.6680	0.0230	4.560	0.178	S12
NGC3201	154.439030	-46.407340	11.5760	0.0190	11.0090	0.0240	10.8270	0.0230	4.300	0.178	S12
NGC3201	154.437420	-46.401530	10.1230	0.0190	9.4450	0.0250	9.2460	0.0210	4.850	0.156	S12
NGC3201	154.431940	-46.394890	12.3650	0.0460	11.7810	0.0460	11.6580	0.0380	3.840	0.242	S12
NGC3201	154.411350	-46.390170	10.7280	0.0180	10.0540	0.0220	9.9340	0.0190	4.780	0.161	S12
NGC3201	154.412340	-46.382180	12.3520	0.0180	11.7930	0.0200	11.7190	0.0190	4.000	0.198	S12
NGC3201	154.409240	-46.377290	9.9280	0.0180	9.1950	0.0220	9.0280	0.0210	5.240	0.175	S12
NGC3201	154.423850	-46.365180	11.9040	0.0210	11.3020	0.0250	11.1630	0.0190	4.140	0.180	S12
NGC3201	154.402220	-46.357640	12.7090	0.0210	12.1470	0.0240	12.0440	0.0210	4.150	0.240	S12
NGC3201	154.448580	-46.463050	12.6300	0.0260	12.0250	0.0250	11.8990	0.0210	4.050	0.291	S12
NGC3201	154.470370	-46.458350	12.3390	0.0260	11.7520	0.0280	11.6100	0.0240	4.180	0.192	S12
NGC3201	154.427440	-46.454010	9.7570	0.0180	9.0370	0.0240	8.8590	0.0210	5.300	0.184	S12
NGC3201	154.422110	-46.446570	12.7150	0.0180	12.1460	0.0210	12.0600	0.0170	3.920	0.250	S12
NGC3201	154.456770	-46.440310	11.9210	0.0210	11.3130	0.0220	11.1960	0.0180	4.500	0.191	S12
NGC3201	154.476150	-46.435080	12.7170	0.0180	12.1590	0.0220	12.0240	0.0240	3.740	0.220	S12
NGC3201	154.439340	-46.425220	11.1700	0.0290	10.5220	0.0310	10.4140	0.2999	4.380	0.149	S12
NGC3201	154.454240	-46.420990	12.0420	0.0380	11.4460	0.0370	11.2880	0.2999	4.040	0.164	S12
NGC6121	245.930140	-26.531660	9.9550	0.0200	9.2470	0.0250	9.0350	0.0190	4.840	0.189	S12
NGC6121	245.920890	-26.525060	9.9200	0.0170	9.1980	0.0200	8.9980	0.0180	4.890	0.164	S12
NGC6121	245.978450	-26.522340	10.4820	0.0190	9.7880	0.0220	9.6050	0.0210	4.490	0.164	S12
NGC6121	245.910840	-26.510590	10.1610	0.0210	9.4390	0.0220	9.2690	0.0210	4.680	0.225	S12
NGC6121	245.920620	-26.502630	10.9600	0.0200	10.2630	0.0200	10.1470	0.0230	4.340	0.242	S12
NGC6121	245.933750	-26.501750	8.7730	0.0190	7.9080	0.0370	7.7140	0.0110	5.170	0.200	S12
NGC6121	245.928500	-26.491040	9.8250	0.0170	9.0770	0.0220	8.9230	0.0210	4.630	0.200	S12
NGC6121	245.959540	-26.490640	10.8170	0.0210	10.1840	0.0250	9.9880	0.0230	4.320	0.226	S12
NGC6121	245.908320	-26.478110	10.8220	0.0310	10.1740	0.0370	9.9720	0.0290	4.440	0.259	S12
NGC6121	245.929730	-26.468730	10.9270	0.0240	10.2540	0.0280	10.0680	0.0210	4.350	0.206	S12

Table 8. continued.

Cluster	ra(J2000)	dec(J2000)	J	σ_J	H	σ_H	K_s	σ_{K_s}	EW	σ_{EW}	source
NGC6121	245.973930	-26.578500	8.9300	0.0150	8.2190	0.0550	7.9990	0.0150	5.120	0.121	S12
NGC6121	245.973220	-26.570840	9.6700	0.0170	8.9190	0.0200	8.7240	0.0170	4.770	0.192	S12
NGC6121	245.974320	-26.564570	10.1160	0.0190	9.4280	0.0220	9.2150	0.0190	4.820	0.180	S12
NGC6121	245.902340	-26.541570	10.5380	0.0340	10.1270	0.0640	9.7330	0.0420	4.580	0.242	S12
NGC6121	245.958900	-26.538710	10.7690	0.0210	10.1220	0.0220	9.9140	0.0190	4.480	0.239	S12
NGC6139	246.913430	-38.854710	11.9750	0.0780	11.1690	0.0920	10.8560	0.0600	4.930	0.170	S12
NGC6139	246.928280	-38.848710	12.3590	0.0610	11.5820	0.0720	11.3290	0.0490	4.700	0.172	S12
NGC6139	246.913380	-38.842030	11.7520	0.0230	10.8680	0.0200	10.5900	0.0340	5.220	0.224	S12
NGC6139	246.916000	-38.838060	11.8450	0.0230	10.8790	0.0220	10.6010	0.0210	5.360	0.215	S12
NGC6139	246.927360	-38.831220	13.4240	0.0350	12.5800	0.0350	12.3830	0.0290	4.500	0.175	S12
NGC6139	246.910180	-38.822870	13.1550	0.0490	12.6020	0.0690	12.2610	0.0470	4.390	0.130	S12
NGC6139	246.908710	-38.818790	13.4120	0.0460	12.6170	0.0510	12.3760	0.0380	4.430	0.149	S12
NGC6139	246.920210	-38.811410	13.0910	0.0180	12.2910	0.0200	12.0490	0.0170	4.470	0.161	S12
NGC6139	246.942580	-38.805490	15.0560	0.0670	14.3820	0.0950	14.2700	0.0840	3.830	0.163	S12
NGC6139	246.929170	-38.799610	13.5460	0.0260	12.7770	0.0280	12.5560	0.0270	4.350	0.157	S12
NGC6139	246.899400	-38.894120	12.7170	0.0210	11.9470	0.0200	11.7060	0.0210	4.720	0.166	S12
NGC6139	246.888640	-38.887020	14.9040	0.0470	14.1520	0.0320	13.9690	0.0520	3.830	0.136	S12
NGC6139	246.917100	-38.881120	14.6720	0.0340	13.8540	0.0490	13.5070	0.2999	3.950	0.150	S12
NGC6139	246.920120	-38.866570	12.8800	0.0380	12.0330	0.0400	11.7880	0.0270	4.840	0.192	S12
NGC6139	246.916330	-38.861330	12.8340	0.0680	11.9280	0.0720	11.6970	0.0550	4.890	0.178	S12
NGC6254	254.316090	-4.102620	13.1740	0.0330	12.6480	0.0360	12.5180	0.0260	3.200	0.149	S12
NGC6254	254.311590	-4.098150	10.0290	0.1870	9.0690	0.2650	9.1430	0.1590	4.410	0.153	S12
NGC6254	254.309230	-4.092510	10.2250	0.0210	9.5440	0.0240	9.3920	0.0210	4.880	0.184	S12
NGC6254	254.303620	-4.084770	12.7820	0.0570	12.2230	0.0210	12.0980	0.0290	3.660	0.153	S12
NGC6254	254.313880	-4.079770	11.0650	0.0250	10.4450	0.0240	10.2510	0.0190	4.420	0.156	S12
NGC6254	254.324820	-4.072610	11.1790	0.0250	10.5240	0.0220	10.3430	0.0190	4.380	0.158	S12
NGC6254	254.305640	-4.064500	11.9590	0.0250	11.3810	0.0210	11.2770	0.0170	3.940	0.148	S12
NGC6254	254.295230	-4.058840	12.4940	0.0450	11.9410	0.0450	11.7550	0.0400	3.720	0.158	S12
NGC6254	254.339890	-4.050990	13.7980	0.0200	13.2390	0.0270	13.1200	0.0230	3.210	0.184	S12
NGC6254	254.322870	-4.045370	11.4320	0.0210	10.8250	0.0210	10.6980	0.0170	4.350	0.139	S12
NGC6254	254.317180	-4.041150	12.8120	0.0230	12.2790	0.0210	12.0910	0.0170	3.650	0.142	S12
NGC6254	254.296090	-4.126930	13.5770	0.0290	13.0430	0.0240	12.8810	0.0310	3.250	0.198	S12
NGC6254	254.321660	-4.116810	13.3810	0.0410	12.7980	0.0380	12.7110	0.0420	3.310	0.150	S12
NGC6325	259.508010	-23.771740	12.5250	0.0350	11.6550	0.0460	11.3650	0.0330	5.100	0.175	S12
NGC6325	259.501210	-23.766900	10.4410	0.0230	9.3790	0.0200	9.0060	0.0230	6.070	0.233	S12
NGC6325	259.489260	-23.759420	13.4160	0.0360	12.6480	0.0390	12.3760	0.0350	4.810	0.189	S12
NGC6325	259.492570	-23.752820	12.7600	0.0320	11.9210	0.0490	11.6330	0.0300	4.840	0.148	S12
NGC6325	259.488020	-23.747100	11.2710	0.0250	10.3190	0.0250	10.0330	0.0230	5.350	0.197	S12
NGC6325	259.485880	-23.723390	14.1290	0.0430	13.3930	0.0480	13.1340	0.0480	4.460	0.164	S12
NGC6325	259.482000	-23.803730	12.3900	0.0190	11.4530	0.0200	11.2200	0.0190	5.060	0.175	S12
NGC6325	259.516940	-23.782600	14.4060	0.0290	13.5420	0.0290	13.2960	0.0350	4.690	0.230	S12
NGC6325	259.487960	-23.778460	11.7700	0.0290	10.8260	0.0320	10.5180	0.0290	5.540	0.186	S12
NGC6356	260.921480	-17.814390	13.9810	0.0490	13.2990	0.0510	13.1370	0.0460	5.840	0.200	S12
NGC6356	260.915630	-17.808790	14.0200	0.0500	13.3020	0.0470	13.1850	0.0490	5.790	0.200	S12
NGC6356	260.927970	-17.796680	13.6660	0.0300	12.8790	0.0300	12.7160	0.0280	5.880	0.200	S12

Table 8. continued.

Cluster	ra(J2000)	dec(J2000)	J	σ_J	H	σ_H	K_s	σ_{K_s}	EW	σ_{EW}	source
NGC6356	260.893260	-17.791780	12.4980	0.0470	11.6010	0.0480	11.4160	0.0440	6.680	0.200	S12
NGC6356	260.923920	-17.784670	13.9980	0.0330	13.2800	0.0300	13.0420	0.0370	5.790	0.200	S12
NGC6356	260.923510	-17.754600	14.0430	0.0300	13.3560	0.0340	13.1360	0.0340	6.090	0.200	S12
NGC6356	260.903940	-17.863810	13.9250	0.0290	13.2040	0.0350	13.0520	0.0300	5.690	0.200	S12
NGC6356	260.870600	-17.856880	13.4440	0.0260	12.6410	0.0300	12.4900	0.0280	6.040	0.200	S12
NGC6356	260.894830	-17.844830	14.1800	0.0330	13.4300	0.0350	13.3070	0.0440	5.760	0.200	S12
NGC6356	260.922280	-17.841960	13.2110	0.0430	12.4040	0.0260	12.1660	0.2999	6.420	0.200	S12
NGC6356	260.911510	-17.830910	12.8940	0.0420	11.9840	0.0000	11.7740	0.2999	6.260	0.200	S12
NGC6380	263.612270	-39.068540	12.2985	0.0057	11.2058	0.0085	10.8563	0.0103	6.030	0.200	S12
NGC6380	263.615370	-39.061460	12.4785	0.0063	11.3568	0.0093	11.0553	0.0086	6.270	0.200	S12
NGC6380	263.626140	-39.055490	11.6306	0.0082	10.3159	0.0154	9.9689	0.0196	6.620	0.200	S12
NGC6380	263.622790	-39.047440	12.6716	0.0058	11.5409	0.0125	11.1859	0.0128	6.110	0.200	S12
NGC6380	263.590740	-39.104890	12.6965	0.0055	11.5668	0.0084	11.2213	0.0073	6.100	0.200	S12
NGC6380	263.600680	-39.094240	11.2495	0.0062	10.0528	0.0118	9.6813	0.0101	6.940	0.200	S12
NGC6380	263.613900	-39.086240	14.0625	0.0062	13.0858	0.0076	12.7663	0.0079	5.400	0.200	S12
NGC6397	265.200350	-53.680320	10.4930	0.0160	9.9900	0.0340	9.8110	0.0260	2.850	0.120	S12
NGC6397	265.136690	-53.674960	9.8780	0.0260	9.2950	0.0280	9.1710	0.0260	3.140	0.135	S12
NGC6397	265.140400	-53.670120	10.9980	0.0230	10.4760	0.0250	10.3900	0.0230	2.760	0.198	S12
NGC6397	265.146980	-53.657950	11.1680	0.0290	10.6640	0.0250	10.5440	0.0250	2.500	0.149	S12
NGC6397	265.162140	-53.656630	11.0100	0.0240	10.4790	0.0270	10.3890	0.0230	2.410	0.128	S12
NGC6397	265.180660	-53.647340	11.6560	0.0260	11.1720	0.0320	11.0660	0.0270	2.350	0.184	S12
NGC6397	265.170100	-53.647100	11.9150	0.0410	11.4440	0.0410	11.3570	0.0380	2.440	0.237	S12
NGC6397	265.217360	-53.644460	12.0330	0.0230	11.5730	0.0240	11.4370	0.0230	2.470	0.269	S12
NGC6397	265.174610	-53.638510	10.6960	0.0230	10.1540	0.0250	10.0560	0.0210	2.840	0.130	S12
NGC6397	265.221230	-53.630000	11.5270	0.0260	11.0550	0.0300	10.9240	0.0260	2.580	0.198	S12
NGC6397	265.092530	-53.718550	11.5020	0.0210	11.0000	0.0220	10.9210	0.0210	2.480	0.233	S12
NGC6397	265.127960	-53.706700	10.0020	0.0210	9.4600	0.0250	9.3450	0.0230	3.130	0.130	S12
NGC6397	265.127430	-53.702640	11.7200	0.0270	11.2220	0.0250	11.1640	0.0290	2.480	0.177	S12
NGC6397	265.133060	-53.697760	10.7770	0.0230	10.2460	0.0240	10.1520	0.0210	2.970	0.156	S12
NGC6397	265.141340	-53.688770	9.9710	0.0230	9.4020	0.0240	9.3100	0.0230	3.130	0.086	S12
NGC6397	265.141080	-53.683220	11.7390	0.0330	11.2610	0.0320	11.2150	0.0340	2.480	0.186	S12
NGC6440	267.206180	-20.366060	11.9888	0.0123	10.8901	0.0244	10.5353	0.0041	6.870	0.200	S12
NGC6440	267.232050	-20.358920	12.6050	0.0115	11.4773	0.0186	11.1800	0.0035	6.350	0.200	S12
NGC6440	267.212100	-20.354570	12.7538	0.0141	11.6941	0.0204	11.4183	0.0037	6.270	0.200	S12
NGC6440	267.234500	-20.348560	11.8280	0.0108	10.6553	0.0193	10.2750	0.0041	6.780	0.200	S12
NGC6440	267.224150	-20.391310	12.7048	0.0104	11.6541	0.0182	11.3473	0.0035	6.170	0.200	S12
NGC6440	267.219370	-20.385210	10.9068	0.0168	9.7291	0.0217	9.3613	0.0050	6.990	0.200	S12
NGC6440	267.226990	-20.378350	13.5038	0.0126	12.5331	0.0191	12.2653	0.0032	6.220	0.200	S12
NGC6440	267.231070	-20.372060	12.9488	0.0100	11.8361	0.0195	11.5503	0.0035	6.330	0.200	S12
NGC6441	267.52623	-37.05202	14.1800	0.0119	13.3800	0.0141	13.2300	0.0121	5.610	0.326	S12
NGC6441	267.57042	-37.04656	13.9500	0.0083	13.1700	0.0108	12.9800	0.0126	5.710	0.233	S12
NGC6441	267.56729	-37.03987	13.8600	0.0085	13.0500	0.0111	12.9000	0.0117	6.110	0.273	S12
NGC6441	267.56177	-37.02637	12.0700	0.0095	11.0800	0.0140	10.8400	0.0149	6.540	0.264	S12
NGC6441	267.56130	-37.01749	14.5600	0.0083	13.8800	0.0098	13.7300	0.0123	5.510	0.275	S12
NGC6441	267.52817	-37.00574	14.2100	0.0084	13.3800	0.0109	13.2300	0.0104	5.450	0.255	S12

Table 8. continued.

Cluster	ra(J2000)	dec(J2000)	J	σ_J	H	σ_H	K_s	σ_{Ks}	EW	σ_{EW}	source
NGC6441	267.54013	-37.06483	14.0700	0.0120	13.2400	0.0153	13.0400	0.0189	5.660	0.256	S12
NGC6528	271.20135	-30.06009	11.1900	0.0432	10.1800	0.0558	9.9820	0.0374	6.620	0.332	S12
NGC6528	271.20703	-30.05372	12.3200	0.0132	11.4300	0.0147	11.1500	0.0124	6.260	0.295	S12
NGC6528	271.19694	-30.05007	13.0600	0.0101	12.2300	0.0127	12.0000	0.0117	5.660	0.259	S12
NGC6528	271.20272	-30.04346	12.8800	0.0116	12.0200	0.0141	11.8100	0.0120	5.920	0.279	S12
NGC6528	271.18283	-30.06262	11.8700	0.0127	10.9500	0.0171	10.6800	0.0133	6.800	0.200	S12
NGC6528	271.19277	-30.06265	12.7100	0.0121	11.8200	0.0156	11.5600	0.0125	6.340	0.200	S12
NGC6528	271.20760	-30.06783	12.7600	0.0111	11.9200	0.0125	11.6700	0.0116	6.440	0.200	S12
NGC6553	272.32879	-25.91109	10.9700	0.0249	9.9850	0.0193	9.6200	0.0205	6.790	0.286	S12
NGC6553	272.34392	-25.90719	12.1800	0.0207	11.3500	0.0282	11.0900	0.0208	6.160	0.304	S12
NGC6553	272.32582	-25.88831	10.2700	0.0199	9.3210	0.0312	8.7930	0.0244	6.840	0.326	S12
NGC6553	272.31620	-25.87955	12.1600	0.0152	11.2800	0.0209	11.0000	0.0135	6.280	0.264	S12
NGC6553	272.32670	-25.87332	11.1700	0.0189	10.1200	0.0221	9.8020	0.0163	6.560	0.277	S12
NGC6553	272.35071	-25.86364	12.0700	0.0150	11.2200	0.0201	10.9700	0.0125	6.380	0.268	S12
NGC6553	272.35361	-25.84971	11.9000	0.0157	11.0300	0.0212	10.7200	0.0160	6.440	0.277	S12
NGC6553	272.34409	-25.96301	11.7500	0.0151	10.8100	0.0188	10.5300	0.0140	6.570	0.318	S12
NGC6553	272.32808	-25.94363	11.4000	0.0139	10.4300	0.0230	10.1300	0.0155	6.510	0.295	S12
NGC6553	272.31580	-25.93005	10.9000	0.0233	9.9130	0.0314	9.6140	0.0199	6.610	0.304	S12
NGC6553	272.32357	-25.92491	12.0400	0.0136	11.1800	0.0197	10.9200	0.0140	6.550	0.304	S12
NGC6558	272.575780	-31.778840	14.1741	0.0068	13.5640	0.0089	13.4282	0.0064	4.750	0.213	S12
NGC6558	272.563700	-31.766630	13.1701	0.0067	12.4990	0.0093	12.3432	0.0064	5.050	0.172	S12
NGC6558	272.589970	-31.757050	13.0921	0.0077	12.4220	0.0118	12.2792	0.0071	5.020	0.225	S12
NGC6558	272.579670	-31.746990	13.0721	0.0062	12.3680	0.0085	12.2212	0.0066	4.870	0.170	S12
NGC6569	273.422660	-31.827060	13.1161	0.0074	12.3215	0.0102	12.1431	0.0060	5.430	0.228	S12
NGC6569	273.409170	-31.789720	13.7401	0.0068	12.9585	0.0102	12.7711	0.0066	5.020	0.256	S12
NGC6569	273.433630	-31.770430	14.1061	0.0086	13.3575	0.0110	13.1881	0.0063	4.880	0.208	S12
NGC6569	273.422840	-31.845770	13.4261	0.0117	12.6555	0.0155	12.4781	0.0072	5.090	0.210	S12
NGC6569	273.408070	-31.841600	14.0321	0.0124	13.3015	0.0185	13.1511	0.0080	4.810	0.205	S12
NGC6656	279.172800	-23.910870	11.8699	0.0108	11.3166	0.0158	11.1604	0.0069	3.430	0.099	S12
NGC6656	279.171160	-23.909170	13.0749	0.0105	12.5576	0.0145	12.4284	0.0062	2.650	0.200	S12
NGC6656	279.176160	-23.907840	12.5169	0.0121	11.9836	0.0149	11.8424	0.0073	3.310	0.144	S12
NGC6656	279.155890	-23.904610	11.4979	0.0124	10.9336	0.0161	10.7614	0.0082	3.190	0.094	S12
NGC6656	279.151130	-23.900460	10.1429	0.0205	9.4506	0.0201	9.3284	0.0112	3.870	0.112	S12
NGC6656	279.129690	-23.896270	12.1519	0.0109	11.5826	0.0142	11.4644	0.0077	3.340	0.158	S12
NGC6656	279.170270	-23.895210	11.5749	0.0136	11.0006	0.0162	10.8374	0.0083	3.340	0.113	S12
NGC6656	279.153790	-23.888850	11.4209	0.0125	10.8566	0.0184	10.7004	0.0086	3.240	0.094	S12
NGC6656	279.149770	-23.888820	10.2239	0.0237	9.5416	0.0170	9.4054	0.0117	4.380	0.142	S12
NGC6656	279.133050	-23.887930	9.8269	0.0175	9.1596	0.0226	8.9964	0.0130	3.970	0.112	S12
NGC6656	279.119060	-23.885510	9.6599	0.0137	9.0026	0.0179	8.8304	0.0106	4.110	0.136	S12
NGC6656	279.149930	-23.885380	11.4129	0.0150	10.8376	0.0181	10.6784	0.0083	3.890	0.128	S12
NGC6656	279.143070	-23.878710	12.2459	0.0112	11.6906	0.0150	11.5564	0.0070	2.850	0.094	S12
NGC6656	279.164990	-23.878410	11.5959	0.0109	11.0396	0.0186	10.8774	0.0080	3.260	0.120	S12
NGC6656	279.168030	-23.876270	12.0709	0.0112	11.5276	0.0150	11.3704	0.0078	3.010	0.141	S12
NGC6656	279.124180	-23.870710	11.5519	0.0139	10.9686	0.0176	10.8444	0.0089	3.170	0.114	S12

Table 8. continued.

Cluster	ra(J2000)	dec(J2000)	J	σ_J	H	σ_H	K_s	σ_{K_s}	EW	σ_{EW}	source
NGC6656	279.133280	-23.869340	11.1149	0.0169	10.5086	0.0244	10.3644	0.0114	3.740	0.113	S12
NGC6656	279.145490	-23.868820	11.1849	0.0155	10.5826	0.0214	10.4384	0.0113	4.050	0.126	S12
NGC6656	279.155720	-23.865530	11.2329	0.0165	10.6676	0.0183	10.5134	0.0099	3.190	0.122	S12
NGC6656	279.177640	-23.864640	9.9499	0.0185	9.2996	0.0252	9.1184	0.0107	3.820	0.103	S12
NGC6656	279.135920	-23.862870	12.1289	0.0117	11.5626	0.0175	11.4244	0.0081	3.550	0.136	S12
NGC6656	279.133760	-23.858610	9.5089	0.0131	8.8236	0.0177	8.6284	0.0108	4.020	0.122	S12
NGC6656	279.128960	-23.857150	12.5989	0.0109	12.0286	0.0173	11.9054	0.0078	3.140	0.150	S12
NGC6656	279.111160	-23.856070	10.1599	0.0261	9.4546	0.0234	9.3444	0.0163	4.740	0.148	S12
NGC6656	279.122800	-23.852450	11.7139	0.0195	11.1166	0.0296	10.9944	0.0105	3.580	0.127	S12
NGC6656	279.120340	-23.850280	9.2349	0.0187	8.4656	0.0261	8.3124	0.0136	4.280	0.121	S12
NGC6656	279.148720	-23.849680	11.3719	0.0138	10.7406	0.0201	10.6234	0.0090	3.570	0.122	S12
NGC6656	279.120070	-23.848090	13.2289	0.0143	12.6866	0.0217	12.5704	0.0091	2.920	0.208	S12
NGC6656	279.177450	-23.847720	12.3749	0.0120	11.8266	0.0149	11.6794	0.0071	3.230	0.156	S12
NGC6656	279.134480	-23.955270	11.9759	0.0140	11.3786	0.0157	11.2554	0.0094	3.090	0.094	S12
NGC6656	279.129160	-23.953670	10.9939	0.0177	10.3736	0.0186	10.2274	0.0126	3.440	0.112	S12
NGC6656	279.143390	-23.950910	12.0119	0.0138	11.4226	0.0156	11.2934	0.0095	2.910	0.086	S12
NGC6656	279.117740	-23.949230	11.8489	0.0109	11.2566	0.0140	11.1274	0.0099	3.290	0.120	S12
NGC6656	279.130670	-23.946030	12.4659	0.0157	11.9126	0.0193	11.7544	0.0102	3.290	0.166	S12
NGC6656	279.129800	-23.942410	11.5859	0.0131	10.9776	0.0157	10.8354	0.0100	3.450	0.135	S12
NGC6656	279.137950	-23.940480	9.8179	0.0205	9.1366	0.0257	8.9784	0.0225	4.010	0.089	S12
NGC6656	279.121380	-23.934020	11.4209	0.0139	10.8376	0.0169	10.6864	0.0095	3.590	0.141	S12
NGC6656	279.138660	-23.933710	11.5939	0.0128	10.9886	0.0163	10.8344	0.0087	3.540	0.130	S12
NGC6656	279.164700	-23.932740	12.8469	0.0116	12.2866	0.0152	12.1734	0.0070	3.630	0.205	S12
NGC6656	279.164210	-23.928830	11.7009	0.0124	11.0916	0.0164	10.9744	0.0077	3.110	0.106	S12
NGC6656	279.138180	-23.928780	11.3179	0.0148	10.7006	0.0160	10.5624	0.0087	3.180	0.106	S12
NGC6656	279.128090	-23.927380	10.4979	0.0193	9.8436	0.0238	9.6904	0.0116	3.970	0.094	S12
NGC6656	279.144670	-23.922690	13.2049	0.0121	12.6766	0.0131	12.5624	0.0073	3.000	0.213	S12
NGC6656	279.132900	-23.920350	12.9149	0.0116	12.3566	0.0165	12.2254	0.0075	3.060	0.178	S12
NGC6656	279.148910	-23.919140	11.6669	0.0118	11.0676	0.0167	10.9354	0.0080	3.820	0.144	S12
NGC6656	279.186990	-23.915770	9.3729	0.0128	8.6676	0.0167	8.4544	0.0109	4.810	0.158	S12
NGC6656	279.138790	-23.914400	11.4939	0.0148	10.9116	0.0170	10.7834	0.0095	3.210	0.114	S12
NGC6656	279.159600	-23.900340	10.0320	0.0210	9.3440	0.0190	9.2070	0.0200	4.120	0.191	S12
NGC6656	279.127260	-23.880040	9.8150	0.0180	9.1300	0.0200	8.9520	0.0170	4.500	0.144	S12
NGC6656	279.113770	-23.957900	12.1310	0.0230	11.5480	0.0290	11.4070	0.0270	2.920	0.130	S12
NGC6656	279.113220	-23.956850	10.9680	0.0410	10.3300	0.0480	10.2040	0.0380	4.090	0.114	S12
NGC6838	298.447690	18.781370	8.5730	0.0350	7.6790	0.0470	7.4490	0.0130	6.680	0.277	S12
NGC6838	298.442240	18.791100	10.3360	0.0260	9.5430	0.0310	9.3950	0.0180	6.040	0.283	S12
NGC6838	298.490080	18.799590	10.9060	0.0260	10.1920	0.0310	10.0420	0.0160	5.690	0.264	S12
NGC6838	298.451090	18.801120	9.1770	0.0330	8.2700	0.0210	8.0940	0.0250	6.490	0.277	S12
NGC6838	298.463290	18.809050	12.0010	0.0470	11.2940	0.0450	11.2200	0.0380	5.340	0.233	S12
NGC6838	298.460960	18.819220	10.2150	0.0340	9.4460	0.0350	9.2710	0.0250	5.900	0.242	S12
NGC6838	298.457900	18.830150	12.2640	0.0240	11.5990	0.0300	11.5190	0.0200	5.080	0.304	S12
NGC6838	298.452100	18.747480	12.3240	0.0390	11.7320	0.0370	11.5980	0.0280	5.250	0.269	S12
NGC6838	298.490220	18.749620	12.3210	0.0220	11.7530	0.0280	11.6370	0.0180	5.150	0.314	S12
NGC6838	298.486330	18.761590	12.1970	0.0330	11.5290	0.0340	11.4550	0.0220	5.030	0.256	S12

Table 8. continued.

Cluster	ra(J2000)	dec(J2000)	J	σ_J	H	σ_H	K_s	σ_{Ks}	EW	σ_{EW}	source
NGC6838	298.449680	18.764200	11.8740	0.0410	11.2320	0.0400	11.1080	0.0270	5.560	0.264	S12
NGC7078	322.531270	12.164500	14.1030	0.0180	13.6010	0.0700	13.5900	0.0430	2.050	0.198	S12
NGC7078	322.523520	12.171420	12.1560	0.0180	11.5960	0.0230	11.4800	0.0190	2.850	0.114	S12
NGC7078	322.519050	12.176160	11.8580	0.0190	11.2720	0.0250	11.1650	0.0170	2.930	0.064	S12
NGC7078	322.517820	12.182660	11.4590	0.0190	10.8930	0.0230	10.7570	0.0170	2.930	0.057	S12
NGC7078	322.509200	12.189740	10.2270	0.0210	9.5820	0.0300	9.4330	0.0190	3.710	0.086	S12
NGC7078	322.502060	12.194030	12.3410	0.0220	11.8160	0.0300	11.6920	0.0220	2.840	0.114	S12
NGC7078	322.561110	12.203340	13.7560	0.0190	13.2380	0.0180	13.1460	0.0330	1.980	0.205	S12
NGC7078	322.499400	12.208470	13.5710	0.0290	13.0690	0.0390	12.9600	0.0380	2.720	0.192	S12
NGC7078	322.533280	12.215460	12.1800	0.0160	11.6220	0.0230	11.4700	0.0170	2.800	0.127	S12
NGC7078	322.521420	12.222710	12.3110	0.0180	11.7240	0.0230	11.6130	0.0150	2.460	0.086	S12
NGC7078	322.513060	12.225080	12.1800	0.0180	11.6590	0.0210	11.5060	0.0170	2.840	0.170	S12
NGC7078	322.511350	12.115950	11.9180	0.0180	11.3880	0.0230	11.2470	0.0190	3.090	0.120	S12
NGC7078	322.523020	12.118580	13.6300	0.0260	13.1450	0.0300	12.9930	0.0310	2.220	0.156	S12
NGC7078	322.501380	12.127220	11.5350	0.0180	10.9440	0.0250	10.8470	0.0170	2.970	0.086	S12
NGC7078	322.531000	12.137590	11.9000	0.0210	11.2850	0.0280	11.2070	0.0170	2.930	0.081	S12
NGC7078	322.537000	12.147420	12.8150	0.0220	12.3180	0.0330	12.1840	0.0270	2.470	0.122	S12
NGC7078	322.516410	12.149830	13.0030	0.0370	12.4830	0.0520	12.3640	0.0430	2.410	0.120	S12
NGC7078	322.527190	12.156610	13.4950	0.0310	12.9870	0.0460	12.8510	0.0390	2.330	0.135	S12
Pal7	272.688940	-7.214170	11.9690	0.0360	11.0180	0.0400	10.7240	0.0360	5.860	0.242	S12
Pal7	272.690750	-7.208330	11.0460	0.0260	9.9220	0.0270	9.5840	0.0240	6.650	0.273	S12
Pal7	272.685660	-7.202940	10.7800	0.0260	9.6490	0.0280	9.3070	0.0260	6.400	0.292	S12
Pal7	272.694060	-7.196020	11.8360	0.0000	11.4320	0.0300	10.5570	0.2999	5.650	0.266	S12
Pal7	272.681500	-7.189500	11.1590	0.0210	10.0580	0.0220	9.7240	0.0230	6.500	0.273	S12
Pal7	272.654260	-7.182170	11.0170	0.0190	9.8770	0.0220	9.5510	0.0210	5.960	0.286	S12
Pal7	272.703810	-7.173710	10.4060	0.0170	9.2170	0.0220	8.8730	0.0210	6.520	0.295	S12
Pal7	272.694190	-7.165590	12.3210	0.0350	11.3000	0.0360	10.9740	0.0330	5.890	0.228	S12
Pal7	272.712920	-7.153860	12.5310	0.0160	11.4270	0.0210	11.1630	0.0210	5.890	0.242	S12
Pal7	272.664410	-7.257900	11.0650	0.0000	9.9510	0.0000	9.5780	0.0370	6.550	0.286	S12
Pal7	272.666790	-7.249910	12.4420	0.0310	11.4460	0.0280	11.1760	0.2999	5.770	0.260	S12
Pal7	272.648130	-7.244750	12.1490	0.0290	11.0460	0.0000	10.7870	0.0290	5.730	0.279	S12
Pal7	272.635010	-7.234980	12.5330	0.0190	11.5450	0.0210	11.2440	0.0230	5.750	0.268	S12
Pal7	272.673930	-7.221060	12.7700	0.0230	11.7370	0.0250	11.4940	0.0240	5.770	0.251	S12
NGC2808	138.096140	-64.942785	10.7670	0.0230	9.9040	0.0200	9.7110	0.0220	5.730	0.070	R97
NGC2808	137.873670	-64.916161	11.6070	0.0190	10.9930	0.0200	10.8720	0.0210	5.190	0.060	R97
NGC2808	137.877910	-64.893799	11.4300	0.0190	10.6760	0.0200	10.5400	0.0210	5.000	0.040	R97
NGC2808	137.834690	-64.905189	12.8810	0.0190	12.5940	0.0200	12.5080	0.0230	4.290	0.070	R97
NGC2808	138.052200	-64.940138	11.7060	0.0210	10.9600	0.0200	10.7960	0.0210	4.930	0.080	R97
NGC2808	137.922770	-64.900869	12.3100	0.0380	11.6500	0.0430	11.4900	0.0330	4.520	0.050	R97
NGC2808	138.088430	-64.906621	12.3490	0.0210	11.6740	0.0240	11.5120	0.0170	4.770	0.120	R97
NGC2808	138.088930	-64.936812	12.5400	0.0210	11.8940	0.0200	11.7600	0.0220	4.690	0.100	R97
NGC2808	138.057760	-64.952639	12.5860	0.0390	11.8910	0.0380	11.7300	0.0370	4.790	0.090	R97
NGC2808	137.842890	-64.875190	12.5150	0.0230	11.7850	0.0220	11.7010	0.0240	4.480	0.100	R97
NGC2808	138.054160	-64.944861	13.0010	0.0210	12.3960	0.0200	12.3070	0.0270	4.900	0.170	R97
NGC2808	137.858270	-64.893801	12.8570	0.0180	12.2230	0.0200	12.1570	0.0210	4.470	0.090	R97

F. Mauro et al.: Deriving Metallicities from CaT in combination with nIR Photometry

Table 8. continued.

Cluster	ra(J2000)	dec(J2000)	J	σ_J	H	σ_H	K_s	σ_{Ks}	EW	σ_{EW}	source
NGC2808	138.012490	-64.924800	13.0940	0.0390	12.5280	0.0410	12.4210	0.0420	4.750	0.140	R97
NGC2808	137.889050	-64.902408	13.0510	0.0230	12.3860	0.0220	12.2290	0.0210	4.630	0.120	R97
NGC2808	137.809490	-64.893239	13.0640	0.0190	12.4110	0.0200	12.2800	0.0230	4.600	0.110	R97
NGC2808	137.978440	-64.916442	13.3710	0.0310	12.7670	0.0270	12.6540	0.0280	4.520	0.170	R97
NGC2808	137.901140	-64.891710	13.4870	0.0290	12.8650	0.0300	12.8220	0.0330	4.520	0.160	R97
NGC2808	137.862840	-64.878940	13.5480	0.0250	12.9560	0.0240	12.7720	0.0260	4.120	0.120	R97
NGC2808	138.041660	-64.921620	14.9130	0.0800	14.4000	0.0480	14.4040	0.0740	3.720	0.290	R97
NGC3201	154.427190	-46.454324	9.7570	0.0180	9.0370	0.0240	8.8590	0.0210	5.030	0.030	R97
NGC3201	154.353020	-46.408506	9.9370	0.0230	9.2290	0.0250	9.0290	0.0190	4.840	0.070	R97
NGC3201	154.408990	-46.377665	9.9280	0.0180	9.1950	0.0220	9.0280	0.0210	4.790	0.030	R97
NGC3201	154.434410	-46.424042	9.9600	0.0180	9.2390	0.0240	9.0830	0.0190	4.880	0.070	R97
NGC3201	154.437200	-46.401818	10.1230	0.0190	9.4450	0.0250	9.2460	0.0210	4.560	0.070	R97
NGC3201	154.360270	-46.414062	10.2440	0.0240	9.5560	0.0240	9.3850	0.0210	4.780	0.070	R97
NGC3201	154.361880	-46.429062	10.2270	0.0260	9.5580	0.0340	9.3730	0.0230	4.550	0.030	R97
NGC3201	154.411010	-46.390442	10.7280	0.0180	10.0540	0.0220	9.9340	0.0190	4.390	0.050	R97
NGC3201	154.336890	-46.431836	10.9230	0.0210	10.3650	0.0240	10.2280	0.0210	4.160	0.080	R97
NGC3201	154.362680	-46.431284	11.1010	0.0230	10.4800	0.0240	10.3570	0.0230	4.170	0.030	R97
NGC3201	154.440520	-46.473483	11.0770	0.0210	10.4000	0.0240	10.2640	0.0230	4.320	0.120	R97
NGC3201	154.454550	-46.416528	11.4380	0.0210	10.8110	0.0240	10.6680	0.0230	4.100	0.060	R97
NGC3201	154.334900	-46.386002	11.6230	0.0210	11.0650	0.0240	10.9370	0.0190	3.670	0.110	R97
NGC3201	154.438820	-46.407650	11.5760	0.0190	11.0090	0.0240	10.8270	0.0230	3.890	0.070	R97
NGC3201	154.375180	-46.443506	11.7200	0.0210	11.1410	0.0240	11.0460	0.0190	3.720	0.150	R97
NGC3201	154.307910	-46.390714	11.9710	0.0210	11.3890	0.0220	11.2580	0.0190	4.000	0.130	R97
NGC3201	154.456600	-46.440693	11.9210	0.0210	11.3130	0.0220	11.1960	0.0180	3.820	0.110	R97
NGC4372	186.337370	-72.626595	9.2600	0.0190	8.5240	0.0330	8.2670	0.0370	3.710	0.040	R97
NGC4372	186.292200	-72.647006	9.7210	0.0190	8.9630	0.0250	8.7670	0.0190	3.430	0.040	R97
NGC4372	186.523930	-72.647522	9.7200	0.0190	8.9450	0.0200	8.7490	0.0190	3.530	0.040	R97
NGC4372	186.532140	-72.614210	9.9220	0.0190	9.1920	0.0220	8.9720	0.0170	3.240	0.070	R97
NGC4372	186.623880	-72.667607	10.1840	0.0190	9.4670	0.0200	9.2660	0.0190	3.070	0.050	R97
NGC4372	186.480260	-72.610036	10.7720	0.0230	10.0530	0.0220	9.8360	0.0190	2.730	0.080	R97
NGC4372	186.356790	-72.615861	10.9100	0.0210	10.2350	0.0200	10.0500	0.0190	2.480	0.070	R97
NGC4372	186.582850	-72.638361	10.8670	0.0190	10.1200	0.0200	9.9680	0.0210	3.000	0.140	R97
NGC4372	186.592970	-72.679804	11.0060	0.0210	10.3000	0.0220	10.1200	0.0190	3.030	0.120	R97
NGC4372	186.545850	-72.691257	11.1760	0.0190	10.4970	0.0200	10.3220	0.0170	2.830	0.100	R97
NGC4372	186.569680	-72.657287	11.2160	0.0210	10.4970	0.0250	10.2990	0.0170	2.660	0.100	R97
NGC4372	186.591820	-72.649098	11.1840	0.0230	10.4580	0.0250	10.3040	0.0210	3.140	0.090	R97
NGC4372	186.622500	-72.648425	11.3120	0.0190	10.5990	0.0200	10.4650	0.0170	2.790	0.080	R97
NGC4372	186.532280	-72.683287	11.4280	0.0190	10.7840	0.0220	10.6160	0.0170	2.380	0.120	R97
NGC4372	186.321430	-72.632609	11.3880	0.0190	10.7120	0.0240	10.5700	0.0210	2.510	0.070	R97
NGC4372	186.342010	-72.641532	11.3890	0.0180	10.7090	0.0200	10.5400	0.0170	2.740	0.170	R97
NGC4372	186.578820	-72.651541	11.5070	0.0230	10.8180	0.0270	10.6350	0.0190	2.360	0.080	R97
NGC4372	186.486450	-72.625976	11.6060	0.0310	10.9120	0.0340	10.7700	0.0340	2.590	0.150	R97
NGC4372	186.464830	-72.621373	11.5980	0.0190	10.9500	0.0200	10.8060	0.0190	2.110	0.190	R97
NGC4372	186.505680	-72.626699	11.6080	0.0230	10.9320	0.0200	10.8010	0.0210	2.410	0.090	R97
NGC4372	186.315590	-72.637770	11.7890	0.0230	11.1790	0.0300	11.0340	0.0240	2.360	0.060	R97

Table 8. continued.

Cluster	ra(J2000)	dec(J2000)	J	σ_J	H	σ_H	K_s	σ_{Ks}	EW	σ_{EW}	source
NGC4372	186.424880	-72.628676	11.8080	0.0260	11.1910	0.0310	10.9800	0.0260	2.490	0.110	R97
NGC4372	186.542710	-72.628857	11.7610	0.0230	11.0170	0.0220	10.8520	0.0190	2.640	0.080	R97
NGC4372	186.588000	-72.664034	12.0340	0.0190	11.3720	0.0270	11.2000	0.0210	2.290	0.150	R97
NGC4372	186.352400	-72.610689	12.1190	0.0230	11.4660	0.0270	11.3040	0.0240	2.490	0.130	R97
NGC4372	186.550890	-72.629431	12.1540	0.0230	11.5160	0.0220	11.3730	0.0170	2.000	0.140	R97
NGC4372	186.453270	-72.626250	12.1620	0.0390	11.4640	0.0530	11.3440	0.0370	2.460	0.100	R97
NGC4590	189.843810	-26.753191	10.4740	0.0210	9.8490	0.0200	9.7070	0.0190	3.600	0.050	R97
NGC4590	189.889410	-26.720411	11.0800	0.0190	10.4660	0.0200	10.3520	0.0170	3.040	0.050	R97
NGC4590	189.816190	-26.754142	11.2700	0.0210	10.6040	0.0200	10.5160	0.0210	3.040	0.050	R97
NGC4590	189.891370	-26.729956	11.5070	0.0210	10.8560	0.0200	10.7720	0.0190	2.890	0.060	R97
NGC4590	189.828750	-26.828418	11.4660	0.0210	10.9550	0.0270	10.7900	0.0190	3.000	0.040	R97
NGC4590	189.862700	-26.797581	11.6450	0.0210	11.0440	0.0200	10.9240	0.0170	2.760	0.060	R97
NGC4590	189.817520	-26.796216	11.7570	0.0260	11.1840	0.0270	11.0630	0.0210	2.990	0.060	R97
NGC4590	189.832100	-26.737906	11.8370	0.0210	11.2670	0.0200	11.1440	0.0210	2.640	0.070	R97
NGC4590	189.821000	-26.760666	12.3240	0.0210	11.7630	0.0200	11.6590	0.0210	2.700	0.070	R97
NGC4590	189.906700	-26.754452	12.3630	0.0230	11.8350	0.0220	11.7120	0.0240	2.620	0.070	R97
NGC4590	189.877700	-26.693994	12.6940	0.0210	12.1710	0.0200	12.0700	0.0230	2.080	0.090	R97
NGC4590	189.797750	-26.754366	12.8920	0.0190	12.3980	0.0200	12.2740	0.0190	2.240	0.100	R97
NGC4590	189.825980	-26.777851	12.8720	0.0210	12.2970	0.0200	12.2030	0.0210	2.200	0.110	R97
NGC4590	189.816180	-26.769893	13.2220	0.0230	12.7900	0.0250	12.6820	0.0290	2.170	0.140	R97
NGC4590	189.905310	-26.715148	13.2240	0.0260	12.7490	0.0260	12.6230	0.0270	2.430	0.140	R97
NGC4590	189.839800	-26.804811	13.4340	0.0250	12.9100	0.0200	12.7590	0.0230	2.360	0.100	R97
NGC4590	189.917520	-26.793705	13.4250	0.0260	12.9100	0.0200	12.9120	0.0370	2.260	0.110	R97
NGC6121	245.957490	-26.566356	8.3360	0.0070	7.5120	0.0330	7.2300	0.0130	4.960	0.030	R97
NGC6121	245.995110	-26.663545	8.6800	0.0170	7.9440	0.0410	7.7550	0.0270	4.580	0.030	R97
NGC6121	245.974040	-26.578352	8.9300	0.0150	8.2190	0.0550	7.9990	0.0150	4.630	0.050	R97
NGC6121	245.947500	-26.529458	8.9160	0.0130	8.1510	0.0290	7.9740	0.0130	4.530	0.070	R97
NGC6121	245.819580	-26.574519	8.8510	0.0230	8.0380	0.0310	7.8320	0.0170	4.560	0.070	R97
NGC6121	245.985700	-26.650349	9.0590	0.0190	8.2940	0.0630	8.0380	0.0310	4.900	0.030	R97
NGC6121	246.054130	-26.605109	9.0700	0.0170	8.2380	0.0330	8.0730	0.0170	4.720	0.030	R97
NGC6121	245.808090	-26.556742	9.0690	0.0210	8.2440	0.0130	8.0720	0.0290	4.740	0.080	R97
NGC6121	245.942860	-26.540850	9.1940	0.0230	8.3560	0.0350	8.1570	0.0150	4.820	0.060	R97
NGC6121	246.066190	-26.585098	9.6560	0.0170	8.9540	0.0200	8.7510	0.0230	4.400	0.030	R97
NGC6121	245.973140	-26.570752	9.6700	0.0170	8.9190	0.0200	8.7240	0.0170	4.300	0.040	R97
NGC6121	245.993280	-26.594346	9.8450	0.0170	9.1120	0.0200	8.9650	0.0190	4.300	0.080	R97
NGC6121	245.974480	-26.564752	10.1160	0.0190	9.4280	0.0220	9.2150	0.0190	4.260	0.070	R97
NGC6121	245.941310	-26.560847	10.0970	0.0170	9.4190	0.0250	9.2420	0.0230	4.410	0.030	R97
NGC6121	245.945660	-26.562233	10.1430	0.0190	9.4390	0.0200	9.2620	0.0190	4.340	0.040	R97
NGC6121	245.874490	-26.390200	10.1860	0.0180	9.4490	0.0200	9.2640	0.0170	4.250	0.040	R97
NGC6121	245.912050	-26.428511	10.3300	0.0180	9.6370	0.0200	9.4620	0.0170	4.360	0.050	R97
NGC6121	245.885070	-26.438944	10.2870	0.0180	9.5590	0.0200	9.3870	0.0170	4.160	0.040	R97
NGC6397	265.116000	-53.619300	8.2660	0.0200	7.5920	0.0340	7.4650	0.0210	3.320	0.050	R97
NGC6397	265.288000	-53.653900	8.8820	0.0230	8.2590	0.0240	8.1360	0.0290	3.340	0.080	R97
NGC6397	265.264000	-53.660800	9.3140	0.0320	8.7110	0.0440	8.5860	0.0210	3.120	0.080	R97
NGC6397	265.064000	-53.670900	9.2560	0.0240	8.7030	0.0510	8.5390	0.0210	2.980	0.070	R97

Table 8. continued.

Cluster	ra(J2000)	dec(J2000)	J	σ_J	H	σ_H	K_s	σ_{Ks}	EW	σ_{EW}	source
NGC6397	265.187000	-53.734600	9.5100	0.0240	8.9460	0.0280	8.8080	0.0250	2.700	0.100	R97
NGC6397	265.119000	-53.642300	9.6000	0.0230	8.9940	0.0240	8.8430	0.0200	2.880	0.050	R97
NGC6397	265.100000	-53.714800	9.7100	0.0210	9.1150	0.0220	9.0060	0.0210	2.760	0.050	R97
NGC6397	265.306000	-53.625900	10.1410	0.0240	9.6830	0.0280	9.4730	0.0200	2.460	0.070	R97
NGC6397	265.128000	-53.707200	10.0020	0.0210	9.4600	0.0250	9.3450	0.0230	2.830	0.080	R97
NGC6397	265.287000	-53.625600	10.2600	0.0210	9.7160	0.0260	9.5730	0.0230	2.690	0.050	R97
NGC6397	265.049000	-53.657200	10.5480	0.0210	9.9920	0.0240	9.9510	0.0210	2.690	0.130	R97
NGC6397	265.267000	-53.637800	10.5340	0.0210	10.0580	0.0260	9.8970	0.0210	2.550	0.070	R97
NGC6397	265.133000	-53.698400	10.7770	0.0230	10.2460	0.0240	10.1520	0.0210	2.560	0.110	R97
NGC6397	265.117000	-53.623800	11.1670	0.0240	10.6550	0.0250	10.5610	0.0210	2.220	0.100	R97
NGC6397	265.221000	-53.630400	11.5270	0.0260	11.0550	0.0300	10.9240	0.0260	2.080	0.120	R97
NGC6522	270.901560	-30.030666	10.8374	0.0181	9.9523	0.0237	9.7242	0.0145	4.980	0.050	R97
NGC6522	270.895910	-30.039841	11.3554	0.0124	10.5403	0.0163	10.3202	0.0116	4.870	0.040	R97
NGC6522	270.888530	-30.042341	11.7604	0.0104	10.9673	0.0174	10.7412	0.0111	4.880	0.060	R97
NGC6522	270.906930	-30.036624	13.0284	0.0084	12.4073	0.0119	12.2542	0.0093	3.780	0.080	R97
NGC6522	270.897660	-30.029130	12.7394	0.0101	11.9973	0.0117	11.8172	0.0090	3.990	0.090	R97
NGC6522	270.900830	-30.028706	12.7484	0.0101	12.0173	0.0118	11.8372	0.0094	4.530	0.080	R97
NGC6522	270.902520	-30.037906	13.0874	0.0090	12.4483	0.0119	12.2742	0.0087	3.850	0.070	R97
NGC6522	270.898860	-30.039038	13.5634	0.0103	12.8933	0.0126	12.7162	0.0099	3.870	0.080	R97
NGC6522	270.895380	-30.027055	13.2584	0.0120	12.5333	0.0163	12.3512	0.0146	4.130	0.090	R97
NGC6528	271.189090	-30.063042	11.8699	0.0127	10.9529	0.0171	10.6790	0.0133	6.140	0.080	R97
NGC6528	271.203810	-30.063170	12.2459	0.0131	11.3789	0.0158	11.1100	0.0134	5.780	0.080	R97
NGC6528	271.213860	-30.068241	12.7579	0.0111	11.9169	0.0125	11.6660	0.0116	6.130	0.120	R97
NGC6528	271.210910	-30.063342	12.8349	0.0107	11.9889	0.0130	11.7620	0.0111	5.850	0.120	R97
NGC6528	271.199040	-30.063076	12.7099	0.0121	11.8199	0.0156	11.5580	0.0125	6.360	0.100	R97
NGC6528	271.211400	-30.062349	13.0989	0.0128	12.2439	0.0142	11.9990	0.0125	5.290	0.110	R97
NGC6528	271.212120	-30.066603	13.7789	0.0103	13.0179	0.0120	12.8190	0.0104	6.040	0.110	R97
NGC6541	272.037000	-43.767200	10.2480	0.0220	9.5890	0.0230	9.4230	0.0230	4.520	0.070	R97
NGC6541	271.948650	-43.706280	10.7950	0.0230	10.1410	0.0210	10.0190	0.0190	4.070	0.070	R97
NGC6541	272.061400	-43.751800	10.9100	0.0220	10.2500	0.0210	10.1290	0.0230	4.020	0.100	R97
NGC6541	271.978600	-43.668650	11.1560	0.0220	10.5060	0.0210	10.4200	0.0240	3.660	0.120	R97
NGC6541	272.094500	-43.694620	11.2940	0.0240	10.6270	0.0230	10.4940	0.0210	3.950	0.100	R97
NGC6541	272.079800	-43.696470	11.5080	0.0270	10.8880	0.0240	10.7190	0.0190	4.020	0.120	R97
NGC6541	271.955220	-43.705200	11.7580	0.0260	11.1420	0.0210	11.0190	0.0210	3.900	0.170	R97
NGC6541	272.051050	-43.665800	12.1230	0.0260	11.5600	0.0290	11.4180	0.0270	3.470	0.180	R97
NGC6541	272.073000	-43.673900	12.2260	0.0300	11.5620	0.0350	11.4880	0.0270	3.420	0.140	R97
NGC6544	271.821160	-24.989815	10.2679	0.0225	9.4242	0.0190	9.2359	0.0272	3.590	0.080	R97
NGC6544	271.851630	-24.975938	10.3729	0.0179	9.5092	0.0213	9.2599	0.0212	4.090	0.100	R97
NGC6544	271.842540	-24.974314	10.6889	0.0186	10.0222	0.0394	9.7449	0.0214	3.670	0.140	R97
NGC6544	271.849760	-25.013621	10.7279	0.0136	9.8532	0.0163	9.7029	0.0217	3.850	0.100	R97
NGC6544	271.831170	-25.014447	11.2279	0.0118	10.4752	0.0226	10.2519	0.0209	3.600	0.110	R97
NGC6544	271.848810	-24.987848	11.0969	0.0182	10.3262	0.0230	10.1139	0.0269	3.770	0.120	R97
NGC6544	271.818010	-24.983324	10.6809	0.0212	9.7512	0.0218	9.5949	0.0324	4.000	0.070	R97
NGC6544	271.857630	-25.011463	11.3329	0.0130	10.5392	0.0219	10.3419	0.0178	3.660	0.110	R97
NGC6544	271.820510	-25.009073	11.5979	0.0108	10.8562	0.0204	10.6439	0.0154	3.420	0.150	R97

Table 8. continued.

Cluster	ra(J2000)	dec(J2000)	J	σ_J	H	σ_H	K_s	σ_{Ks}	EW	σ_{EW}	source
NGC6544	271.820420	-25.007336	11.4699	0.0127	10.7172	0.0226	10.5039	0.0185	3.680	0.160	R97
NGC6544	271.840056	-24.982136	9.3480	0.0220	8.4140	0.0150	8.1090	0.0200	4.650	0.070	R97
NGC6553	272.335020	-25.916079	10.7154	0.0234	9.6184	0.0261	9.4212	0.0193	6.180	0.070	R97
NGC6553	272.333930	-25.912852	11.4874	0.0329	10.5454	0.0352	10.0842	0.0229	6.370	0.110	R97
NGC6553	272.328130	-25.914426	10.9684	0.0249	9.9854	0.0193	9.6202	0.0205	6.170	0.060	R97
NGC6553	272.319930	-25.906701	10.9854	0.0245	9.9854	0.0262	9.6812	0.0221	5.660	0.100	R97
NGC6553	272.329550	-25.920776	12.1914	0.0170	11.2874	0.0205	11.0142	0.0161	5.470	0.130	R97
NGC6553	272.328860	-25.921909	12.1064	0.0191	11.2284	0.0221	10.9672	0.0153	6.020	0.160	R97
NGC6553	272.319430	-25.911748	10.2640	0.0490	9.1750	0.0420	8.7820	0.0350	5.970	0.090	R97
NGC6553	272.331670	-25.913027	10.2450	0.0320	9.1940	0.0370	8.8280	0.0340	6.380	0.110	R97
NGC6624	275.938420	-30.355234	12.9299	0.0088	12.2717	0.0117	12.1608	0.0093	5.680	0.120	R97
NGC6624	275.910010	-30.331587	12.2139	0.0081	11.6387	0.0098	11.5098	0.0098	5.090	0.100	R97
NGC6624	275.901620	-30.350888	11.7339	0.0109	10.8897	0.0119	10.7188	0.0138	4.700	0.170	R97
NGC6624	275.929650	-30.379375	11.9369	0.0106	11.1587	0.0157	10.9928	0.0112	5.460	0.120	R97
NGC6624	275.914510	-30.380723	11.8489	0.0087	11.0007	0.0134	10.8318	0.0105	5.480	0.130	R97
NGC6624	275.937200	-30.354595	12.1869	0.0094	11.3927	0.0119	11.2228	0.0115	5.180	0.160	R97
NGC6624	275.946020	-30.369740	12.2389	0.0102	11.5027	0.0115	11.3288	0.0109	5.360	0.100	R97
NGC6624	275.898760	-30.345880	12.5839	0.0087	11.8987	0.0093	11.7688	0.0113	5.030	0.200	R97
NGC6624	275.904870	-30.367484	12.3579	0.0146	11.5607	0.0148	11.4198	0.0145	5.480	0.140	R97
NGC6624	275.943960	-30.354774	12.6229	0.0089	11.9297	0.0103	11.8038	0.0097	5.080	0.150	R97
NGC6624	275.927820	-30.380025	12.5229	0.0107	11.7527	0.0148	11.5988	0.0110	5.340	0.080	R97
NGC6624	275.908530	-30.348299	11.3819	0.0141	10.5087	0.0212	10.3308	0.0144	4.970	0.210	R97
NGC6624	275.947730	-30.342786	12.8689	0.0088	12.1187	0.0116	11.9838	0.0097	4.740	0.150	R97
NGC6624	275.953230	-30.360993	13.1839	0.0081	12.5567	0.0083	12.4228	0.0089	5.180	0.170	R97
NGC6624	275.902740	-30.371356	13.1729	0.0120	12.4577	0.0132	12.3288	0.0119	4.610	0.200	R97
NGC6624	275.925500	-30.335833	13.2649	0.0089	12.5527	0.0090	12.4198	0.0110	4.610	0.180	R97
NGC6624	275.943490	-30.368702	13.3139	0.0086	12.6147	0.0094	12.4798	0.0098	5.050	0.170	R97
NGC6624	275.925490	-30.380779	13.9249	0.0078	13.3647	0.0103	13.2678	0.0086	4.470	0.250	R97
NGC6626	276.149840	-24.837034	10.7893	0.0088	10.0662	0.0135	9.8998	0.0115	4.320	0.090	R97
NGC6626	276.175110	-24.858400	11.1093	0.0091	10.3512	0.0104	10.1978	0.0105	5.140	0.110	R97
NGC6626	276.099570	-24.867621	11.4923	0.0080	10.7642	0.0114	10.5798	0.0096	4.420	0.130	R97
NGC6626	276.098900	-24.876100	11.5643	0.0126	10.8812	0.0194	10.7068	0.0166	4.710	0.100	R97
NGC6626	276.165770	-24.859210	11.7843	0.0084	11.1082	0.0099	10.9798	0.0100	5.160	0.130	R97
NGC6626	276.140220	-24.911129	11.7513	0.0093	11.0172	0.0116	10.8628	0.0113	4.550	0.080	R97
NGC6626	276.159820	-24.895232	12.1903	0.0076	11.5882	0.0085	11.4288	0.0090	4.740	0.210	R97
NGC6626	276.103280	-24.891095	11.8383	0.0111	11.1112	0.0149	10.9338	0.0138	4.640	0.130	R97
NGC6626	276.161760	-24.882580	12.2483	0.0082	11.5712	0.0094	11.4218	0.0094	4.410	0.190	R97
NGC6626	276.141310	-24.902104	12.6253	0.0094	11.9882	0.0109	11.8408	0.0092	4.530	0.150	R97
NGC6626	276.104340	-24.898918	12.9323	0.0180	12.3452	0.0180	12.2208	0.0164	4.550	0.140	R97
NGC6626	276.094190	-24.869700	13.0403	0.0086	12.4082	0.0118	12.2568	0.0091	4.000	0.150	R97
NGC6637	277.831110	-32.347872	10.4451	0.0188	9.5161	0.0249	9.3030	0.0126	5.990	0.040	R97
NGC6637	277.835720	-32.376780	11.8141	0.0197	11.0928	0.0272	10.9530	0.0120	5.750	0.070	R97
NGC6637	277.831350	-32.354689	11.1771	0.0150	10.3312	0.0186	10.1560	0.0107	5.900	0.060	R97
NGC6637	277.842140	-32.361624	12.1285	0.0127	11.4456	0.0130	11.3110	0.0082	5.470	0.090	R97
NGC6637	277.830170	-32.335277	12.0632	0.0141	11.2822	0.0167	11.1560	0.0111	5.390	0.050	R97

Table 8. continued.

Cluster	ra(J2000)	dec(J2000)	J	σ_J	H	σ_H	K_s	σ_{Ks}	EW	σ_{EW}	source
NGC6637	277.839250	-32.368119	12.8718	0.0108	12.2755	0.0115	12.1540	0.0111	4.800	0.140	R97
NGC6637	277.828560	-32.352250	12.8128	0.0131	12.1440	0.0128	12.0170	0.0082	5.290	0.100	R97
NGC6637	277.822330	-32.357247	13.7167	0.0099	13.3563	0.0081	13.2600	0.0066	4.960	0.120	R97
NGC6637	277.816430	-32.362244	13.1428	0.0112	12.4995	0.0101	12.3710	0.0074	5.430	0.110	R97
NGC6637	277.823910	-32.351319	13.6966	0.0152	13.1957	0.0150	13.1010	0.0088	4.610	0.100	R97
NGC6637	277.820270	-32.360449	14.1267	0.0121	13.6532	0.0080	13.5560	0.0070	5.260	0.130	R97
NGC6637	277.822210	-32.356119	14.1623	0.0120	13.6934	0.0100	13.5950	0.0077	5.140	0.100	R97
NGC6637	277.872920	-32.357453	11.8140	0.0220	11.0710	0.0260	10.9410	0.0190	5.290	0.080	R97
NGC6637	277.875100	-32.347411	9.7870	0.0230	8.8500	0.0590	8.6030	0.0230	6.520	0.050	R97
NGC6637	277.863280	-32.364886	12.9030	0.0220	12.3020	0.0240	12.1630	0.0210	5.040	0.140	R97
NGC6638	277.753960	-25.494728	11.1816	0.0120	10.2643	0.0201	10.0351	0.0093	5.550	0.080	R97
NGC6638	277.747190	-25.514728	11.2556	0.0113	10.3623	0.0271	10.1091	0.0088	5.400	0.110	R97
NGC6638	277.709840	-25.485283	12.0176	0.0079	11.1743	0.0190	10.9831	0.0068	5.190	0.080	R97
NGC6638	277.743270	-25.510178	12.3916	0.0093	11.5963	0.0152	11.4051	0.0064	4.970	0.150	R97
NGC6638	277.729720	-25.478459	12.8456	0.0074	12.1483	0.0139	11.9991	0.0057	5.080	0.180	R97
NGC6638	277.734210	-25.482252	13.1096	0.0082	12.4633	0.0135	12.3301	0.0054	4.980	0.190	R97
NGC6638	277.753050	-25.478493	12.9926	0.0066	12.3323	0.0143	12.1861	0.0054	4.620	0.140	R97
NGC6638	277.747070	-25.476430	12.9396	0.0069	12.2763	0.0149	12.1111	0.0062	5.470	0.120	R97
NGC6638	277.708590	-25.508143	12.7366	0.0072	11.9833	0.0138	11.8071	0.0057	5.390	0.120	R97
NGC6638	277.717510	-25.474371	13.4746	0.0064	12.8283	0.0121	12.6911	0.0052	4.630	0.150	R97
NGC6809	294.998500	-30.919460	9.2960	0.0200	8.6080	0.0370	8.4410	0.0210	4.270	0.040	R97
NGC6809	294.983400	-30.921370	9.2890	0.0200	8.6660	0.0190	8.4700	0.0200	4.290	0.040	R97
NGC6809	294.960900	-30.928380	10.2590	0.0210	9.6120	0.0250	9.5040	0.0200	3.970	0.040	R97
NGC6809	294.896070	-30.993520	10.7160	0.0200	10.1060	0.0250	9.9850	0.0200	3.640	0.030	R97
NGC6809	294.875900	-30.988590	11.1600	0.0210	10.5410	0.0250	10.3980	0.0230	3.560	0.030	R97
NGC6809	295.016950	-30.999800	11.1720	0.0210	10.5820	0.0230	10.4690	0.0210	3.640	0.040	R97
NGC6809	294.932600	-30.925550	11.5730	0.0210	11.0110	0.0260	10.9140	0.0210	3.080	0.050	R97
NGC6809	294.960350	-30.918480	12.1210	0.0260	11.8710	0.0330	11.8010	0.0250	3.090	0.050	R97
NGC7099	325.070990	-23.168264	10.3600	0.0210	9.7800	0.0250	9.6300	0.0210	3.480	0.040	R97
NGC7099	325.075230	-23.173839	10.4870	0.0210	9.9420	0.0270	9.7750	0.0210	3.030	0.050	R97
NGC7099	325.057860	-23.150794	11.0600	0.0210	10.5380	0.0250	10.3890	0.0210	2.910	0.040	R97
NGC7099	325.160670	-23.182993	11.6500	0.0200	11.1030	0.0270	10.9790	0.0210	3.040	0.140	R97
NGC7099	325.077120	-23.146500	13.3360	0.0280	12.8560	0.0360	12.7770	0.0330	2.210	0.190	R97

NGC2808 (R97 ; C09c)

NGC2808 (S12 ; C09c)

NGC6139 (S12 ; C09)

NGC2808 (R97 ; H10)

NGC2808 (S12 ; H10)